UNIVERSITY OF LIVERPOOL

Inverse Vulcanised Sulfur Polymers for Heavy Metal Remediation

Thesis submitted in accordance with the requirements of the University of Liverpool for the degree of Doctor of Philosophy

By

Douglas J. Parker BSc(Hons), MSc(Res)

Department of Chemistry, University of Liverpool

September 2019

DECLARATION

The research contained in this thesis documents was undertaken within the Department of Chemistry at the University of Liverpool between October 2015 and March 2019. The research presented herein is entirely my own work, unless otherwise stated in the preface or indicated in the text. I have read the PGR Code of Practice and declare that this document adheres to the academic standards defined in Appendix 4. This thesis does not exceed the specified maximum word count and complies with the requirements as set out by the Faculty of Science & Engineering.

Douglas J. Parker

September 2019

ACKNOWLEDGEMENTS

I would like to start by thanking my supervisor *Dr Tom Hasell* for not only giving me the opportunity to study in his group, but also for all his help and support throughout my PhD programme. I would also like to thank all members of the Hasell Group both past and present for making the last three and half years some of the most entertaining and enjoyable I have had; with a special thanks to *Jess*, *Sam* and *Bowen*.

Although a PhD is the culmination of research by a single person, it would most certainly not have been possible to achieve this without the help and support of many individuals. Thanks are due to both *Sam Petcher* and *Bowen Zhang* from the Hasell Group for providing me with high resolution SEM micrographs and gas sorprtion data of my samples. The analytical services team here in the Department of Chemistry for providing NMR and CHNS analysis, and a big thank you to *Stephen Moss* who runs the departmental ICP-OES service. Without his expert knowledge, can do attitude and flexibility (thanks for fitting in all my awkward unstabilised toxic heavy metal samples!) this project would not have been as successful as it has been.

I would also like to thank *Professor Andy Cooper* and his group for allowing the use of their analytical equipment and for collaborating on certain projects, especially *Duncan Woods* for running GPC analysis on my samples, *Jet-Sing Lee* for collaborating with our group on the carbonisation of S-DCPD polymers and to *Rob Clowes* for keeping all the analytical instruments running (even when our samples did occasionally break them). Special thanks also go to *Dr Sam Chong* and her group for analysing several of my samples on the I11 Beamline at Diamond.

Finally I'd like to thank my friends and family for their never ending support during my PhD; and I am especially grateful to my *mum*, *step-dad* and my *girlfriend* who not only supported me throughout my PhD programme but also put up with me through the highs and lows that go along with it (and for suffering through and proof-reading this thesis!).

ABSTRACT

Inverse Vulcanised Sulfur Polymers for Heavy Metal Remediation

Douglas J. Parker

This thesis describes the work undertaken between two interlinked fields of chemical research; the synthesis of novel sustainable inverse vulcanised sulfur polymers and their applications for the remediation of heavy metals.

Chapter 1 includes an introduction to sulfur and its chemistry, inverse vulcanisation and its processes and a discussion of previously reported work in the field. The potential applications for inverse vulcanised sulfur polymers and background information relating to heavy metals, their toxicity and environmental contamination are also contained in this chapter.

Research into new crosslinkers and the route to establishing an adaptable synthetic method suitable for the inverse vulcanisation of multiple different sustainable crosslinking agents is presented in **Chapters 2** and **3**. These chapters cover early initial reactions, background information on potential new crosslinkers and the synthesis and analysis of nine new polymeric materials.

Chapter 4 discusses the potential application for these polymers as sorbents for heavy metal remediation. This chapter discusses routes to enhancing the surface area of these novel polymeric materials, followed by the results from in situ testing of these materials against a range of inorganic and organometallic heavy metal compounds.

Detailed experimental methods and heavy metal testing protocols, information relating to the instrumentation used to generate the data presented in this thesis and the relevant analytical theory behind these techniques, is to be found in **Chapter 5**.

Chapter 6 covers the main conclusions drawn from this research and suggests how this project could be continued in the future.

TABLE OF CONTENTS

Chapter 2: Cyclical and Complex Terpenoid Mixtures for Crosslinking

Chapter 3: Linear Terpenoid Derived Crosslinkers

Chapter 4: Applications for Heavy Metal Remediation

Chapter 5: Synthesis, Characterisation and Analytical Theory

LIST OF PUBLICATIONS

The worked presented in this thesis has contributed to the following publications:

I. **Catalytic inverse vulcanization**

X. Wu, J. A. Smith, S. Petcher, B. Zhang, **D. J. Parker**, J. M. Griffin and T. Hasell, Nature Communications, 2019, 10, 647

II. **Sustainable inverse-vulcanised sulfur polymers**

D. J. Parker, S. Y. Chong and T. Hasell, RSC Advances, 2018, 8, 27892-27899

III. **High surface area sulfur-doped microporous carbons from inverse-vulcanised polymers**

J.-S. Lee, **D. J. Parker**, A. I. Cooper and T. Hasell, Journal of Materials Chemistry A, 2017, 5, 18603-18609

IV. **Low cost and renewable sulfur-polymers by inverse vulcanisation**

D. J. Parker, H. A. Jones, S. Petcher, L. Cervini, J. M. Griffin, R. Akhtar and T. Hasell, Journal of Materials Chemistry A, 2017, 5, 11682-11692

V. **Porous inverse vulcanised polymers for mercury capture**

T. Hasell, **D. J. Parker**, H. A. Jones, T. McAllister and S. M. Howdle, Chemical Communications, 2016, 52, 5383-5386

LIST OF ABBREVIATIONS

AC	Activated Carbon
AES	Atomic Emission Spectroscopy
AR	Analytical Reagent
ASGM	Artisanal and Small-scale Gold Mining
BDET	1,3-benzenediamidoethanethiolate
BET	Brunauer Emmett Teller theory
BHT	Butylated Hydroxytoluene
C	Critical point
CCD	Charge Coupled Device
$CDCl_3$	Chloroform (deuterated)
C_{con}	Control solution
CFE-SEM	Cold Field Emission Scanning Electron Microscope
CNS	Central Nervous System
CO_2	Carbon Dioxide
COD	Crystallography Open Database
Cp	Heat capacity
C_{test}	Test solution
DCPD	Dicyclopentadiene
DI	Deionised Water
DIB	Diisopropenyl benzene
DSC	Differential Scanning Calorimetry
DVB	Divinyl benzene
E. coli	*Escherichia coli*
EPA	Environmental Protection Agency

ESP	Electrostatic Precipitators
FGD	Flue Gas Desulfurisation
FF	Fabric Filters
FIB-SEM	Focused Ion Beam Scanning Electron Microscope
FT-IR	Fourier Transform-Infrared Spectroscopy
GPC	Gel Permeation Chromatography
GPR	General Purpose Reagent
$HAuCl_4$	Chloroauric acid
HPLC	High Performance Liquid Chromatography
H_2S	Hydrogen Sulfide
ICP	Inductively Coupled Plasma
ICP-OES	Inductively Coupled Plasma – Optical Emission Spectroscopy
ICSD	Inorganic Crystal Structure Database
IR	Infrared
IUPAC	International Union of Pure and Applied Chemistry
K_2CO_2	Potassium Carbonate
KBr	Potassium Bromide
KOH	Potassium Hydroxide
Li-S	Lithium – sulfur
mAh^{-1}	Milliampere hour
mbar	Millibar
M_p	Polymer mass
MPa	Megapascals
Ms	Sorbent mass
M_w	Molecular weight

Na-S	Sodium – sulfur
NMR	Nuclear Magnetic Resonance
OES	Optical Emission Spectroscopy
P_C	Critical pressure
PDF	Powder Diffraction File
PES	Polyethersulfone
ppb	Parts per Billion
ppm	Parts per Million
PVDF	polyvinyl difluoride
pXRD	Powder X-Ray Diffraction
Q_P	Polymer capacity
Q_s	Sorbent capacity
RI	Refractive Index
ROP	Ring Opening Polymerisation
$scCO_2$	Supercritical Carbon Dioxide
SCF	Supercritical Fluid
scXRD	Single crystal X-Ray Diffraction
S-DCPD	Sulfur – DCPD copolymer
S-DIB	Sulfur – DIB copolymer
SEM	Scanning Electron Microscope
S-FAR	Sulfur – Farnesene copolymer
S-FSOL	Sulfur – Farnesol copolymer
S-HOP	Sulfur – Hop oil copolymer
S-LIM	Sulfur – Limonene copolymer
S-MYR	Sulfur – Myrcene copolymer

S-NER	Sulfur – Nerolidol copolymer
SO_2	Sulfur Dioxide
S-PER	Sulfur – Perillyl alcohol copolymer
S-PERT	Sulfur – Perillartine copolymer
S-SQ	Sulfur – Squalene copolymer
T	Triple point
TAC	Triallyl cyanurate
T_C	Critical temperature
T_c	Crystallisation transition temperature
T_g	Glass transition temperature
THF	Tetrahydrofuran
T_m	Melting transition temperature
TVTCSi	1,3,5,7-Tetravinyl 1,3,5,7-tetramethylcyclotetrasiloxane
UV	Ultraviolet
wt.%	Weight percent
$Zn(DTC)_2$	Zinc diethyldithiocarbamate

LIST OF EQUATIONS

LIST OF FIGURES

LIST OF SCHEMES

LIST OF TABLES

Chapter 1: Introduction and Literature Review

Contents

1.1 INTRODUCTION – THE SULFUR PROBLEM

1.1.1 BACKGROUND

Sulfur is one of the most abundant mineral elements found on the planet,[1] and until the turn of the 20th century it was most commonly extracted from the soil surrounding volcanoes especially on the island of Sicily.[2] Due to relative abundance in the environment, man has found a diverse range of applications requiring elemental sulfur; from explosives and medicines to functional materials and fine chemicals.[3-5] With this increased demand for sulfur, a new method was required to extract larger quantities. First proposed and subsequently patented by Herman Frasch at the end of the 19th century, the Frasch process enabled the extraction of sulfur from salt dome deposits.[6] By liquefying sulfur within geological deposits using superheated water and then pumping the molten sulfur to the surface, the Frasch process allowed the extraction of higher purity sulfur to be rapidly extracted for processing (compared to traditional mining methods).[7]

The Frasch process would remain the predominant method for the extraction of sulfur until the early 1970s, when the rise of environmental concerns surrounding SO_2 emissions and acid rain caused by the combustion of petroleum based products required industry to remove sulfur from crude petroleum products.[5] Industry responded to these concerns by using the hydrodesulfurisation process to remove sulfur from natural gas and petroleum, however this led to sulfur becoming an increasingly significant waste by-product with the vast majority of elemental sulfur being stockpiled at large refining sites as production outstrips demand.[4] United States Geological Survey statistics show that there was approximately 72.4 million metric tons of sulfur produced in 2014.[8]

Although elemental sulfur has uses in specific areas of chemistry; for example the production of sulfuric acid, fertilisers and in niche chemical applications

such as vulcanisation, these processes make limited demands on the huge amount of available sulfur. This large abundance of sulfur makes it a relatively cheap feedstock for exploitation if suitable uses and reactions can be derived.

1.1.2 CHEMISTRY OF SULFUR

Elemental sulfur is a yellow crystalline solid that exhibits a number of polymorphs. Primarily found in its orthorhombic state (also known as the α-sulfur polymorph) at temperatures lower than 100 °C, sulfur is a cyclical compound with an average "sulfur ring" comprising eight sulfur atoms (S_8).[4] At temperatures above 95 °C and below 120 °C, the monoclinic or β-sulfur polymorph is the increasingly favoured species with similar sulfur rings as found in α-sulfur polymorphs albeit arranged and packed into a different orientation.[9]

Continued heating of elemental sulfur above 120 °C leads to the sulfur melting into a thin yellow liquid and above 159 °C the sulfur starts to undergo Ring Opening Polymerisation (ROP), shown in Scheme 1.1.1, with itself leading to the formation of a thick viscous liquid.[9, 10] As the molten sulfur is heated further, it undergoes an equilibrium polymerisation process up to approximately 200 °C where it is transformed into a red solid polymeric material.[11-15] During this heating process the molten sulfur exhibits several colour changes as it undergoes polymerisation, from yellow to orange and finally red.[9] It is still unclear as to why sulfur undergoes this colour change, however it has been suggested by Meyer *et al.* that polymeric sulfur does in fact retain its yellow colour (as shown when thin films of polymeric sulfur were quenched at 200 °C) and that the red colour is caused by small organic impurities or small cyclical sulfur molecules such as S_3 and S_4.[16, 17] Polymeric sulfur is formed of sulfur chains that are terminated in radical thiyl groups,

making the material intrinsically unstable and readily able to depolymerise back into elemental sulfur due to the backbiting effect attributed to the thiyl groups present.[17]

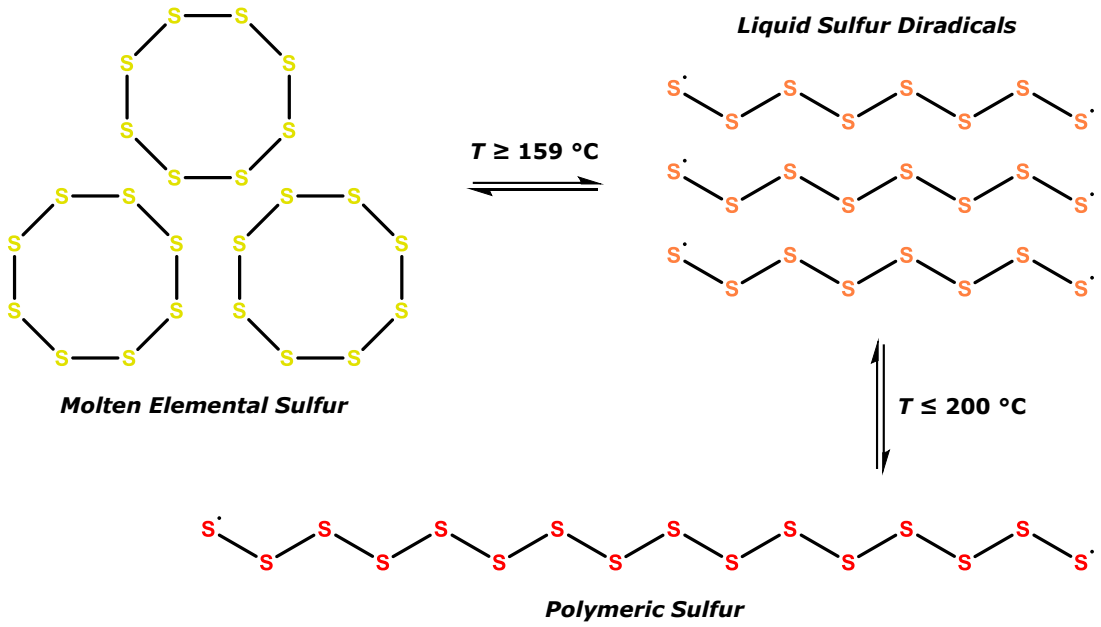

Scheme 1.1.1 ROP of elemental sulfur into polymeric sulfur. Adapted from[18]

1.2 VULCANISATION AND INVERSE VULCANISATION

1.2.1 THE VULCANISATION PROCESS

Charles Goodyear is often credited with the discovery of the vulcanisation process in the early 1800s.[19] The structure of natural rubber allows the polyisoprene chains to move freely and this leads to a material that is easily deformable and lacking in useful physical properties. However by introducing a small quantity of sulfur to natural rubber these properties can be greatly enhanced and modified. The sulfur forms crosslinks between the polyisoprene chains, which prevents them from moving freely. By varying the quantity of sulfur and other additives, vulcanised materials with varying properties can synthesised. Despite rapidly approaching the bicentennial of the invention of vulcanised rubber, its physical properties and our

understanding of the material properties are still limited with most of the research pioneered by Arthur V. Tobolsky.[9, 10, 20-23]

1.2.2 INVERSE VULCANISATION OF ELEMENTAL SULFUR

Inverse vulcanisation is the process by which sulfur is utilised as the polymeric material backbone with organic monomers used as crosslinking agents, in a process that is the polar opposite of conventional vulcanisation. However unlike vulcanisation, which typically has a low sulfur crosslinker content, inverse vulcanised polymers tend to have a higher crosslinker content between 10 to 50 wt.%. This method of utilising sulfur as a polymeric backbone was first proposed in 2013 by Pyun *et al.* and relies heavily on the fact that sulfur can ring open and readily form polymeric chains.[24, 25]

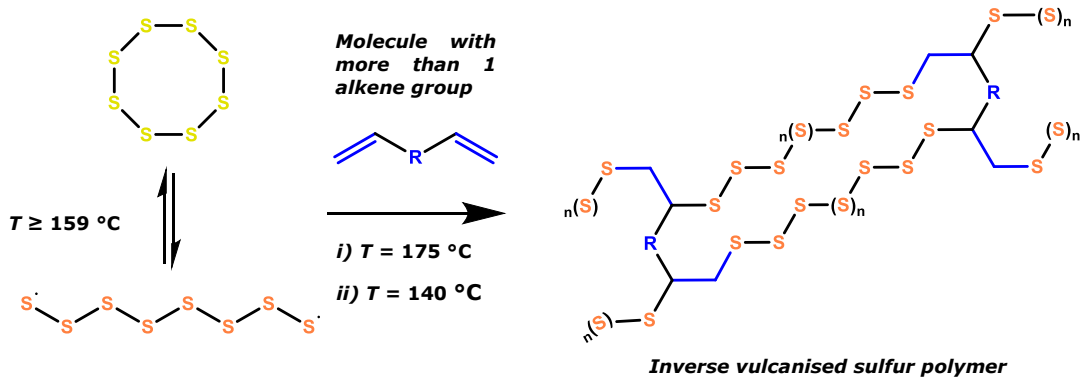

Scheme 1.2.1 Simplified scheme showing the process of inverse vulcanisation

As shown in the scheme above (Scheme 1.2.1), the process of inverse vulcanisation differs very little from that of the heating and subsequent "polymerisation" of elemental sulfur. By utilising sulfur in its molten state, inverse vulcanised polymers are inherently green due to the lack of solvent required and thus also making these reactions highly atom efficient. These properties align closely with the principles of green chemistry and by using waste by-products or renewable sources for crosslinking agents, the green credentials of inverse vulcanised polymers can only be enhanced further.

As well as being used to synthesise "pure" polymeric materials, inverse vulcanisation can be used as part of a process for synthesising a multi-component material. It is possible to incorporate inverse vulcanised polymers with metal nanoparticle precursors to form nanocomposite materials and to synthesise novel composite materials by blending inverse vulcanised polymers with other polymeric materials, such as polybenzoxazines, aromatic diynes and aliphatic amines.[26-28]

1.2.3 SYNTHESIS OF EARLY INVERSE VULCANISED POLYMERS

Recently there has been a renewed interest in sulfur polymeric materials, with papers focusing on crosslinking sulfur with 1,3-diisopropenyl benzene (DIB),[24] and limonene.[29] The work by Pyun *et al.* in using DIB as a crosslinker was a breakthrough for modern sulfur polymer materials.[24] The sulfur - DIB copolymer produced (Scheme 1.2.2) exhibits good physical properties, with respect to shape persistence (which is important if porosity is to be induced) and thermal properties such as glass transition temperature, and has been demonstrated for potential applications, such as IR transparent lenses and Li-S batteries, however the high cost of DIB relative to sulfur would limit this material commercially to certain applications.

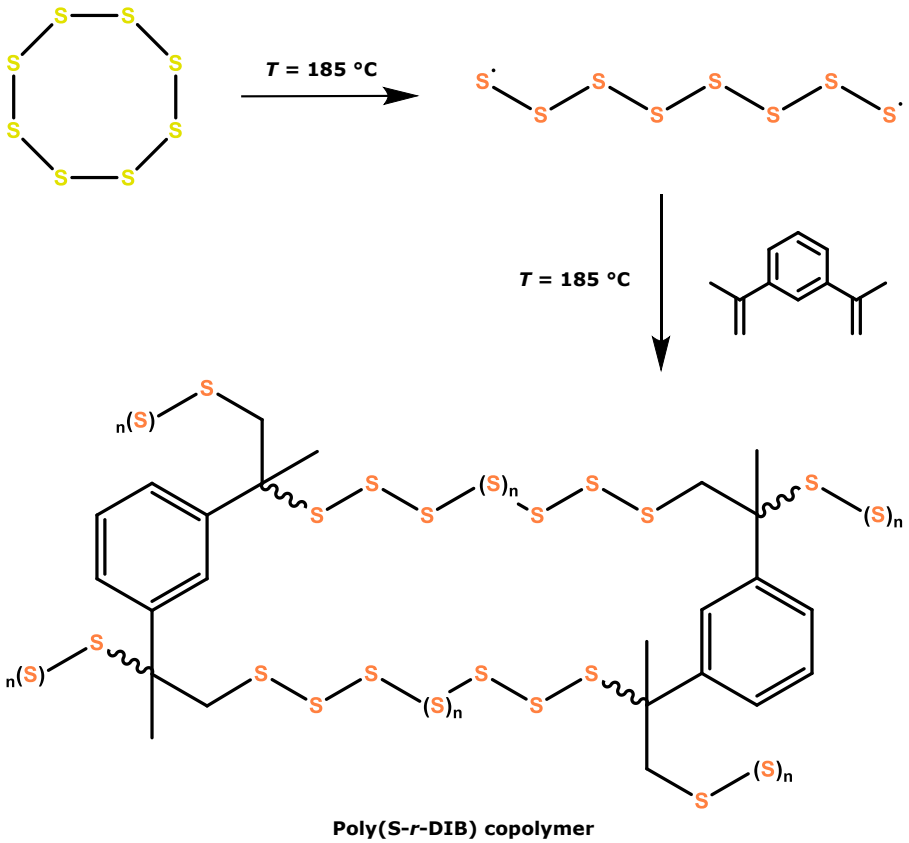

Scheme 1.2.2 The copolymerisation of S_8 with DIB. Adapted from[24]

In 2015, Chalker *et al.* developed a novel sulfur - limonene polymer which had aimed to address the issue of affordability by developing a suitable polymeric material from cheaper feedstocks.[29] Although limonene is much cheaper than DIB and comes from a renewable feedstock (it is removed from citrus peel), the physical properties of the resultant polymeric materials were much poorer than S-DIB and lacked shape persistence (Figure 1.2.1). In addition to this, the S-LIM copolymer exhibited a very low glass transition temperature (-20 °C). This lack of shape persistence is likely caused by the synthesis of low molecular weight species, rather than a high molecular weight complex polymeric material. However the material has been shown to have applications in the remediation of mercury from water. Despite this useful and desirable ability, the severe lack of shape persistence also bars this material from widespread commercial adoption.

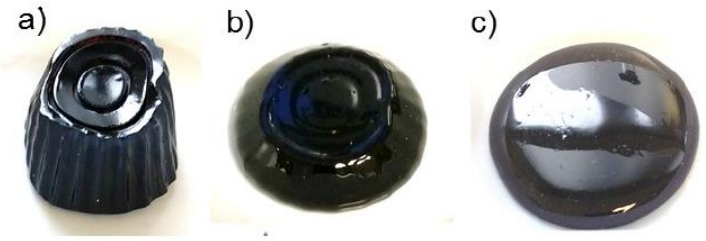

Figure 1.2.1 Images of sulfur-limonene copolymer a) after removal from mould, b) 2 hours at room temperature and c) 24 hours at room temperature

1.2.4 CURRENT TRENDS IN INVERSE VULCANISED SULFUR POLYMERS

Moreover, there have been recent attempts at redressing these issues. Yagci *et al*. reported in 2016, the successful synthesis of sulfur polybenzoxazines copolymers with a high molecular weight (38,650 to 112,100 $gmol^{-1}$), high sulfur content (between 50 and 90 wt.% sulfur content) and some tunability of the material properties.[27] The use of polybenzoxazines has gained increasing importance as the crosslinking backbone in synthetic resin synthesis due in part to polybenzoxazines possessing several physiochemical properties such as: a high T_g;[30] the tuneabilty to provide better resistance to UV light;[31] and chemical exposure.[32] Combining a well-known and studied compound with the ability to crosslink with sulfur meets the aims of making a more functional material although the issue of material costs is still a consideration. Similarly, Salman *et al*. reported the use of divinylbenzene (DVB) as a crosslinker for the inverse-vulcanisation of sulfur.[33] DVB has a similar structure to DIB, except it excludes the additional methyl groups of the latter. It would be reasonable therefore, to expect the physical properties to be similar to those that were reported to DIB. At higher sulfur content the polymers perform similarly according to DSC but as crosslinker content is increased DIB has a higher T_g with the 30 wt.% sulfur DIB copolymer having a T_g almost 5 °C higher than sulfur DVB copolymer. This lower T_g however is

somewhat mitigated by the much lower cost of DVB as raw material and feed stock for polymer synthesis.

Since the first reported use of limonene as a biorenewable crosslinking agent by Chalker *et al.*, there have been further reports of other crosslinking agents that were derived from sustainable and renewable sources suitable for inverse vulcanisation reactions. In 2016, Mecerreyes *et al.* reported the use of diallyl disulfide as a biorenewable crosslinking agent for inverse vulcanisation.[34] When reacted with sulfur, diallyl disulfide rapidly formed a homogenous mixture, before the copolymer was cured for 24 hours. The resultant inverse vulcanised copolymers produced dark red/black rubbery shape persistent films that proved impervious to a selection of common laboratory solvents, with only the 40 wt.% diallyl disulfide copolymer dissolving carbon disulfide.

Following on from this Theato *et al*. have studied the use of eugenol and vegetable oils as suitable crosslinking agents.[35] In the case of eugenol, although it reacted with sulfur at 175 °C, the resultant copolymer composition was unstable and after 24 hours started to depolymerise. Theato postulated that the lack of allylic groups present in eugenol contributed to instability in the copolymer, therefore eugenol was modified via a Williamson ether synthesis to form eugenol allyl ether. When reacted with sulfur, eugenol allyl ether successfully forms a dark coloured stable inverse vulcanised polymer suggesting that the additional allylic groups present on the crosslinker allow additional C-S bonds to form stabilising the copolymer composition.

Theato *et al*. also investigated the use of various vegetable oils to synthesise inverse vulcanised materials for Li-S battery applications.[36] Their research showed that it was possible to form stable sulfur copolymer composites with an 80 wt.% content of sulfur using linseed, sunflower and olive oils as biorenewable crosslinking agents, although trace amounts of crystalline S_8 were detected suggesting that not all sulfur had been consumed in the

reactions or the samples had started to slowly degrade. Despite all three oils possessing different fatty acid compositions, the sulfur copolymers synthesised exhibited very similar physiochemical properties with the sulfur content of the copolymer being the defining element. All inverse vulcanised copolymers synthesised took 30 to 40 minutes to reach their respective gel points before additional heating "cured" the polymeric materials forming, brown rubbery materials.

Although these new materials have made some progress in minimising cost implications and improving the usability of sulfur materials, the need to further improve these factors requires the development of new novel polymeric sulfur materials.

1.3 HEAVY METALS AND THE ENVIRONMENT

1.3.1 MERCURY

Heavy metals, such as mercury, are becoming increasingly problematical for the environment as they are persistent and can bio-accumulate in plants, animals and organisms. Exposure to mercury can lead to a multitude of health problems including serious neurological issues, embryotoxic effects and in severe cases even death.[37] Due to the extremely toxic nature of mercury and its associated compounds, there have been multiple reviews studying the anthropogenic causes of mercury contamination, its sources and methods of remediation.[38, 39]

Data released in the 2018 UN Global Mercury Assessment report, shows that the two largest sources of anthropogenic mercury pollution are from Artisanal and Small-scale Gold Mining (ASGM) and burning of coal.[40] ASGM and the burning of coal release a combined average of over 1,300 tonnes of mercury pollution per year and account for over 60% of all anthropogenic mercury

pollution, shown in Figure 1.3.1 are the ten largest sectors and processes that generate mercury waste.

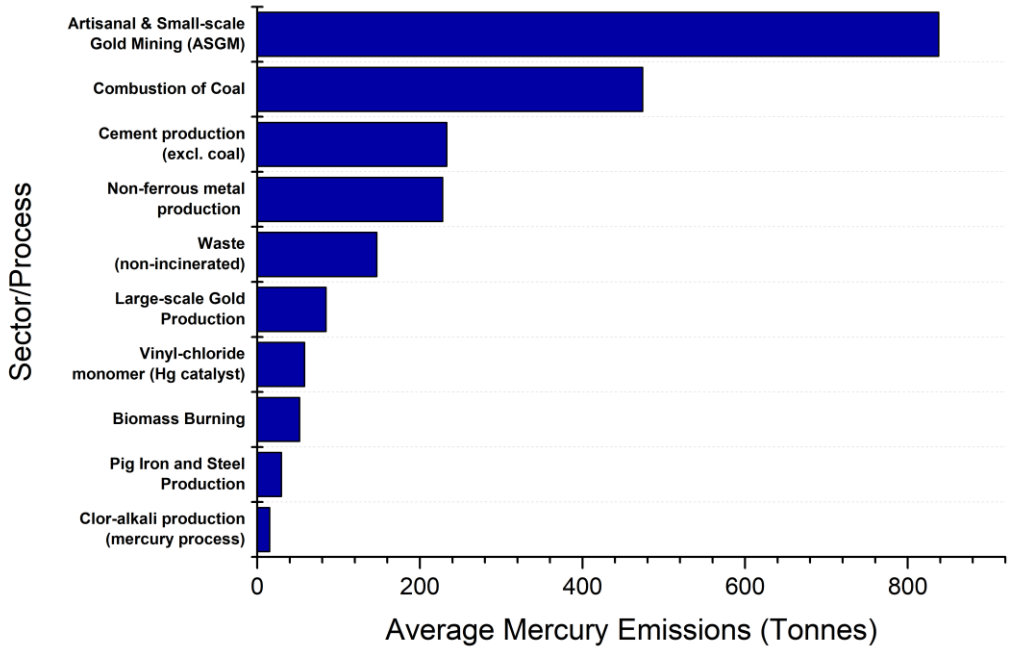

Figure 1.3.1 Ten largest sources of anthropogenic mercury pollution. Adapted from[40]

ASGM is the single largest producer of anthropogenic mercury pollution, which uses elemental mercury as a lixiviant in the extraction of gold. It is thought that between 400 to 1400 tonnes of mercury are released into the environment each year through ASGM activities, accounting for almost 40% of global mercury pollution.[41]

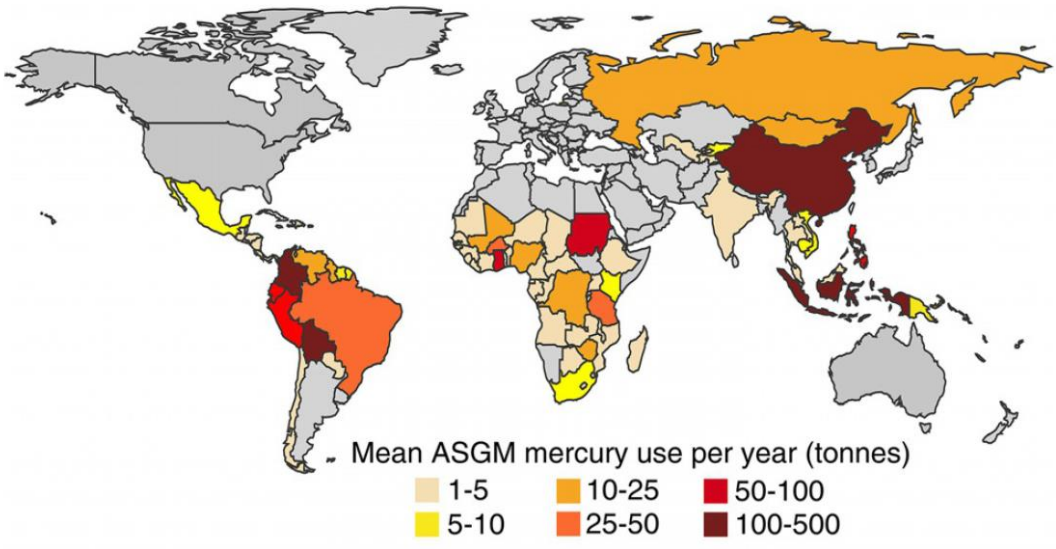

Figure 1.3.2 Map of global mercury usage for ASGM activities, reproduced from[42]

ASGM is an extremely prevalent activity, employing an estimated 10 to 20 million miners predominately working in South America, Africa and Asia.[41, 43, 44] However it is difficult to accurately estimate the number of miners due to the unlicensed and unregulated nature of ASGM. Large quantities of mercury are lost in the extraction and recovery process, with between 50 and 5000 mg of mercury present in a kilogram of tailings produced.[43, 45] Even after the extraction process, the gold isolated typically contains 5% residual mercury by mass due to amalgamation.[46] To recover as much gold as possible, the ASGM industry usually treats the gold tailings with cyanide containing compounds to extract up to 90% of the residual gold.[47] However in doing so, the cyanide also complexes with mercury forming highly soluble mercury species that can readily enter the environment through waste streams.[45] This increased mobility allows these highly toxic mercury containing species to be more readily methylated by bacteria and therefore increases the bioaccumulation of methylmercury.[47]

In ASGM communities there is an even greater risk of mercury exposure, by either organic or inorganic mercury, due to the high levels of mercury that can accumulate in food and water supplies.[37, 48] In children and developing

foetuses exposure to mercury is extremely life threatening and can lead to the increased likelihood of physical and neurological deformities occurring and can lower IQ.[49-51] Acute exposure to mercury in adults, especially from mercury vapour, can cause tremors, memory loss and other neurological symptoms such as psychosis, respiratory distresses and ultimately death.[52, 53] Exposure to methylmercury is also extremely harmful as it is highly nephrotoxic and can damage the Central Nervous System (CNS) leading to nerve, brain damage and in worse cases death.[37] Second only to ASGM, the burning of coal (other fossil fuels such as oil do contain trace amounts of mercury) contributes almost 500 tonnes on average to the global mercury problem. The problem is multifaceted with the generation of elemental mercury, Hg^{2+} species and mercury bound to particulate matter all being produced in the combustion cycle.[54] In more developed countries, methods to ameliorate the flue gasses released from the burning of coal in power stations and other large scale applications has led to the development of emission control equipment such as Electrostatic Precipitators (ESP), Flue Gas Desulfurisation (FGD) and Fabric Filters (FF).[55] It has been reported that the average mercury content present in coal is in the range of 0.1 to 0.15 mg Kg^{-1},[56] and that concentration of mercury in flue gasses can vary between 1 to 20 μg m^3.[57] Despite the use of technologies such as ESP and FF (FGD is more limited in its usefulness in controlling mercury emissions), the amount of mercury species removed from the flue gasses and particulates varies widely depending upon the type and quality of the coal burnt.[58] Under favourable conditions emission control equipment can scrub 98% of the mercury generated from the combustion of coal, however if the poorest quality of coal is used (lignite forms) this can be reduced to 0% in certain instances as shown in Table 1.3.1.[59]

Table 1.3.1 Average mercury capture by coal type and emission control configuration. Adapted from[59]

Emission Control Equipment configuration	Average percentage of Hg captured from various coal types (%)		
	Bituminous	Subbituminous	Lignite
FF	90	72	N/A
PS	N/A	9	N/A
CS-ESP	36	3	-4
HS-ESP	9	6	N/A
SDA + ESP	N/A	35	N/A
SDA +FF	98	24	0
SDA + FF +SCR	98	N/A	N/A
FF + wet FGD	98	N/A	N/A
PS + wet FGD	12	-8	33
CS-ESP + wet FGD	74	29	44
HS-ESP + wet FGD	50	29	N/A

CS-ESP = Cold Side-ESP, HS-ESP = Hot Side-ESP, PS = Particulate Scrubber, SDA = Spray Dryer Adsorber, SCR = Selective Catalytic Reduction

1.3.2 LEAD, CHROMIUM AND OTHER METALS

Despite the attempts at reducing the amount of lead released into the environment, for example replacing leaded petrol with unleaded substitutes, lead pollution is a continuing problem with lead still required in many processes and previous sources of lead contamination, (such as ceramic factories, lead paint and leaded pipework) all contributing to water and soil contamination.[60, 61] Even when activities causing the release of lead into the environment have ceased, such as in the case of leaded petrol and former lead mines, high levels of lead can be detected in the surrounding environment.[62, 63] Despite the known detrimental effects on health caused by lead toxicity, some industries, including those in the smelting and electronic waste recycling

sectors, still produce excessive amounts of lead waste that is easily transported into the local environment contaminating houses and other premises, water sources and soil.[64, 65]

Chronic exposure to lead in adults can lead to a multitude of health problems, including but not limited to renal failure, cardiovascular disease, hypertension and stokes. In children the effects of lead toxicity are even more troubling, with only low levels of lead present in blood required to cause neurodevelopmental toxicity which can cause long-term neurological damage, especially with repeated exposure.[66, 67] Additionally due to lead readily binding to sulfhydryl groups in proteins, it can readily attack the CNS by distorting the structural proteins and enzymes.[68]

First row transition metals such as iron, copper, chromium, nickel and manganese, are all vital trace elements found in the body. However in larger doses and in specific forms these metals can be acutely toxic to humans and other organisms.[69-72] Of the first row transition metals, chromium especially in its hexavalent state is probably regarded as the most toxic although both nickel and manganese compounds can be equally as toxic, if less well known.

Chromium is typically found in its trivalent state (III) which is its most stable form, however it may also be found in its hexavalent form (VI) which is an extremely powerful oxidising agent. Trivalent chromium is an important trace metal for the human body as it is used in the metabolism of insulin. In industry, chromium complexes in a variety of oxidation states are used for a multitude of applications including tanning of leather (III), corrosion resistance (VI), cleaning solutions (VI) and in colour pigments (III and VI).[73] Trivalent chromium compounds are poorly absorbed by the body but have a lower toxicity compared to hexavalent species. Hexavalent chromium, is a known carcinogen when inhaled and therefore the mostly likely route of exposure to humans is via occupational exposure routes.[74] Unfortunately due

to the wide variety of uses for hexavalent chromium compounds, they can easily contaminate groundwater and soil located near industry leading to the pollution of local water courses and therefore exposure to hexavalent chromium form oral routes is also possible.

Manganese and nickel complexes are employed widely, for their uses in metal alloys, electrochemical products and in corrosion resistance. Exposure to manganese complexes are usually from occupational sources but can occur from contaminated produce and from polluted water sources. Manganese is readily absorbed by the body through oral and inhalation routes and once exposed to a high concentration, symptoms similar to Parkinson's disease have been noted.[75] Similarly exposure to nickel in toxic concentrations usually occurs via occupation routes, although contaminated soils, groundwater and industrial vapours can all lead to increased exposure to the general populace. In lower doses nickel can cause allergic reactions such as contact dermatitis, however occupational workers who handle nickel compounds have been found to have an increased risk of upper respiratory tract cancers due to inhalation of nickel or nickel compounds in their workplaces.[76]

Precious metals such as gold and palladium are becoming an increasing problem also. As discussed previously in 1.3.1 the extraction of gold has led to devastating mercury pollution. Similarly palladium is an extremely valuable noble metal predominantly used as a catalyst in various organic reactions, and due to its high cost its recovery from chemical waste streams is desirable for industry.[77, 78] Due to its versatility as a catalyst, palladium along with other precious metals can be found in catalytic converters. Research conducted by Barbante *et al.* has found that palladium is now being leached into the environment via the exhaust gasses it is catalysing.[79]

1.3.3 CURRENT METHODS OF REMEDIATION

One of the most common sorbents used by itself or as a scaffold for advanced materials is activated carbon (AC). AC has several advantages, however the two most important being that it is thermally stable at high temperatures and can be generated from renewable sources.[80, 81] The high thermal stability means that AC can be used in waste gas / thermal desorption systems, as shown by Chang *et al.*,[82] as well as aqueous ones. Additionally, AC can be pre-treated with chemicals to improve its absorptivity and selectivity, as shown in Nelson's patent.[83]

Other popular porous materials investigated are zeolites. Zeolites can be either naturally occurring or synthetic, with both containing regular repeating crystal structures. Although natural zeolites are not as uniform as their synthetic counterparts, the overall uniformity with respect to porosity is a significant advantage over AC. Chojnacki *et al.* studied naturally occurring clinoptilolite zeolites for their potential as sorbents for mercury from effluent streams.[84] It was reported that the natural zeolites had good mercury absorption properties and the uptake was relatively quick, with an equilibrium reached after only 15 minutes. As with AC, zeolites can be pre-treated with chemicals to achieve better selectivity and absorptivity as reported by Morency.[85]

There are other novel materials that have been demonstrated to have mercury remediation properties. One such novel group of materials are temperature responsive biopolymers, which have been reported by Kostal *et al.* as having suitable mercury uptake for low-level mercury waste in aqueous conditions.[86] These polymers have the advantage that they can undergo thermal precipitation at different temperatures, meaning that they can be reused to trap mercury. Another possible way to remove mercury from aqueous systems is to use a chelating ligand, such as 1,3-benzenediamidoethanethiolate

(BDET) as reported by Blue *et al.*[87] BDET (Figure 1.3.3), has been shown to successfully bind with mercury and reduce the concentration of mercury in solution to below that of the detection limit of ICP-OES, approximately 0.05 ppb.

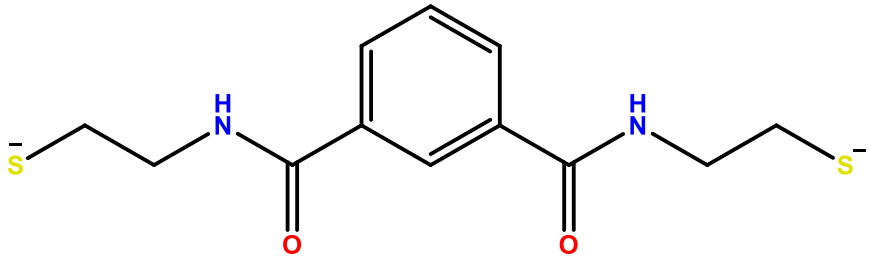

Figure 1.3.3 Structure of BDET

It has been reported by Guedron *et al.* that it is possible to use calcium hydroxide as a simple flocculant to treat gold mining tailing ponds.[88] The calcium hydroxide flocculant can aid in the reduction or even possibly prevent the methylation of waste mercury by causing the suspended particles of inorganic mercury to flocculate and therefore facilitate easier removal before methylation can occur.

1.4 APPLICATIONS FOR INVERSE VULCANISED POLYMERS

1.4.1 BATTERIES

With the ever increasing demand for increased electrical generation to support our technologically driven society, there is a clear and rapidly developing need for research into methods of supporting sustainable energy generation and its storage.[89, 90] Both lithium and sodium can be combined with sulfur to form batteries having enhanced properties when compared with pre-existing battery materials, the research into these alternatives starting in the 1960s.[91] From the middle of the twentieth century research into sodium – sulphur (Na-S) batteries increased due to their potentially high power density and

cyclability, making these batteries potentially desirable for industrial applications.[92, 93] However due to issues arising from early Na-S batteries, namely the high operating temperature and the potential to catch fire if the cell was breached and the inner components exposed to air or water, research and popularity stagnated whilst alternatives were sought. Despite these issues research continued and recently there has been a renewed interest in Na-S batteries due to advancements in available materials and chemical understanding.[94]

Lithium-sulfur (Li-S) batteries have an operating voltage range of 2.1 Volts and a theoretical capacity of 1675 mAh^{-1} per gram of material, potentially making these batteries safer, smaller and cheaper than currently available commercial batteries. However, by replacing the positive electrode currently available in lithium ion batteries with sulfur, the battery lifecycle is decreased to approximately 200 cycles.[91, 95, 96] Despite this limitation, Li-S batteries have a far higher theoretical energy density and specific energy compared to traditional lithium ion batteries.[91, 96] One of the main issues surrounding the implementation of Li-S batteries is the general instability of the sulfur cathode under cycling conditions, due to the formation of polysulfides. These polysulfides reduce the coulombic efficiency of the battery, leading to a large decrease in capacity.[95] One potential method to help stabilise the sulfur cathode, is to use an inverse vulcanised polymer.[3]

In using an inverse vulcanised sulfur - DIB (S-DIB) copolymer as the cathodic material for a Li-S battery, Pyun *et al.* reported an almost fivefold increase in the capacity *versus* a traditional lithium ion battery. Although this remarkable capacity was at the expense of the battery's cycle life, which was much reduced compared with lithium ion batteries.[3] This can be rectified however, by introducing 1,3-diethynylbenzene or 1,4-diphenylbutadiyne as an additional monomer, in the synthesis process.[97, 98] The use of 1,4-diphenylbutadiyne in

the sulfur copolymer leads to a cathode with a specific capacity of 800 mAh per gram of material and a cycle life of approximately 300.[99] Similarly Park *et al.* have reported an organosulfur based cathode for use in Li-S batteries that can achieve 99% coulombic efficiency over 450 cycles with a capacity of 850 mAh^{-1} per gram.[100] It has been reported by Dirlam *et al.* that it is possible to produce a battery with capacities nearing 1000 mAh^{-1} per gram using inverse vulcanised sulfur polymers for the cathode material.[97] It is hypothesised that the improvement in performance noted in Li-S batteries using inverse vulcanised sulfur polymers for the cathodic material is due in part to the stability of the sulfur in the cathode and therefore the sulfur polymer reduces lithium sulfide formation.[25]

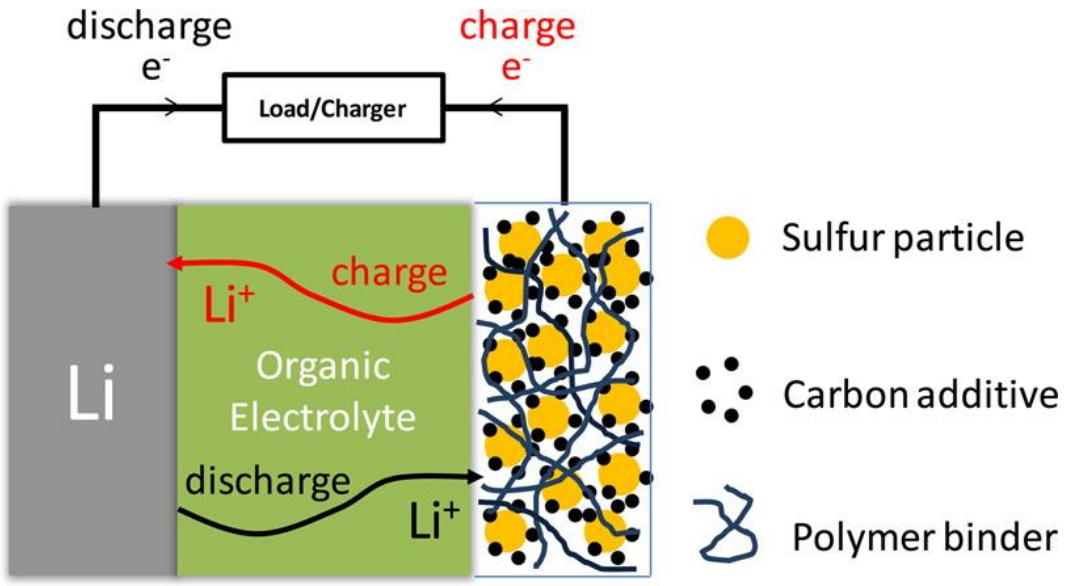

Figure 1.4.1: Diagrammatic illustration of Li-S cell, reproduced from[101]

1.4.2 OPTICAL

To increase the optical properties of a polymeric material (*eg* to increase its refractive index) sulfur can be incorporated into the structure of the material replacing part of the polymer's backbone or as additional units from the backbone itself.[102] Pyun *et al.* have successfully shown that high sulfur content inverse vulcanised polymers are highly transparent to infrared radiation,

despite their red colour under ambient light conditions, and possess refractive indices (n) that are extremely high for polymeric materials ($n > 1.80$).[103]

Due to the reversibility of sulfur-sulfur bonds, certain inverse-vulcanised polymers can exhibit vitrimeric properties. If optical lenses were synthesised from one of these materials, then any physical surface damage could be repaired by simply reheating and reshaping the lens back to its original shape and structure.[103, 104] Work by Bear *et al.* has shown that it is possible to incorporate a myriad of nanoparticles into S-DIB copolymers; nanoparticles incorporated included quantum dots, iron oxide and gold.[105] It should be noted that the colour of the S-DIB copolymer varied slightly depending on the nanoparticle incorporated into its structure, but the wavelength absorption data showed a marked change between the different inverse vulcanised nanocomposite materials (Figure 1.4.2).

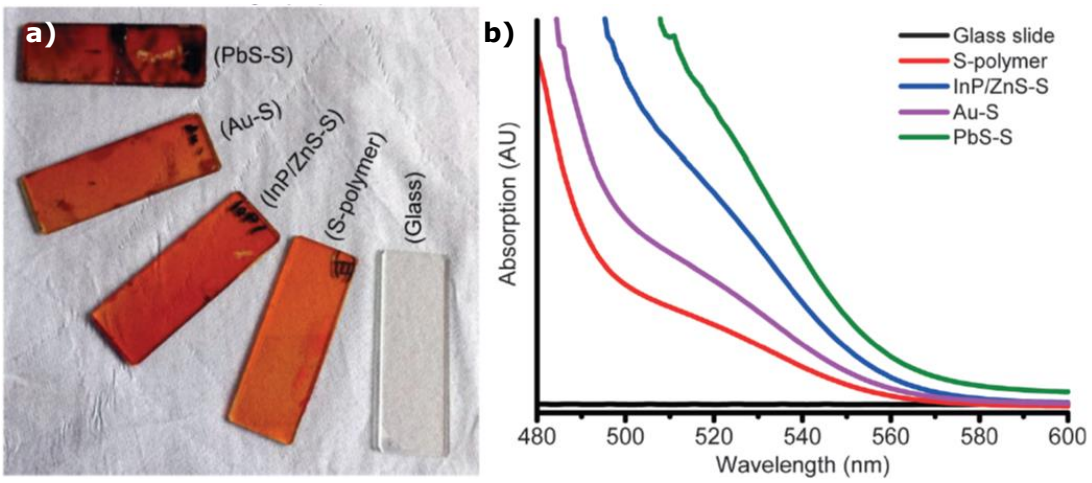

Figure 1.4.2 a) S-DIB nanocomposites compared to glass, b) wavelength absorption data, reproduced from[105]

1.4.3 HEAVY METAL REMEDIATION

Despite the field of inverse vulcanised polymers being relatively young, there have been a small number of papers published relating to the ability of sulfur copolymers in the remediation of mercury, in the form of mercury chloride,

from aqueous solutions. It is interesting to note the almost polar opposite methods of tackling this problem.

The research published by Chalker *et al.* focused heavily on the green and sustainable properties of inverse vulcanised polymers by using the renewable crosslinkers, limonene and canola oil.[29, 106] The advantage of using these inexpensive crosslinkers is that it helps keep the total costs of producing large quantities low, potentially making these materials readily available globally. However these cheap crosslinkers do have a detrimental effect on the physical properties of the polymers, with respect to issues such as shape persistence and lower glass transition temperatures compared to S-DIB. Both polymers exhibit good specificity towards mercury and remediate the majority of mercury present in test solutions over a 24 hour period. Additionally in the case of S-LIM, the polymer is also self-indicating for mercury as it changes colour from dark brown to yellow, as shown in Figure 1.4.3.

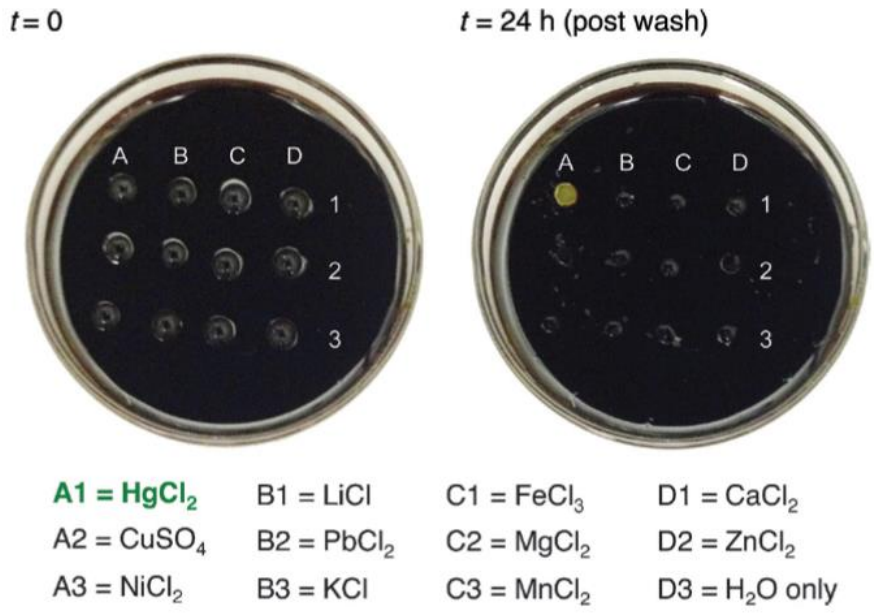

Figure 1.4.3 S-LIM polysulfide at t=0 and at t=24 hours after exposure to metal solutions. Note A1 exhibiting a colour change after exposure to $HgCl_2$, reproduced from[29]

In contrast to these extremely cheap, although low capacity sulfur polymers Theato *et al.* focused on improving the performance of the already published S-DIB by electrospinning the polymer into fibres.[107] By electrospinning S-DIB into fibres, the surface area per gram of polymer used is rapidly increased and therefore there is a greater inherent ability to adsorb mercury. A capacity of 440 mg g^{-1} has been reported for these electrospun fibres, with an uptake of approximately 98% of mercury from solution happening within minutes. However the process of electrospinning is not cheap, as it requires additional solvents and high voltages, and is a batch process. These reasons coupled with the relatively expensive crosslinker used (DIB), means these sulfur copolymer fibres have a limited utility for mercury remediation as the primary driving force is the price per gram of material used.

1.5 PROJECT OVERVIEW AND AIMS

The main aim of this research is to synthesise and develop a library of novel inorganic functional materials, whose composition comprises a majority of elemental sulfur with crosslinking agents that are either renewable bio-derived compounds or by-products from industry. These materials must meet the demanding requirement of good physical properties *versus* affordability for industry to adopt them in sufficient quantities to begin to overcome the excess sulfur problem. This necessitates a material which is shape persistent, chemically stable and with the ability to either be coated onto a solid support or have porosity induced into the copolymer in order to sufficiently increase the surface area to make it a suitable sorbent material for the remediation of mercury and other metals.

1.6 REFERENCES

1. A. A. Yaroshevsky, *Geochemistry International*, 2006, **44**, 48-55.
2. H.-F. Graf, J. Feichter and B. Langmann, *Journal of Geophysical Research: Atmospheres*, 1997, **102**, 10727-10738.
3. W. J. Chung, J. J. Griebel, E. T. Kim, H. Yoon, A. G. Simmonds, H. J. Ji, P. T. Dirlam, R. S. Glass, J. J. Wie, N. A. Nguyen, B. W. Guralnick, J. Park, Á. Somogyi, P. Theato, M. E. Mackay, Y.-E. Sung, K. Char and J. Pyun, *Nat Chem*, 2013, **5**, 518-524.
4. G. Kutney, *Sulfur : history, technology, applications & industry*, Toronto : ChemTec Publishing, 2013. Second edition., 2013.
5. J. A. Ober, *Materials flow of sulfur*, US Geological Survey, Reston, Va, 2003.
6. H. Frasch, *US Patent*, No. US 461431 A, 1891.
7. T. L. Brown, *Chemistry : The Central Science*, Prentice Hall, Upper Saddle River, N.J. ;, 9th ed. edn., 2003.
8. L. E. Apodaca, *Mineral Commodity Summaries: Sulfur*, U.S. Geological Survey, 2015.
9. A. Eisenberg and A. V. Tobolsky, *Journal of Polymer Science*, 1960, **46**, 19-28.
10. A. V. Tobolsky, *Journal of Polymer Science Part C: Polymer Symposia*, 1966, **12**, 71-78.
11. J. Chiu, *Analytical Chemistry*, 1963, **35**, 933-934.
12. G. W. Miller, *Journal of Applied Polymer Science*, 1971, **15**, 1985-1994.
13. B. R. Currell and A. J. Williams, *Thermochimica Acta*, 1974, **9**, 255-259.
14. G. Gee, *Transactions of the Faraday Society*, 1952, **48**, 515-526.
15. A. V. Tobolsky, *Journal of Polymer Science*, 1957, **25**, 220-221.
16. B. Meyer, T. V. Oommen and D. Jensen, *The Journal of Physical Chemistry*, 1971, **75**, 912-917.
17. B. Meyer, *Chemical Reviews*, 1976, **76**, 367-388.
18. J. Lim, J. Pyun and K. Char, *Angewandte Chemie International Edition*, 2015, **54**, 3249-3258.

19. S. Ramarad, M. Khalid, C. T. Ratnam, A. L. Chuah and W. Rashmi, *Progress in Materials Science*, 2015, **72**, 100-140.

20. M. Mochulsky and A. V. Tobolsky, *Industrial & Engineering Chemistry*, 1948, **40**, 2155-2163.

21. D. Katz and A. V. Tobolsky, *Journal of Polymer Science Part A: General Papers*, 1964, **2**, 1595-1605.

22. S. L. Cooper and A. V. Tobolsky, *Journal of Applied Polymer Science*, 1967, **11**, 1361-1369.

23. A. V. Tobolsky, P. F. Lyons and N. Hata, *Macromolecules*, 1968, **1**, 515-519.

24. W. J. Chung, J. J. Griebel, E. T. Kim, H. Yoon, A. G. Simmonds, H. J. Ji, P. T. Dirlam, R. S. Glass, J. J. Wie, N. A. Nguyen, B. W. Guralnick, J. Park, SomogyiÁrpád, P. Theato, M. E. Mackay, Y.-E. Sung, K. Char and J. Pyun, *Nat Chem*, 2013, **5**, 518-524.

25. J. J. Griebel, R. S. Glass, K. Char and J. Pyun, *Progress in Polymer Science*, 2016, **58**, 90-125.

26. E. T. Kim, W. J. Chung, J. Lim, P. Johe, R. S. Glass, J. Pyun and K. Char, *Polymer Chemistry*, 2014, **5**, 3617-3623.

27. M. Arslan, B. Kiskan and Y. Yagci, *Macromolecules*, 2016, **49**, 767-773.

28. W. Li, X. Wu, Z. Zhao, A. Qin, R. Hu and B. Z. Tang, *Macromolecules*, 2015, **48**, 7747-7754.

29. M. P. Crockett, A. M. Evans, M. J. H. Worthington, I. S. Albuquerque, A. D. Slattery, C. T. Gibson, J. A. Campbell, D. A. Lewis, G. J. L. Bernardes and J. M. Chalker, *Angewandte Chemie International Edition*, 2015, **55**, 1714-1718.

30. H. Ishida and Y. Rodriguez, *Polymer*, 1995, **36**, 3151-3158.

31. J. A. Macko and H. Ishida, *Journal of Polymer Science Part B: Polymer Physics*, 2000, **38**, 2687-2701.

32. H.-D. Kim and H. Ishida, *Journal of Applied Polymer Science*, 2001, **79**, 1207-1219.

33. M. K. Salman, B. Karabay, L. C. Karabay and A. Cihaner, *Journal of Applied Polymer Science*, 2016, **133**.

34. I. Gomez, O. Leonet, J. A. Blazquez and D. Mecerreyes, *ChemSusChem*, 2016, **9**, 3419-3425.

35. A. Hoefling, D. T. Nguyen, Y. J. Lee, S.-W. Song and P. Theato, *Materials Chemistry Frontiers*, 2017, **1**, 1818-1822.

36. A. Hoefling, Y. J. Lee and P. Theato, *Macromolecular Chemistry and Physics*, 2017, **218**, 1600303.

37. P. B. Tchounwou, W. K. Ayensu, N. Ninashvili and D. Sutton, *Environmental Toxicology*, 2003, **18**, 149-175.

38. Q. Wang, D. Kim, D. D. Dionysiou, G. A. Sorial and D. Timberlake, *Environmental Pollution*, 2004, **131**, 323-336.

39. A. R. Hutchison and D. A. Atwood, *Journal of Chemical Crystallography*, 2003, **33**, 631-645.

40. U. N. E. Programme, *Global Mercury Assessment 2018*, United Nations Environment Programme, 2019.

41. J. Seccatore, M. Veiga, C. Origliasso, T. Marin and G. De Tomi, *Science of the Total Environment*, 2014, **496**, 662-667.

42. L. J. Esdaile and J. M. Chalker, *Chemistry – A European Journal*, 2018, **24**, 6905-6916.

43. P. Cordy, M. M. Veiga, I. Salih, S. Al-Saadi, S. Console, O. Garcia, L. A. Mesa, P. C. Velásquez-López and M. Roeser, *Science of the Total Environment*, 2011, **410-411**, 154-160.

44. M. M. Veiga and J. J. Hinton, *Natural Resources Forum*, 2002, **26**, 15-26.

45. M. M. Veiga, D. Nunes, B. Klein, J. A. Shandro, P. C. Velasquez and R. N. Sousa, *Journal of Cleaner Production*, 2009, **17**, 1373-1381.

46. P. Cordy, M. Veiga, B. Crawford, O. Garcia, V. Gonzalez, D. Moraga, M. Roeser and D. Wip, *Environmental Research*, 2013, **125**, 82-91.

47. M. M. Veiga, G. Angeloci, M. Hitch and P. Colon Velasquez-Lopez, *Journal of Cleaner Production*, 2014, **64**, 535-544.

48. H. Gibb and K. G. O'Leary, *Environmental Health Perspectives*, 2014, **122**, 667-672.

49. I. A. Brown and D. W. Austin, *Toxicological & Environmental Chemistry*, 2012, **94**, 1610-1627.

50. S. Bose-O'Reilly, B. Lettmeier, R. Matteucci Gothe, C. Beinhoff, U. Siebert and G. Drasch, *Environmental Research*, 2008, **107**, 89-97.

51. D. C. Bellinger, K. O'Leary, H. Rainis and H. J. Gibb, *Environmental Research*, 2016, **147**, 159-163.

52. S. Bose-O'Reilly, R. Schierl, D. Nowak, U. Siebert, J. F. William, F. T. Owi and Y. I. Ir, *Environmental Research*, 2016, **149**, 274-281.

53. M. T. Solis, E. Yuen, P. S. Cortez and P. J. Goebel, *The American Journal of Emergency Medicine*, 2000, **18**, 599-602.

54. A. Kolker, C. L. Senior and J. C. Quick, *Applied Geochemistry*, 2006, **21**, 1821-1836.

55. M. Rallo, M. A. Lopez-Anton, M. L. Contreras and M. M. Maroto-Valer, *Environmental Science and Pollution Research*, 2012, **19**, 1084-1096.

56. S. H. Lee, Y. J. Rhim, S. P. Cho and J. I. Baek, *Fuel*, 2006, **85**, 219-226.

57. B. Wu, T. W. Peterson, F. Shadman, C. L. Senior, J. R. Morency, F. E. Huggins and G. P. Huffman, *Fuel Processing Technology*, 2000, **63**, 93-107.

58. P. Chu and D. B. Porcella, *Water, Air, and Soil Pollution*, 1995, **80**, 135-144.

59. H. Yang, Z. Xu, M. Fan, A. E. Bland and R. R. Judkins, *Journal of Hazardous materials*, 2007, **146**, 1-11.

60. D. A. Gidlow, *Occupational Medicine*, 2004, **54**, 76-81.

61. M. Vinceti, S. Rovesti, M. Bergomi, E. Calzolari, S. Candela, A. Campagna, M. Milan and G. Vivoli, *Science of the Total Environment*, 2001, **278**, 23-30.

62. I. Guagliardi, D. Cicchella, R. De Rosa and G. Buttafuoco, *Journal of Environmental Sciences*, 2015, **33**, 179-187.

63. J. A. Rodríguez Martín, C. Gutiérrez, M. Escuer, M. T. García-González, R. Campos-Herrera and N. Águila, *Science of the Total Environment*, 2014, **473-474**, 518-529.

64. A. L. Morrison, *Science of the Total Environment*, 2003, **303**, 125-138.

65. Q. Song and J. Li, *Environmental Pollution*, 2015, **196**, 450-461.

66. P. J. Landrigan, R. Fuller, N. J. R. Acosta, O. Adeyi, R. Arnold, N. Basu, A. B. Baldé, R. Bertollini, S. Bose-O'Reilly, J. I. Boufford, P. N. Breysse, T. Chiles, C. Mahidol, A. M. Coll-Seck, M. L. Cropper, J. Fobil, V. Fuster, M. Greenstone, A. Haines, D. Hanrahan, D. Hunter, M. Khare, A. Krupnick, B. Lanphear, B. Lohani, K. Martin, K. V. Mathiasen, M. A. McTeer, C. J. L. Murray, J. D. Ndahimananjara, F. Perera, J. Potočnik, A. S. Preker, J. Ramesh, J. Rockström, C. Salinas, L. D. Samson, K. Sandilya, P. D. Sly, K. R. Smith, A. Steiner, R. B. Stewart, W. A. Suk, O. C. P. van Schayck, G. N. Yadama, K. Yumkella and M. Zhong, *The Lancet*, 2018, **391**, 462-512.

67. K. C. Staudinger and V. S. Roth, *Am Fam Physician*, 1998, **57**, 719-726, 731-712.

68. H. Needleman, *Annual Review of Medicine*, 2004, **55**, 209-222.

69. E. R. Alt, I. Sternlieb and S. Goldfischer, in *International Review of Experimental Pathology*, eds. G. W. Richter and K. I. M. Solez, Academic Press, 1990, vol. 31, pp. 165-188.

70. D. R. Winge and R. K. Mehra, in *International Review of Experimental Pathology*, eds. G. W. Richter and K. I. M. Solez, Academic Press, 1990, vol. 31, pp. 47-83.

71. P. Aisen, G. Cohen and J. O. Kang, in *International Review of Experimental Pathology*, eds. G. W. Richter and K. I. M. Solez, Academic Press, 1990, vol. 31, pp. 1-46.

72. J. A. Alcedo and K. E. Wetterhahn, in *International Review of Experimental Pathology*, eds. G. W. Richter and K. I. M. Solez, Academic Press, 1990, vol. 31, pp. 85-108.

73. D. G. Barceloux and D. Barceloux, *Journal of Toxicology: Clinical Toxicology*, 1999, **37**, 173-194.

74. H. Sun, J. Brocato and M. Costa, *Current Environmental Health Reports*, 2015, **2**, 295-303.

75. S. L. O'Neal and W. Zheng, *Current Environmental Health Reports*, 2015, **2**, 315-328.

76. D. Schaumlöffel, *Journal of Trace Elements in Medicine and Biology*, 2012, **26**, 1-6.

77. K. C. Nicolaou, P. G. Bulger and D. Sarlah, *Angewandte Chemie International Edition*, 2005, **44**, 4442-4489.

78. C. Torborg and M. Beller, *Advanced Synthesis & Catalysis*, 2009, **351**, 3027-3043.

79. C. Barbante, A. Veysseyre, C. Ferrari, K. Van De Velde, C. Morel, G. Capodaglio, P. Cescon, G. Scarponi and C. Boutron, *Environmental Science & Technology*, 2001, **35**, 835-839.

80. Suhas, P. J. M. Carrott and M. M. L. Ribeiro Carrott, *Bioresource Technology*, 2007, **98**, 2301-2312.

81. F.-S. Zhang, J. O. Nriagu and H. Itoh, *Water Research*, 2005, **39**, 389-395.

82. T. C. Chang and J. H. Yen, *Journal of Hazardous materials*, 2006, **128**, 208-217.

83. S. G. Nelson, *US Patent*, No. US 6953494 B2, 2005.

84. A. Chojnacki, K. Chojnacka, J. Hoffmann and H. Górecki, *Minerals Engineering*, 2004, **17**, 933-937.

85. J. Morency, *Filtration & Separation*, 2002, **39**, 24-26.

86. J. Kostal, A. Mulchandani, K. E. Gropp and W. Chen, *Environmental Science & Technology*, 2003, **37**, 4457-4462.

87. L. Y. Blue, M. A. Van Aelstyn, M. Matlock and D. A. Atwood, *Water Research*, 2008, **42**, 2025-2028.

88. S. Guedron, D. Cossa, M. Grimaldi and L. Charlet, *Applied Geochemistry*, 2011, **26**, 222-229.

89. S. Chu and A. Majumdar, *Nature*, 2012, **488**, 294.

90. M. Armand and J. M. Tarascon, *Nature*, 2008, **451**, 652.

91. X. Ji and L. F. Nazar, *Journal of Materials Chemistry*, 2010, **20**, 9821-9826.

92. J. L. Sudworth, *Journal of Power Sources*, 1984, **11**, 143-154.

93. J. T. Kummer and N. Weber, 1967.

94. T. Oshima, M. Kajita and A. Okuno, *International Journal of Applied Ceramic Technology*, 2004, **1**, 269-276.

95. Y.-S. Su and A. Manthiram, *Nature Communications*, 2012, **3**, 1166.

96. M.-K. Song, E. J. Cairns and Y. Zhang, *Nanoscale*, 2013, **5**, 2186-2204.

97. P. T. Dirlam, A. G. Simmonds, R. C. Shallcross, K. J. Arrington, W. J. Chung, J. J. Griebel, L. J. Hill, R. S. Glass, K. Char and J. Pyun, *ACS Macro Letters*, 2015, **4**, 111-114.

98. Z. Sun, M. Xiao, S. Wang, D. Han, S. Song, G. Chen and Y. Meng, *Journal of Materials Chemistry A*, 2014, **2**, 9280-9286.

99. P. T. Dirlam, A. G. Simmonds, T. S. Kleine, N. A. Nguyen, L. E. Anderson, A. O. Klever, A. Florian, P. J. Costanzo, P. Theato, M. E. Mackay, R. S. Glass, K. Char and J. Pyun, *RSC Advances*, 2015, **5**, 24718-24722.

100. H. Kim, J. Lee, H. Ahn, O. Kim and M. J. Park, *Nature Communications*, 2015, **6**, 7278.

101. A. Manthiram, Y. Fu, S.-H. Chung, C. Zu and Y.-S. Su, *Chemical Reviews*, 2014, **114**, 11751-11787.

102. T. Higashihara and M. Ueda, *Macromolecules*, 2015, **48**, 1915-1929.

103. J. J. Griebel, S. Namnabat, E. T. Kim, R. Himmelhuber, D. H. Moronta, W. J. Chung, A. G. Simmonds, K.-J. Kim, J. van der Laan, N. A. Nguyen, E. L. Dereniak, M. E. Mackay, K. Char, R. S. Glass, R. A. Norwood and J. Pyun, *Advanced Materials*, 2014, **26**, 3014-3018.

104. J. J. Griebel, N. A. Nguyen, S. Namnabat, L. E. Anderson, R. S. Glass, R. A. Norwood, M. E. Mackay, K. Char and J. Pyun, *ACS Macro Letters*, 2015, **4**, 862-866.

105. J. C. Bear, W. J. Peveler, P. D. McNaughter, I. P. Parkin, P. O'Brien and C. W. Dunnill, *Chemical Communications*, 2015, **51**, 10467-10470.

106. M. J. H. Worthington, R. L. Kucera, I. S. Albuquerque, C. T. Gibson, A. Sibley, A. D. Slattery, J. A. Campbell, S. F. K. Alboaiji, K. A. Muller, J. Young, N. Adamson, J. R. Gascooke, D. Jampaiah, Y. M. Sabri, S. K. Bhargava, S. J. Ippolito, D. A. Lewis, J. S. Quinton, A. V. Ellis, A. Johs, G. J. L. Bernardes and J. M. Chalker, *Chemistry – A European Journal*, 2017, **23**, 16219-16230.

107. M. W. Thielke, L. A. Bultema, D. D. Brauer, B. Richter, M. Fischer and P. Theato, *Polymers*, 2016, **8**, 266.

CHAPTER 2: CYCLICAL AND COMPLEX TERPENOID MIXTURES FOR CROSSLINKING

CONTENTS

2.1 INTRODUCTION

To meet the aims set out at the start of this PhD programme, it would be desirable to combine a bioderived or industrial waste by-product that contains multiple allylic units and sulfur to produce suitable sustainable inverse vulcanised polymers. One such family of naturally occurring compounds are terpenes, with over 50,000 naturally occurring terpene and terpenoid compounds reported.[1] They have been extensively studied for their suitability as precursors to sustainable polymeric materials.[2-6]

Terpenes are a unique series of compounds found in most living organisms comprising of isoprene "building blocks". The wide variety and complexity of terpenes biosynthesised in nature can vary from simple terpenes that are often volatile, and found in plant essential oils (imbuing plants with their distinct smell), through to much more complex molecules that are precursors to important bioactive compounds such as cholesterol.[7] The terpene family of compounds can be subdivided into several categories derived from the number of isoprene units present, as shown in Table 2.1.1.

Table 2.1.1 Classification of terpenes, adapted from[8]

Classification	Characteristics		
	Number of isoprene units	General formula	Example
Hemiterpenes	1	C_5H_8	Isoprene
Monoterpenes	2	$C_{10}H_{16}$	Limonene
Sesquiterpenes	3	$C_{15}H_{24}$	Farnesene
Diterpenes	4	$C_{20}H_{32}$	Retinol (Vitamin A1)
Sesterterpenes	5	$C_{25}H_{40}$	Moenocinol
Triterpenes	6	$C_{30}H_{48}$	Squalene

This chapter will briefly discus the previously reported crosslinkers for inverse vulcanisation and initial reactions with cyclical crosslinking agents before discussing in more detail three bioderived and one industrial by-product crosslinking agents, their synthesis and subsequent analysis.

2.2 PRELIMINARY WORK

2.2.1 PREVIOUSLY REPORTED CROSSLINKERS

In order to achieve a better understanding of how sulfur reacts and interacts with allylic containing compounds it was decided that model reactions using the previously reported diisopropenyl benzene and limonene crosslinkers should be undertaken.[9, 10]

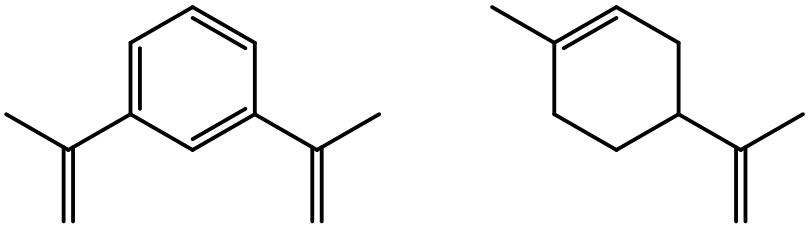

Figure 2.2.1 Previously reported crosslinkers for the synthesis of inverse vulcanised sulfur polymers

Although both crosslinkers successfully reacted with sulfur to form inverse vulcanised polymers, the synthetic methods employed were very different. The synthesis of S-DIB from sulfur and DIB, followed a more traditional "one pot" method in which sulfur was heated until molten and combined with DIB under constant agitation and a reaction temperature of 185 °C. The reaction then rapidly proceeded to a homogenous ruby red solution, at which point it was transferred to an oven and cured at 140 °C overnight. The reaction between sulfur and limonene was markedly different, with the reaction mostly being conducted *in vacuo* and at a temperature of 170 °C. The resultant product was a waxy brown solid of low molecular weight, for a polymeric

material, and suffered from poor shape persistence. The use of vacuum during the synthesis of S-LIM inverse vulcanised polymers, allowed for the removal of both unwanted by-products and low molecular weight polysulfides and thiols that could act as plasticisers in the resultant polymer. Additionally it cannot be overlooked that the addition of a negative pressure in the reaction flask helped to drive the reaction forward to a suitable end point. This is supported by the research published by Wu *et al*. that showed that a S-LIM reaction took 20 hours to solidify without the addition of vaccum or catalyst.[11]

2.2.2 INITIAL REACTIONS WITH CYCLICAL CROSSLINKERS

The first two potential crosslinking agents to be considered were triallyl cyanurate (TAC) and 1,3,5,7-tetravinyl 1,3,5,7-tetramethylcyclotetrasiloxane (TVTCSi), in part due to the multiple alkenyl groups present and their low cost. TAC has been an extensively researched compound, with research going as far back as the late 50s and early 60s into its ability to polymerise and crosslink with other compounds to form usable materials.[12-15] TVTCSi has previously been reported for use in various composite materials, including polymeric films and membranes.[16-18]

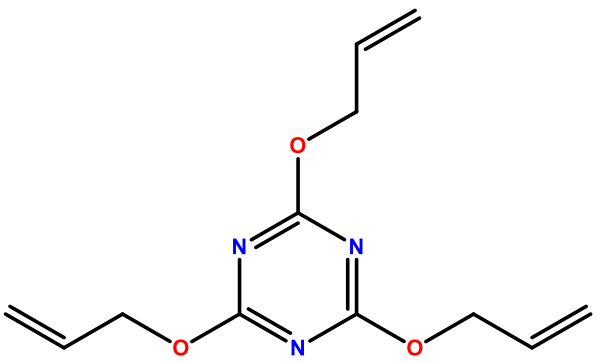

Triallyl cyanurate (TAC)

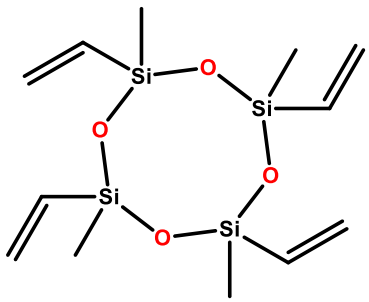

1,3,5,7-Tetravinyl 1,3,5,7-tetramethylcyclotetrasiloxane (TVTCSi)

Figure 2.2.2 Chemical structures of TAC and TVTCSi

Both TAC and TVTCSi are liquids at low temperatures (≤ 40 °C) and therefore it was hoped that these crosslinkers would be somewhat miscible with molten elemental sulfur. Nevertheless, despite varying numerous reaction conditions including the time, temperature and ratio of crosslinker to sulfur all reactions yielded a yellow block of polymeric sulfur and the crosslinkers could be poured back out of the reaction flasks and recovered. The inability of the sulfur radical chains to successfully react with the allylic groups present in TAC and TVTCSi is likely attributed to the stabilising effect of the silicon and heteroatoms present in these molecules (Figure 2.2.2). The electron rich nature of these atoms in the crosslinkers essentially helps to stabilise the allylic bonds from radical attack.

Further work on these crosslinkers was not perused until the reaction between sulfur and TVTCSi was attempted again, this time using a catalytic method developed by other group members. In this study a series of first row transition metal containing complexes were screened to discern their catalytic activity, including metals in their pure, oxide, chloride and ligand forms.[11] This research showed that the optimum catalyst to use was zinc diethyldithiocarbamate, $Zn(DTC)_2$, with as little as 1 wt.% of catalysts added to the reaction mixture. Additionally by using $Zn(DTC)_2$ the reaction temperature can be reduced to 130 °C, almost 30 °C below the floor temperature of elemental sulfur. Shown in Scheme 2.2.1 is the proposed catalytic cycle that occurs during these reactions.

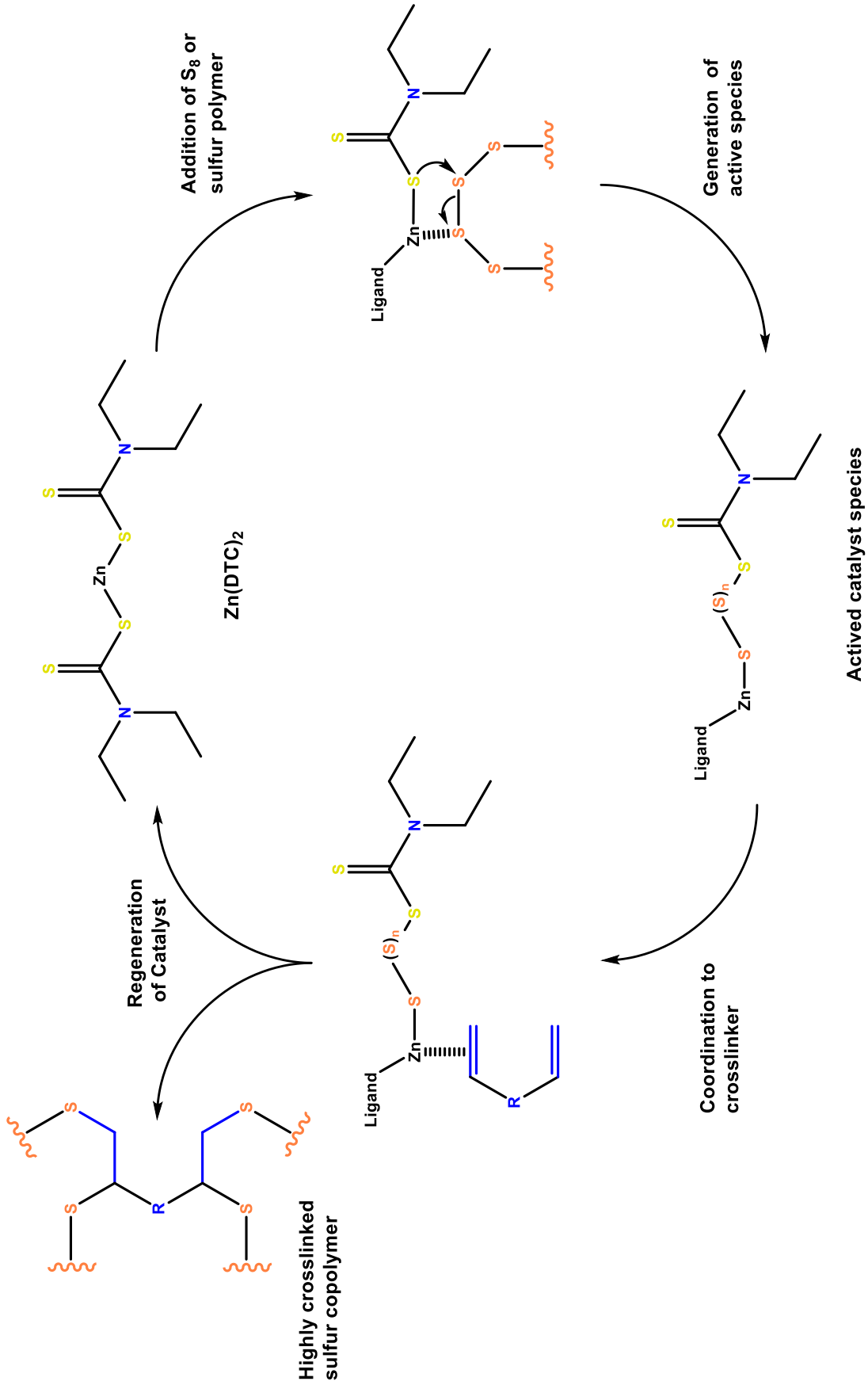

Scheme 2.2.1 Proposed catalytic cycle for the inverse vulcanisation of sulfur copolymers using $Zn(DTC)_2$. Adapted from[11]

2.3 CROSSLINKERS

2.3.1 DICYCLOPENTADIENE

A by-product from the steam cracking of naphtha, dicyclopenatdiene (DCPD) is produced in large quantities with industrial uses in resins, adhesives and rubber containing compounds.[19, 20] DCPD is also used as the precursor to much more commercially attractive cyclopentadiene, which is used in a host of chemical compounds including fine chemicals, fire retardants and pesticides.[21] Due to the allylic bonds and strained configuration, DCPD has been extensively studied as a potential crosslinking agent for various applications.[22-27]

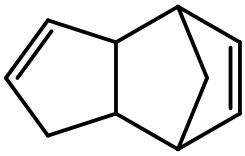

Dicyclopentadiene

Figure 2.3.1 Structure of dicyclopentadiene

2.3.2 PERILLYL ALCOHOL

Perillyl alcohol is a natural monocyclic terpene found in the essential oils of numerous plants, including but not limited to peppermint, lavender and sage.[28] It is a metabolite of limonene and is produced by plants via the mevalonate pathway, whereby limonene is hydroxylated by enzymes in the cytochrome P450 family.[29] Perillyl alcohol is a widely studied molecule with numerous potential uses, however it has been primarily studied for its reported anticancer properties.[30-33] Since cytochrome P450 enzymes are present in many naturally occurring organisms there have been several studies into the biotransformation of limonene into perillyl alcohol by utilising bioreactors coupled with cytochrome P450 modified bacteria, yeasts and

fungi.[34-36] Perillyl alcohol can also be synthetically manufactured in the laboratory, utilising limonene and a four step synthetic method, however the overall yield is less than 40%.[37]

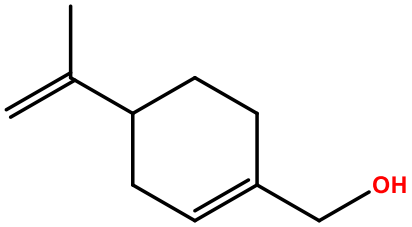

Perillyl alcohol

Figure 2.3.2 Structure of perillyl alcohol

2.3.3 PERILLARTINE

Known since the 1920s as a highly sweet compound, perillartine is reported to be 2000 times sweeter than sucrose.[38] Extracted from *Perilla frutesce*, a Perilla from the Lamiaceae family of flowering mint plants, perillartine is the oxime of perillaldehyde (itself a further metabolite of limonene and perillyl alcohol in the mevalonate pathway). Several studies have been conducted into the structure property relationship between perillartine (including its analogues and derivatives) and the mechanism of the basic taste, sweetness.[39, 40]

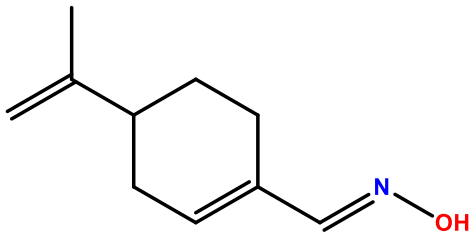

Perillartine

Figure 2.3.3 Structure of perillartine

2.3.4 HOP OIL

Hop oil is the essential oil extracted from the flower of *Humulus lupulus*, which is a perennial flowering species of Cannabaceae family (hemp family). Found

indigenously in several parts of the world, hops are used primarily in the brewing industry to impart aroma and taste to beers. Additionally hops have also been shown to possess preservative effects.[41] The major components found in the extracted essential oil are the terpenes, myrcene, humulene and caryophyllene (Figure 2.3.4).[42] The composition of hop essential oil can significantly differ between different batches of crops and plant varieties, with the humulene content potentially accounting for up to 40% of the total extractable amount of hop oil.[43]

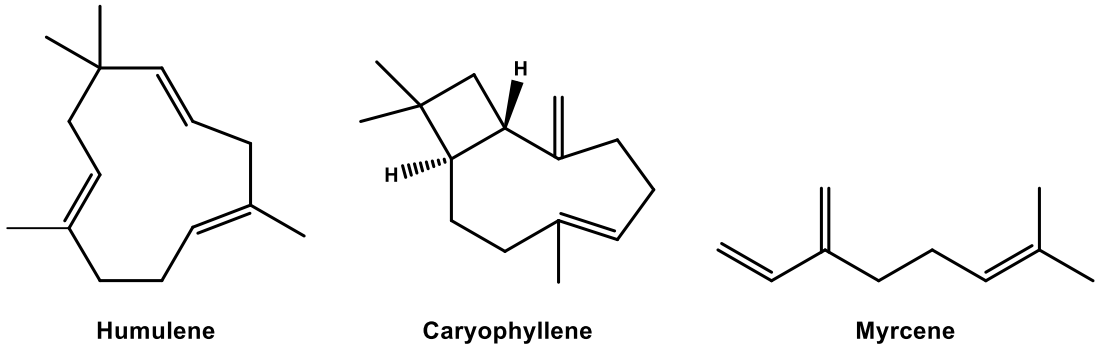

Figure 2.3.4 Structures of the main components of hop oil

Despite the sequiterpenes humulene and caryophyllene being naturally occurring compounds, they have both been studied in depth and can be successfully synthesised in the laboratory via several different routes. The first total synthesis of caryophyllene was reported by Corey *et al*. in 1964.[44] Following on from the work of Corey *et al*. several groups have reported different synthetic methods for synthesising humulene from mimicking the natural biosynthetic method through to the use of metal catalysts.[45, 46] Recently, a greener route to the total synthesis of caryophyllene has been reported by Yang *et al*. who have used modified *Escherichia coli* (*E. coli*) to establish a new biosynthetic route of production.[47]

2.4 RESULTS AND DISCUSSION

By their very nature, polymers synthesised with a high sulfur content are difficult to characterise by traditional analytical chemistry techniques. If a copolymer was to be fully or highly crosslinked then it would be insoluble and therefore GPC and solution NMR cannot be performed. Additionally this lack of solubility prevents sulfur copolymers being analysed via GC-MS and LC-MS. Sulfur can be classed as NMR inactive, since the major isotope of sulfur is ^{32}S which possess a spin state of 0. It is only the ^{33}S isotope that is NMR active with a spin of 3/2 however its relative abundance is extremely low at 0.75%, rendering even solid state NMR analysis extremely difficult. Due to sulfur being IR transparent, difficulties are encountered when using FT-IR to analyse polymeric samples containing high quantities of sulfur. To overcome this, various techniques need to be employed including using a larger than normal sample, increasing the number of scans performed and the use of the spectrometer in transmittance mode with the sample being suspended in a KBr disc.

In order to successfully characterise inverse vulcanised sulfur polymers, analytical techniques that reveal certain properties of these materials by observation of that which is not present, must be employed. For example, we can deduce that a sulfur copolymer has a high molecular weight because it is insoluble in a series of common laboratory solvents and at different temperatures. Disappearance of C=C in an IR spectra when compared to the crosslinking monomer suggesting that a crosslinking reaction has occurred. The presence of a singular broad peak in the pXRD pattern would indicate that material is of an amorphous nature, this coupled with the lack of crystalline S_8 peaks suggests that all the elemental sulfur has been consumed in the reaction and was fully stabilised in the material.

2.4.1 STRUCTURAL AND PHYSICAL PROPERTIES

With the exception of S-DCPD copoylmers, copolymers containing perillartine, perillyl alcohol, and hop oil as crosslinking agents stabilised up to 80 wt.% sulfur containing materials. S-DCPD copolymer composites exceeded this by a further 10%, only showing inhomogeneity and sulfur instability at compositions in excess of 90 wt.% sulfur content. Both S-DCPD and S-PERT copolymers at 50 wt.% produced glassy black materials, which slightly lightened to black/dark brown colour in the case of S-DCPD (Figure 2.4.1) and a black/dark red colour for S-PERT composites at higher sulfur contents. S-PER copolymers were glassy with vibrant red colours, the 50 wt.% copolymer produced a ruby red translucent copolymer. As the wt.% of sulfur increased the S-PER copolymers lost their translucency, turning opaque with a lighter red colour. All S-HOP copolymers, regardless of sulfur content, produced brown copolymer composites.

Figure 2.4.1 Moulded 50 wt.% S-DCPD copolymer samples

Sulfur copolymers were subjected to elemental analysis apart from S-HOP, as the full composition of the hop oil crosslinker was unknown. Shown in Table 2.4.1 are the results from the 50 wt.% compositions against their calculated values. As can be seen from the table there is very little deviance from the predicted values, suggesting very few by-products were formed during the synthesis reactions.

Table 2.4.1 Calculated and observed values for the elemental analysis of 50 wt.% S-DCPD, S-PERT and S-PER

Sample	Calculated			Observed		
	C	H	S	C	H	S
S-DCPD 50:50	45.43	4.57	50.00	40.40	3.64	55.77
S-PERT 50:50	36.35	4.58	50.00	33.18	4.16	52.98
S-PER 50:50	39.45	5.30	50.00	37.66	4.73	53.79

The FT-IR analysis of all inverse vulcanised sulfur copolymers showed similar results and is demonstrated by the stacked FT-IR spectra of S-PER shown in Figure 2.4.2. Stacked FT-IR spectra of S-HOP, S-DCPD and S-PERT copolymers at 50 wt.% can be found in Appendix A1.

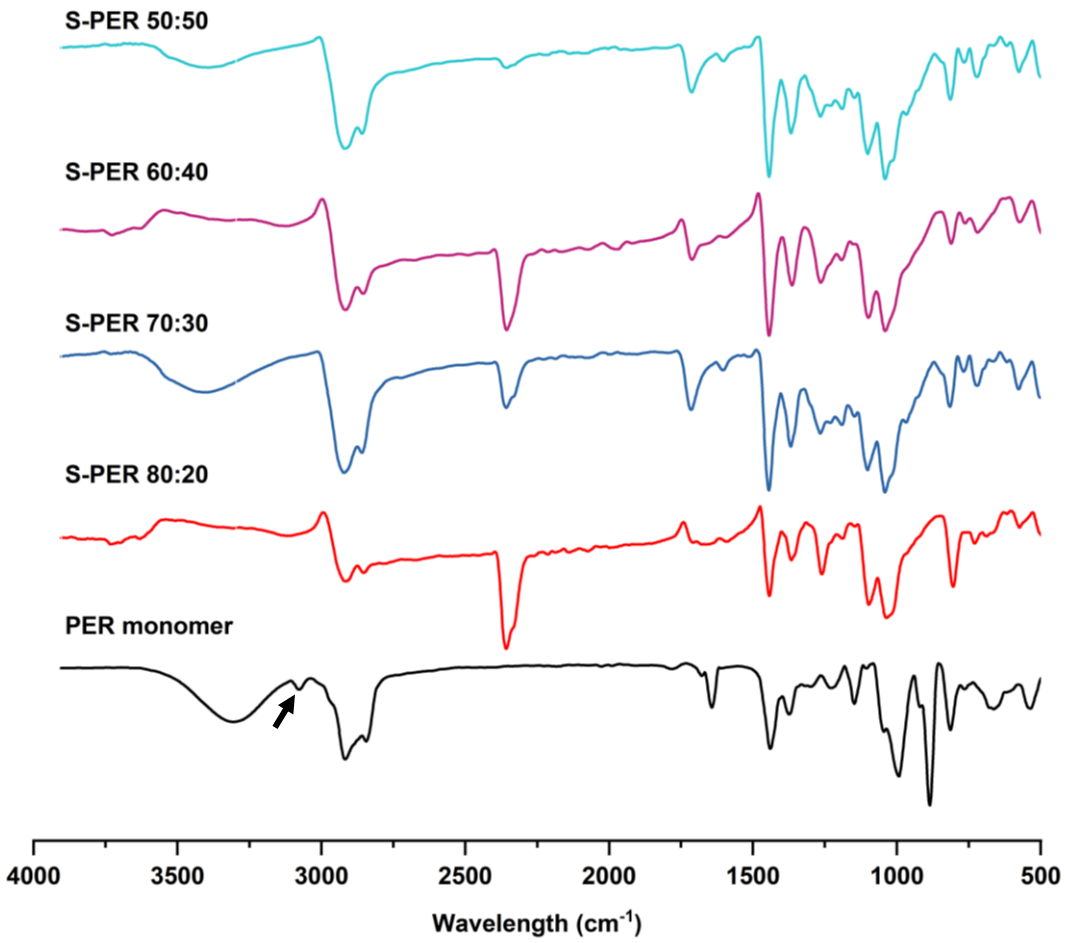

Figure 2.4.2 Stacked FT-IR spectra of S-PER copolymers and PER monomer. An arrow indicates the allylic C=C-H bond present in the monomer at ~ 3100 cm^{-1}

As can be seen from the spectra in Figure 2.4.2, the C=C-H allylic group present in the monomer at ~ 3100 cm^{-1} (see arrow) is not present in any of the copolymer compositions suggesting that crosslinking has occurred and that all of the PER monomer has been consumed in the reactions. This trend was observed across all polymers however there were slight variances noticed in the fingerprint region of the spectra owing to the different structures of the crosslinkers.

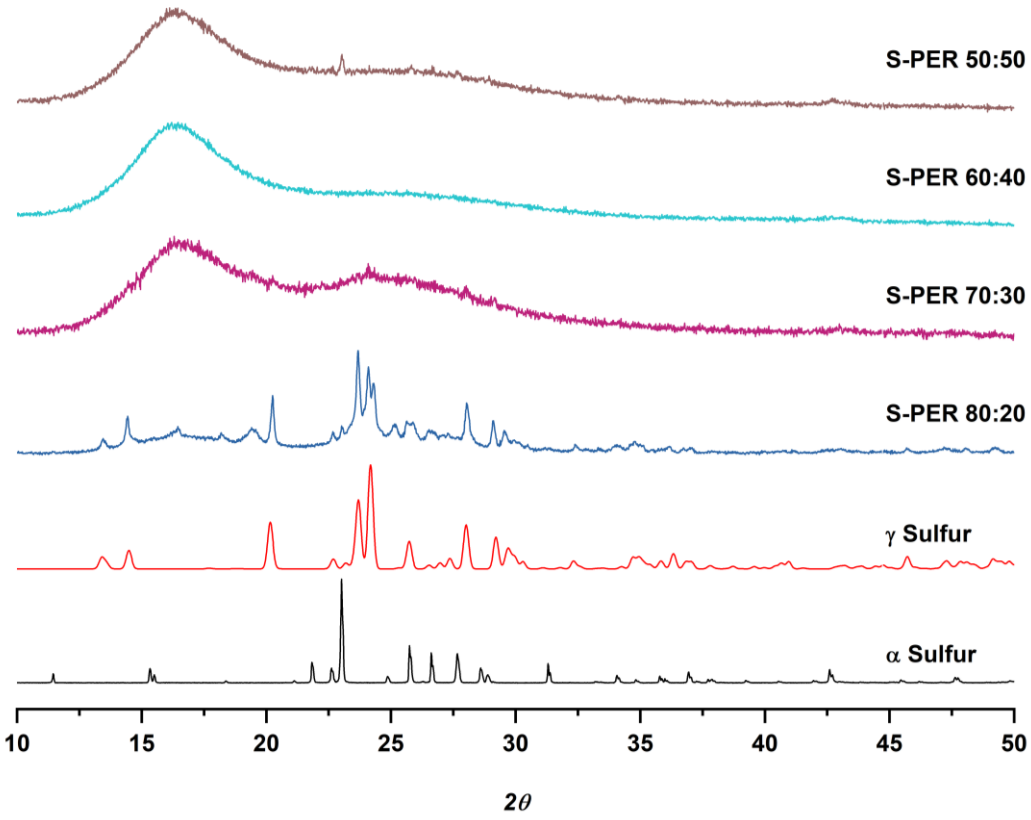

Figure 2.4.3 Stacked pXRD patterns of S-PER copolymers with γ and α polymorphs of sulfur

To ascertain the whether the copolymer reactions had proceeded to completion, pXRD analysis was performed on the sulfur copolymer samples. As demonstrated by the lack of crystalline S_8 peaks observed in the stacked pXRD patterns of 50 to 70 wt.% S-PER copolymers, shown in Figure 2.4.3, it can be assumed with a high degree of certainty that these S-PER copolymers blends underwent a successful inverse vulcanisation reaction and stabilised

all elemental sulfur present in the reaction. At 80 wt.% sulfur content, the pXRD pattern exhibited crystalline sulfur peaks suggesting there was residual elemental sulfur present in this sample either from being unreacted during the synthesis stage or due to instability and depolymerisation occurring. Additionally this trend is also noted in the pXRD patterns of S-HOP and S-PERT copolymers but not in the S-DCPD copolymer samples. S-DCPD exhibited a similar trend, however the crystalline sulfur peaks were first detected at the higher 90 wt.% composition instead of 80 wt.% as found in the pXRD patterns of the aforementioned copolymer samples (found in Appendix A2).

It is interesting to note that the crystalline sulfur peaks detected in the 80 wt.% S-PER copolymer correspond to the peaks that are observed in the γ sulfur polymorph rather than the α sulfur polymorph, this being the normal state in which elemental sulfur is found. The γ sulfur polymorph is typically only found when elemental sulfur is heated to a molten state, where it resides in its β polymorph state before being slowly cooled back down to form the γ polymorph. To confirm this theory several samples were prepared for high resolution variable temperature synchrotron pXRD, data for which was collected on the I11 beamline at Diamond Light Source by Dr S Chong. This data (Figure 2.4.4) showed the transition of elemental sulfur from the stable α polymorph, to the transitional β polymorph at 96 °C before melting at 119 °C.

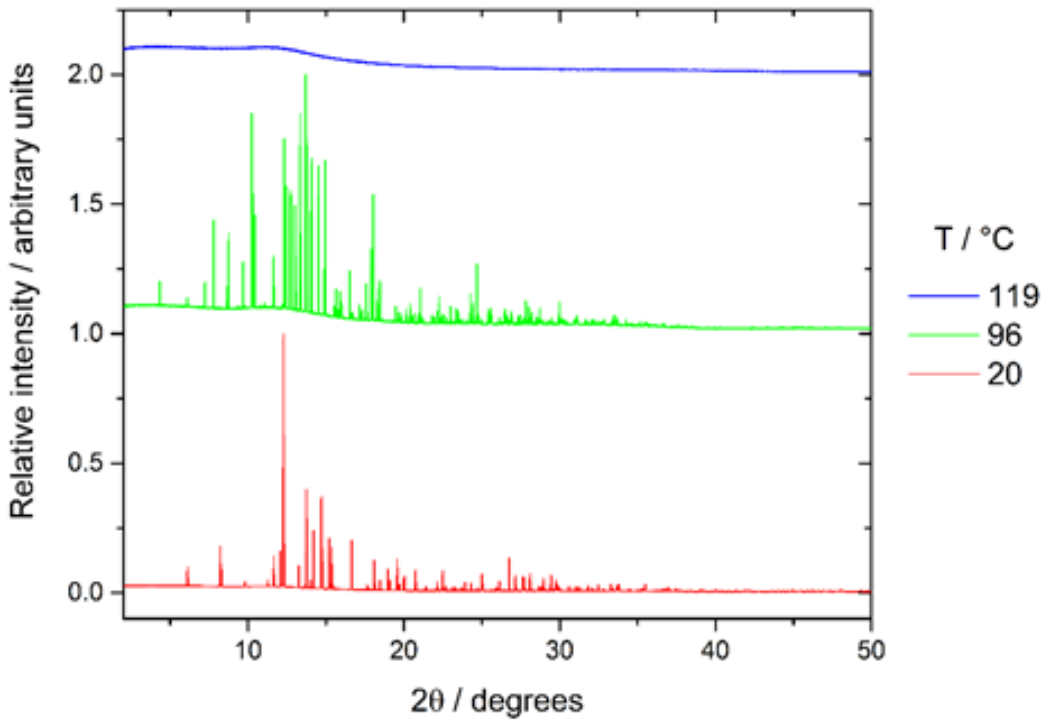

Figure 2.4.4 Variable temperature pXRD patterns (λ = 0.824965 Å) of pure sulfur, packed in a capillary with patterns collected whilst the sample was heated.

Additionally a capillary was packed with a "pre-copolymer" slurry of 70 wt.% S-PER copolymer solution. The "pre-copolymer" slurry was formed by heating elemental sulfur to just above its melting point and adding perillyl alcohol to the solution with vigorous stirring to promote a homogenous solution but before the polymerisation reaction could occur. The reaction mixture was rapidly cooled and packed into a 0.5 mm quartz capillary for analysis. The sample was heated *in situ* once on the beamline with diffraction data collected in real time. As can be seen in Figure 2.4.5 before heating commenced the diffraction showed a mixture of α and β sulfur polymorph peaks, with the β polymorph being the predominant form confirming that the sulfur had indeed melted but had yet to react with the crosslinker. The sample was the heated to 185 °C for one hour to ensure the polymerisation reaction had fully occurred. This is confirmed by the middle pXRD pattern displayed in Figure 2.4.5 showing that the crystalline peaks in the previous pattern have been replaced with a singular amorphous peak. The sample was then cooled

to room temperature before being retested 24 hours later (top pXRD pattern in Figure 2.4.5), which showed little change in the pXRD pattern confirming that polymerisation had occurred and the sulfur remained stable in the material.

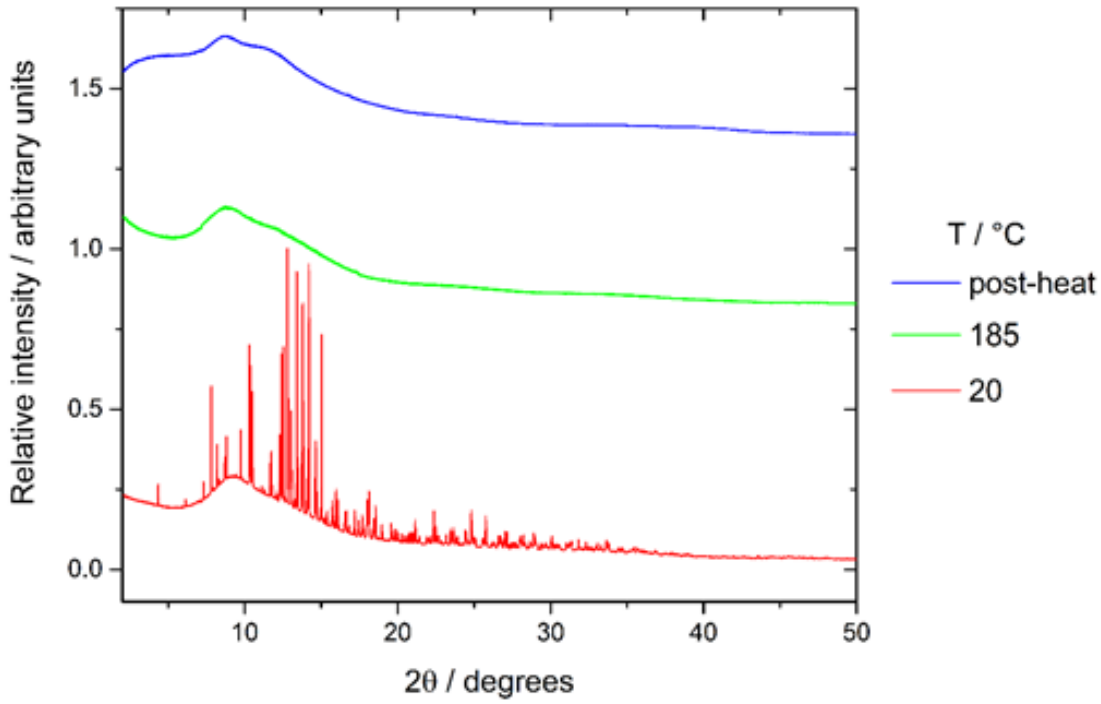

Figure 2.4.5 Stacked pXRD patterns of S-PER before, during and 24 hours post reaction

2.4.2 POLYMERIC TRENDS

Both S-DCPD and S-PERT copolymers proved to be insoluble when tested against a battery of common laboratory solvents. S-PER at 50 wt.% did show some solubility as is shown in Figure 2.4.6, however it was not as soluble as S-LIM and instead showed greater similarity to S-DIB. As shown in Figure 2.4.6, S-PER is readily soluble in polar solvents such as chloroform, THF and toluene but relatively insoluble in non-polar solvents, with it being sparingly soluble in hexane.

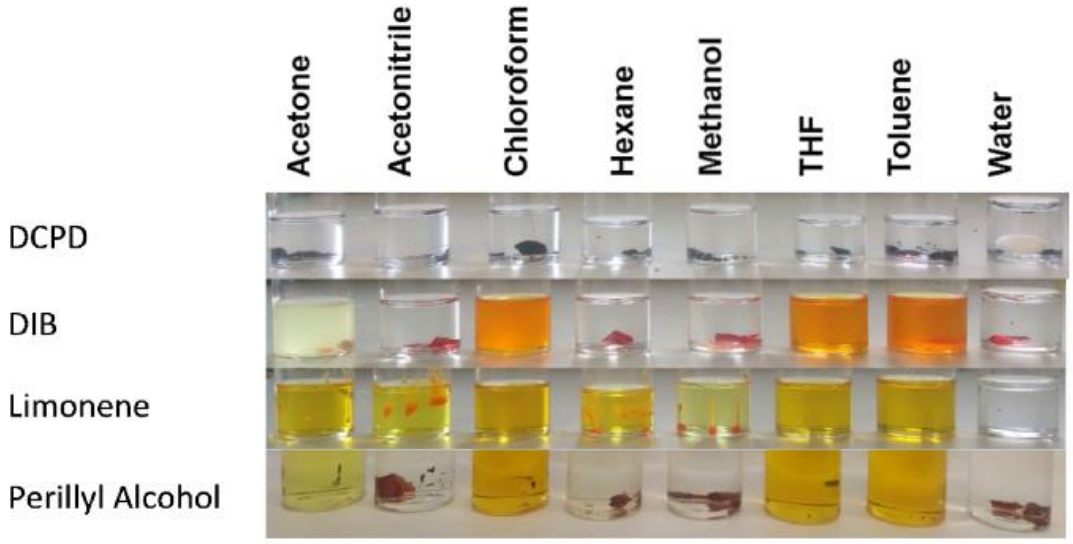

Figure 2.4.6 Solubility tests of S-PER and S-DCPD at 50 wt.% compared to S-LIM and S-DIB

Simple solubility studies were performed on all sulfur copolymers at 50 wt.% composition by placing 100 mg of solid in 10 mL solvent and agitating overnight on a tube roller. After 24 hours all samples were filtered onto pre-weighted filter papers to calculate the mass remaining after 24 hours. Samples that had fully dissolved after 24 hours of agitation were assigned a nominal solubility of ≥ 10.0 mg mL^{-1}. Solubility data for S-PER, S-HOP, S-PERT and S-DCPD are provided in Table 2.4.2.

Table 2.4.2 Solubility data for S-PER, S-HOP, S-PERT and S-DCPD

Solvent	Solubility of sulfur copolymer (mg mL^{-1})			
	S-PER	S-HOP	S-PERT	S-DCPD
Acetone	0.15	0.27	Nil	Nil
Acetonitrile	Nil	Nil	Nil	Nil
Chloroform	≥ 10.0	8.63	Nil	Nil
Hexane	0.31	Nil	Nil	Nil
Methanol	Nil	Nil	Nil	Nil
THF	≥ 10.0	≥ 10.0	Nil	Nil
Toluene	≥ 10.0	9.82	Nil	Nil
Water	Nil	Nil	Nil	Nil

Differential Scanning Calorimetry was used to record the glass transition temperature (T_g) of copolymer samples synthesised and to determine any other structural features present. In all cases only a single T_g was recorded for each sample, if an additional T_g was detected this would have suggest that that the copolymers was inhomogeneous with a region higher in crosslinker content and another region higher in polymeric sulfur.

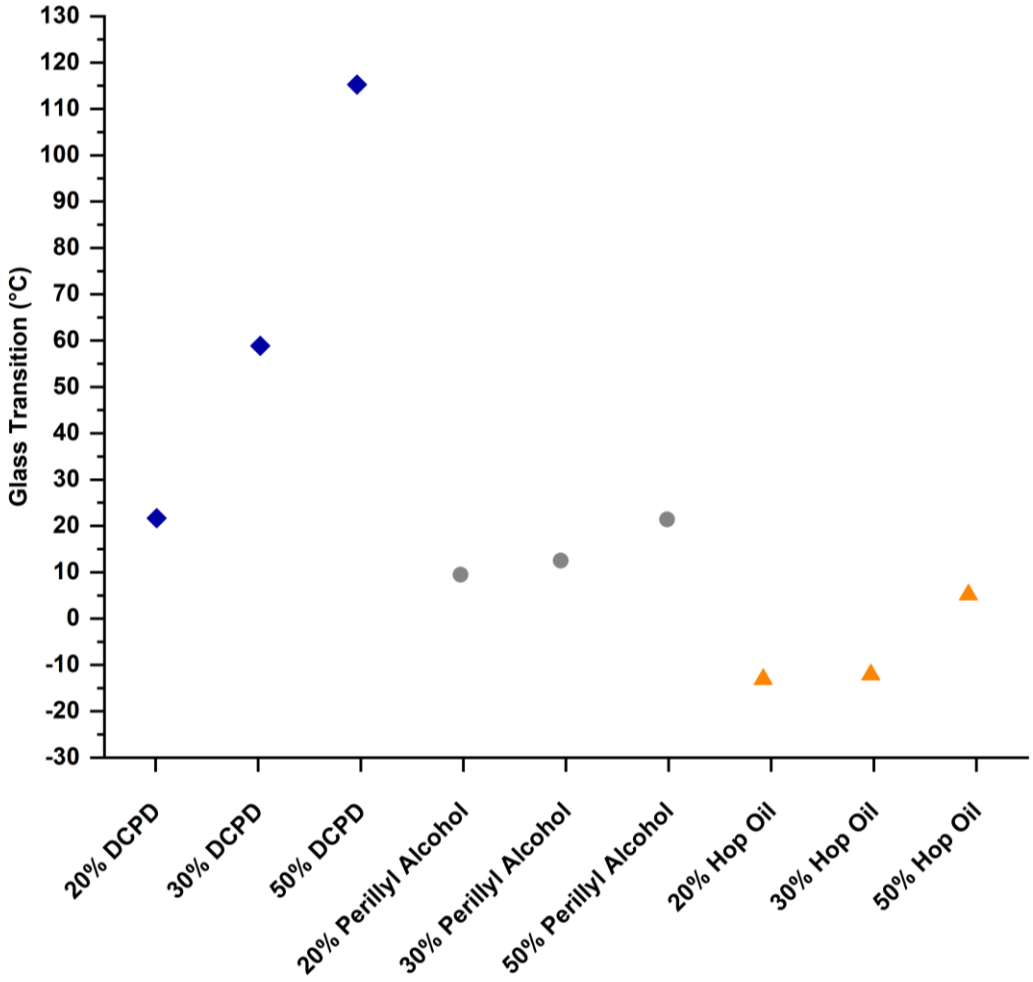

Figure 2.4.7 Plot comparing S-DCPD, S-PER and S-HOP copolymers and their recorded T_g

As shown in Figure 2.4.7 the majority of T_g recorded were below room temperature. The particularly low T_g for S-HOP copolymer is likely explained by the unknown ~ 10% content of the hop oil. The unknown ~ 10% is likely to have prevented full crosslinking from occurring whilst acting like a plasticiser

thereby reducing the T_g from what it would be expected were the hop oil to comprise solely of myrcene, humulene and caryophyllene. It is theorised that the extremely high T_g temperatures recorded for S-DCPD copolymers is due to the inherent rigidity of the DCPD ring structure coupled with the C=C bridge present over the cyclohexene ring, which aids in keeping the DCPD extremely rigid (preventing it from contorting). It is therefore reasonable that a highly crosslinked sulfur copolymer containing this DCPD moiety would require far more energy to reach the T_g when compared to other linear and cyclic crosslinkers.

Additionally, DSC was used to determine whether there was residual elemental sulfur present in samples, as it proved to be more sensitive than the bulk analysis provided by the "in house" pXRD, owing to the distinctive sulfur melting transition at ~ 120 °C present in samples that contained free elemental sulfur.

2.5 CONCLUSIONS

This chapter has shown that it is not only possible to synthesis inverse vulcanised sulfur copolymers from pure commercially available crosslinking agents but it is also possible to form stable copolymers from unrefined plant essential oils high in naturally occurring terpenes, such as hop oil. These sulfur copolymers have exhibited a range of colours, translucency, and physiochemical properties depending on both the crosslinker chosen and the sulfur content present.

Most crosslinkers can stabilise up to 80 wt.% sulfur, with DCPD the exception being able to stabilise up to 90 wt.%. Additionally both S-DCPD and S-PERT copolymers proved to be insoluble against a panel of common laboratory solvents, with both S-PER and S-HOP showing a greater affinity and solubility in polar solvents such as THF. From pXRD studies we can confirm that

elemental sulfur undergoes a transition from the α polymorph state to the β polymorph state before undergoing ROP with the terpenoid based crosslinkers. If there is unreacted sulfur remaining in the copolymer it will crystallise out in γ polymorphic state and not return to the α polymorph.

2.6 REFERENCES

1. S. Serra, in *Studies in Natural Products Chemistry*, ed. R. Atta ur, Elsevier, 2015, vol. 46, ch. Chapter 7 - Recent Developments in the Synthesis of the Flavors and Fragrances of Terpenoid Origin, pp. 201-226.
2. M. Firdaus, L. Montero de Espinosa and M. A. R. Meier, *Macromolecules*, 2011, **44**, 7253-7262.
3. J. Zhao and H. Schlaad, in *Bio-synthetic Polymer Conjugates*, ed. H. Schlaad, Springer Berlin Heidelberg, Berlin, Heidelberg, 2013, ch. Synthesis of Terpene-Based Polymers, pp. 151-190.
4. P. A. Wilbon, F. Chu and C. Tang, *Macromolecular Rapid Communications*, 2013, **34**, 8-37.
5. M. Shibata and M. Asano, *Journal of Applied Polymer Science*, 2013, **129**, 301-309.
6. J. M. Bolton, M. A. Hillmyer and T. R. Hoye, *ACS Macro Letters*, 2014, **3**, 717-720.
7. J. G. Speight, in *Handbook of Industrial Hydrocarbon Processes*, ed. J. G. Speight, Gulf Professional Publishing, Boston, 2011, ch. Chapter 7 - Hydrocarbons from Biomass, pp. 241-279.
8. G. Rubulotta and E. A. Quadrelli, in *Studies in Surface Science and Catalysis*, eds. S. Albonetti, S. Perathoner and E. A. Quadrelli, Elsevier, 2019, vol. 178, ch. Chapter 11 - Terpenes: A Valuable Family of Compounds for the Production of Fine Chemicals, pp. 215-229.
9. W. J. Chung, J. J. Griebel, E. T. Kim, H. Yoon, A. G. Simmonds, H. J. Ji, P. T. Dirlam, R. S. Glass, J. J. Wie, N. A. Nguyen, B. W. Guralnick, J. Park, Á. Somogyi, P. Theato, M. E. Mackay, Y.-E. Sung, K. Char and J. Pyun, *Nat Chem*, 2013, **5**, 518-524.
10. M. P. Crockett, A. M. Evans, M. J. H. Worthington, I. S. Albuquerque, A. D. Slattery, C. T. Gibson, J. A. Campbell, D. A. Lewis, G. J. L. Bernardes and J. M. Chalker, *Angewandte Chemie International Edition*, 2015, **55**, 1714-1718.
11. X. Wu, J. A. Smith, S. Petcher, B. Zhang, D. J. Parker, J. M. Griffin and T. Hasell, *Nature Communications*, 2019, **10**, 647.
12. B. H. Clampitt, D. E. German and J. R. Galli, *Journal of Polymer Science*, 1958, **27**, 515-522.

13. R. W. Roth and R. F. Church, *Journal of Polymer Science*, 1961, **55**, 41-48.

14. J. K. Gillham and C. C. Mentzer, *Journal of Applied Polymer Science*, 1973, **17**, 1143-1164.

15. A. Matsumoto, F. Hirai, Y. Sumiyama, H. Aota, Y. Takayama, A. Kameyama and T. Nakanishi, *European Polymer Journal*, 1999, **35**, 195-199.

16. S. U. A. Redondo, E. Radovanovic, I. L. Torriani and I. V. P. Yoshida, *Polymer*, 2001, **42**, 1319-1327.

17. R. O. Pinho, E. Radovanovic, I. L. Torriani and I. V. P. Yoshida, *European Polymer Journal*, 2004, **40**, 615-622.

18. Y. Yoo, J. B. You, W. Choi and S. G. Im, *Polymer Chemistry*, 2013, **4**, 1664-1671.

19. T. F. Woloszyn and P. C. Jurs, *Analytical Chemistry*, 1993, **65**, 582-587.

20. W.-S. Kong, T.-J. Ju, J.-H. Park, S.-R. Joo, H.-G. Yoon and J.-W. Lee, *International Journal of Adhesion and Adhesives*, 2012, **38**, 38-44.

21. T. T. P. Cheung, in *Encyclopedia of Polymer Science and Technology*, ed. H. F. Mark, John Wiley & Sons, Hoboken, NJ, 1st edn., 2001, ch. Cyclopentadiene and Dicyclopentadiene.

22. B. K. Bordoloi and E. M. Pearce, in *New Uses of Sulfur—II*, AMERICAN CHEMICAL SOCIETY, 1978, vol. 165, ch. 3, pp. 31-53.

23. A. Della Martina, J. G. Hilborn and A. Mühlebach, *Macromolecules*, 2000, **33**, 2916-2921.

24. D. D. Andjelkovic and R. C. Larock, *Biomacromolecules*, 2006, **7**, 927-936.

25. X. Liu, X. Sheng, J. K. Lee and M. R. Kessler, *Journal of Thermal Analysis and Calorimetry*, 2007, **89**, 453-457.

26. M. Valverde, D. Andjelkovic, P. P. Kundu and R. C. Larock, *Journal of Applied Polymer Science*, 2008, **107**, 423-430.

27. P. Henna and R. C. Larock, *Journal of Applied Polymer Science*, 2009, **112**, 1788-1797.

28. P. L. Crowell and C. E. Elson, in *Handbook of nutraceuticals and functional foods*, ed. R. E. C. Wildman, CRC Press, Boca Raton, Fla, 1st edn., 2001, ch. Isoprenoids, Health and Disease, pp. 31–53.

29. T. C. Chen, C. O. D. Fonseca and A. H. Schönthal, *American journal of cancer research*, 2015, **5**, 1580-1593.

30. J. D. Haag and M. N. Gould, *Cancer Chemotherapy and Pharmacology*, 1994, **34**, 477-483.

31. L. Yeruva, K. J. Pierre, A. Elegbede, R. C. Wang and S. W. Carper, *Cancer Letters*, 2007, **257**, 216-226.

32. L. Yeruva, C. Hall, J. A. Elegbede and S. W. Carper, *Anti-Cancer Drugs*, 2010, **21**, 1-9.

33. L. Pan, H. Chai and A. D. Kinghorn, *Phytochemistry Letters*, 2010, **3**, 1-8.

34. S. Lupien, F. Karp, K. Ponnamperuma, M. Wildung and R. Croteau, *Journal*, 1995, **12**, 245.

35. W. A. Duetz, H. Bouwmeester, J. B. van Beilen and B. Witholt, *Applied Microbiology and Biotechnology*, 2003, **61**, 269-277.

36. J. B. van Beilen, R. Holtackers, D. Lüscher, U. Bauer, B. Witholt and W. A. Duetz, *Applied and Environmental Microbiology*, 2005, **71**, 1737-1744.

37. K. Geoghegan and P. Evans, *Tetrahedron Letters*, 2014, **55**, 1431-1433.

38. A. D. Kinghorn and C. M. Compadre, in *Alternative Sweeteners*, ed. L. O. B. Nabors, Marcel Dekker, New York, 3rd ed. edn., 2001, ch. Less Common High-Potency Sweeteners, pp. 209-233.

39. R. W. Bragg, Y. Chow, L. Dennis, L. N. Ferguson, S. Howell, G. Morga, C. Ogino, H. Pugh and M. Winters, *Journal of Chemical Education*, 1978, **55**, 281.

40. Y. Miyashita, Y. Takahashi, C. Takayama, K. Sumi, K. Nakatsuka, T. Ohkubo, H. Abe and S. Sasaki, *Journal of Medicinal Chemistry*, 1986, **29**, 906-912.

41. C. R. Langezaal, A. Chandra and J. J. C. Scheffer, *Pharmaceutisch Weekblad*, 1992, **14**, 353-356.

42. M. Verzele, *Journal of the Institute of Brewing*, 1986, **92**, 32-48.

43. S. T. Katsiotis, C. R. Langezaal and J. J. C. Scheffer, *Planta Medica*, 1989, **55**, 634-634.

44. E. J. Corey, R. B. Mitra and H. Uda, *Journal of the American Chemical Society*, 1964, **86**, 485-492.

45. M. C. Pirrung and A. T. Morehead Jr., in *Total Synthesis of Natural Products*, ed. D. Goldsmith, John Wiley & Sons, Canada, 1997, vol. 10, ch. II. Monocyclic Sesquiterpenes, pp. 29-160.

46. T. Hu and E. J. Corey, *Organic Letters*, 2002, **4**, 2441-2443.

47. J. Yang, Z. Li, L. Guo, J. Du and H.-J. Bae, *Renewable Energy*, 2016, **99**, 216-223.

Chapter 3: Linear Terpenoid Derived Crosslinkers

Contents

3.1 INTRODUCTION

Due to the current lack of low-cost sustainable materials for mercury and other toxic heavy metal waste remediation, there is a need to synthesise and develop novel inorganic functional porous materials. Such copolymers could be synthesised from elemental sulfur using renewable crosslinkers to form inverse vulcanised copolymers, however they need to meet the demanding requirement of good physical properties *versus* affordability for industry. This necessitates a material which is shape persistent, chemically stable and with the ability to induce porosity to enhance the surface area making it suitable as a filter for toxic heavy metals. This chapter will discuss the results of five renewable linear terpenoid derived crosslinkers, the synthesis process, their physical properties and trends within the crosslinkers.

3.2 CROSSLINKERS

3.2.1 MYRCENE

Myrcene is a monoterpene with two isomeric forms, alpha and beta. The most common form of myrcene is β-myrcene and it is an essential oil found in many plants, such as hops and parsley, whereas α-myrcene is not found in nature and is the given name of 2-methyl-6-methylene-1,7-octadiene.[1] Although naturally occurring, myrcene is more commonly synthesised from the pyrolysis of β-pinene.[2] Other synthetic routes for the production of valuble small molecule have been investigated, with a greener route of production using modified *E. coli* proposed by Kim *et al*.[3] Due to its low cost and relative abundance, myrcene has been studied since the late 1940s as a component in various polymerisation reactions.[4-7]

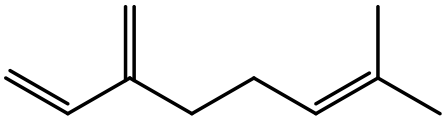

Myrcene

Figure 3.2.1 Structure of myrcene

3.2.2 FARNESENE

Farnesene is the general name given to the family of sesquiterpenes that comprises two isomers and six sterioisomers (Figure 3.2.2). Of the six sterioisomers, three have so have been reported as naturally occurring; (E,E)-α-farnesene, (Z,E)-α-farnesene and (E)-β-farnesene.[8-10] Present in the waxy skins of various fruits, farnesene is most commonly extracted from apples,[11] however it can also be produced via biosynthetic routes using modified *E. coli*.[12] Farnesene has been investigated as a potential biofuel due to its ready availability in nature and its hydrocarbon chain that is a similar length to hydrocarbons found in petroleum based fuels.[13, 14]

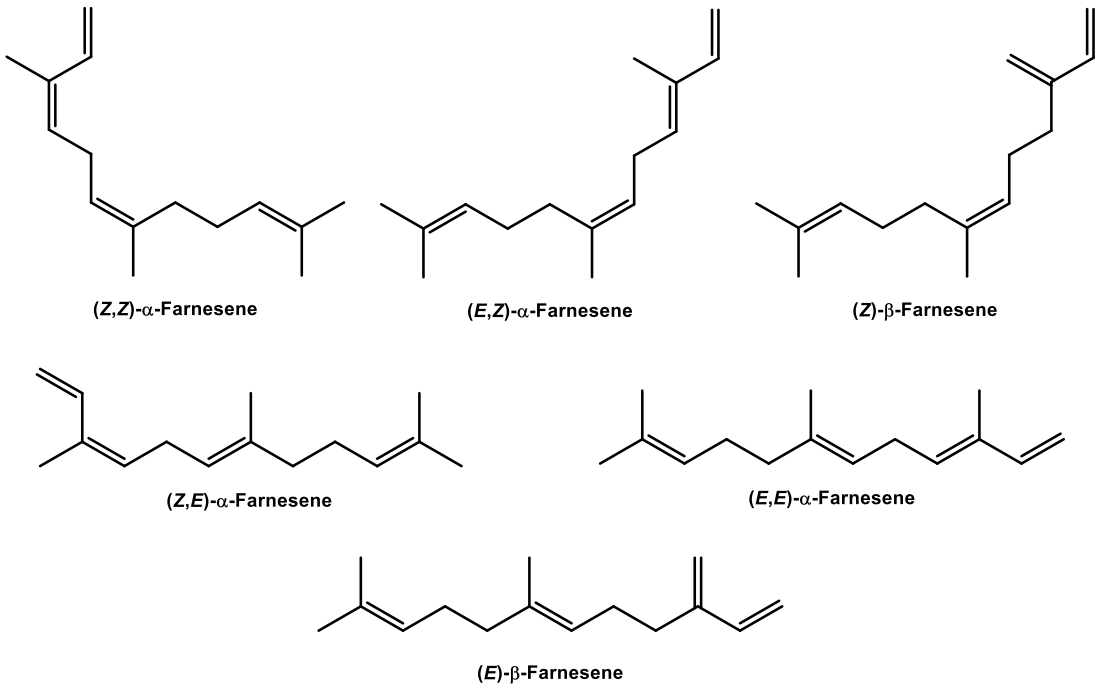

Figure 3.2.2 The six structural isomers of farnesene

3.2.3 FARNESOL

Farnesol is a naturally occurring sesquiterpene alcohol produced by many organisms.[15] Although naturally occurring farnesol can be synthesised via synthetic and biosynthetic routes.[16-18] In certain organisms farnesol and its derivatives are one of the base building blocks used in the synthesis of squalene.[19, 20] Farnesol has been extensively studied for its antimicrobial effects, especially on gram positive bacterial strains such as *Staphylococcus aureus* and *Streptococcus mutans*.[21-24]

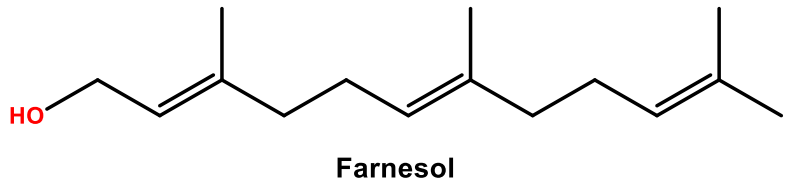

Farnesol

Figure 3.2.3 Structure of farnesol

3.2.4 SQUALENE

Squalene is a naturally occurring triterpene, found in various plant and animal species. It was first reported by Tsujimoto, who proposed the name as the oil was extracted from the livers of the *Squalidae* family of sharks.[25] As a biochemical precursor, squalene is used in the synthesis of various important steroids and sterols such as cholesterol.[26] Due to the increasing use of squalene in both the cosmetics and pharmaceutical industries, alternative methods of synthesis are actively being investigated including the use of engineered microorganisms such as bacteria, yeasts and fungi.[27-29]

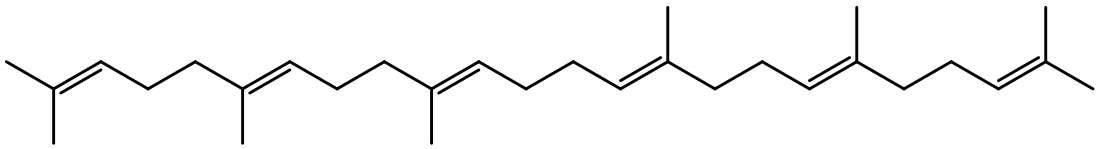

Squalene

Figure 3.2.4 Structure of squalene

3.2.5 NEROLIDOL

Also known as peruviol, nerolidol is a naturally occurring sesquiterpene that was first reported in scientific literature at the turn of the 20th century.[30, 31] Found in both *-cis* and *-trans* configurations, nerolidol is a component of many plant essential oils and is used widely in both cosmetics and non-cosmetics such as detergents.[32, 33] Due to the wide spread use of nerolidol in the cosmetic industry with little or no reported side effects, there has been an increased interest in studying the compound for its pharmacological properties.[34-36]

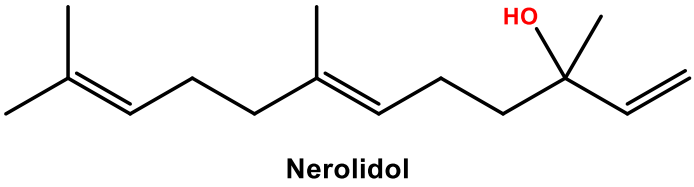

Nerolidol

Figure 3.2.5 Structure of nerolidol

3.3 RESULTS AND DISCUSSION

Unlike the cyclic and complex mixture of terpenoids presented in Chapter 2, the use of linear crosslinkers in this chapter has allowed certain analytical techniques to be used in more detail to gain a better understanding of the structure property relationships of these new materials. This is due to these inverse vulcanised materials being more soluble in specific solvents, allowing both solution NMR and GPC to be performed on specific copolymers.

3.3.1 STRUCTURAL AND PHYSICAL PROPERTIES

Similiarly to the crosslinkers discussed in Chapter 2, the inverse vulcanised sulfur copolymers synthesised from the crosslinkers described in this chapter all managed to stabilise up to 80 wt.% elemental sulfur into a useable material. Depending on the crosslinker chosen and the sulfur content present in the copolymer the colour of final material varied from a brown/burnt umber colour to a fully black glassy material in the case of 50 wt.% myrcene.

All inverse vulcanised sulfur copolymers synthesised were analysed by elemental analysis at least twice with the averages reported in this thesis. The results of the 50 wt.% compositions presented in Table 3.3.1, for full results see Appendix A3. As can be seen in Table 3.3.1, there is a slight variance between S-MYR and its calculated value compared to the other crosslinkers. This is likely caused by myrcene having a boiling point between 166 – 168 °C and the reaction being conducted at a nominal 175 °C (the heating block was set and monitored at 175 °C, with no *in situ* reaction monitoring undertaken), suggesting that a small quantity of crosslinker may have boiled off.

Table 3.3.1 Calculated and observed values for the elemental analysis of 50 wt.% S-MYR, S-FAR, S-FSOL, S-SQ and S-NER

Sample	Calculated			Observed		
	C	H	S	C	H	S
S-MYR 50:50	44.08	5.92	50.00	37.31	4.53	57.28
S-FAR 50:50	44.08	5.92	50.00	41.87	5.22	54.16
S-FSOL 50:50	40.51	5.89	50.00	40.55	5.21	51.86
S-SQ 50:50	43.87	6.13	50.00	43.57	5.91	50.52
S-NER 50:50	40.51	5.89	50.00	40.47	5.19	52.14

Examination of the elemental analysis results for all inverse vulcanised copolymer compositions reveals the loss of hydrogen during the synthesis of these materials. This was calculated by comparing the C:H ratios of the calculated elemental analysis to those of the observed results for all copolymer samples. Detailed analysis shows that in all cases there is a slight reduction in the expected amount of hydrogen for 50 wt.% samples, with the amount of hydrogen being abstracted increasing as the sulfur content of the samples increases. The difference between the calculated and observed C:H ratios, can range from 0.5% for 50 wt.% samples upto a 15% difference in 80 wt.% samples. It is theorised that hydrogen is abstracted via the formation of

hydrogen sulfide (H_2S), which is to be expected as the formation of H_2S has also been reported in the syntheses other sulfur copolymers.[37, 38] This is unsurprising, as in the conventional vulcanisation process the most widely agreed method for the crosslinking reaction to occur is via hydrogen abstraction of the α-position (relative to the double bond) proton. [39-41]

Due to certain copolymers being soluble in deuterated solvents, solution ^{1}H NMR were conducted on specific polymers. In theory, fully crosslinked polymeric materials should be insoluble, due to their structures comprising a fully interconnected network of chemical bonds. However certain inverse vulcanised copolymers synthesised in this chapter proved to be soluble in deuterated solvents and therefore ^{1}H NMR analysis were conducted. The inherent solubility of these copolymers strongly suggests that these materials are not fully crosslinked but instead exhibited a more hyper-branched oligomeric structure We can draw this conclusion from a number of factors; first these polymers exhibit shape persistence and therefore must have some form of complex structure similar to a fully crosslinked network, and secondly (as discussed below) the complex NMR structures of these materials indicate that they are not simple small organic molecules but much larger structures. This is further confirmed by GPC analysis reported later in this chapter, which shows these materials possess molecular weights in excess of 1000 g mol^{-1}.

Despite the complex structure of hyper-branched polymeric materials, NMR analysis revealed two important results. First taking the ^{1}H NMR spectra of S-MYR and its monomer as an example (Figure 3.3.1) there is a complete absence of allylic bonds in the S-MYR sample, confirming the findings of the FT-IR analysis (found in Appendix A1). These complimentary techniques indicate, with a degree of certainty that a reaction occurred at these sites. Secondly, there is the presence of a broad peak between 2 - 4 ppm in the S-MYR spectra but not in the monomer. This broad peak is attributed to the proton adjacent

to a carbon atom which is bonded to a sulfur atom, further confirming that ROP has occurred during the reaction at the sites of the allylic groups present in the monomer. The ^{1}H NMR spectra for the other soluble sulfur copolymers from this chapter show the same pattern of results and can be found in Appendix A4.

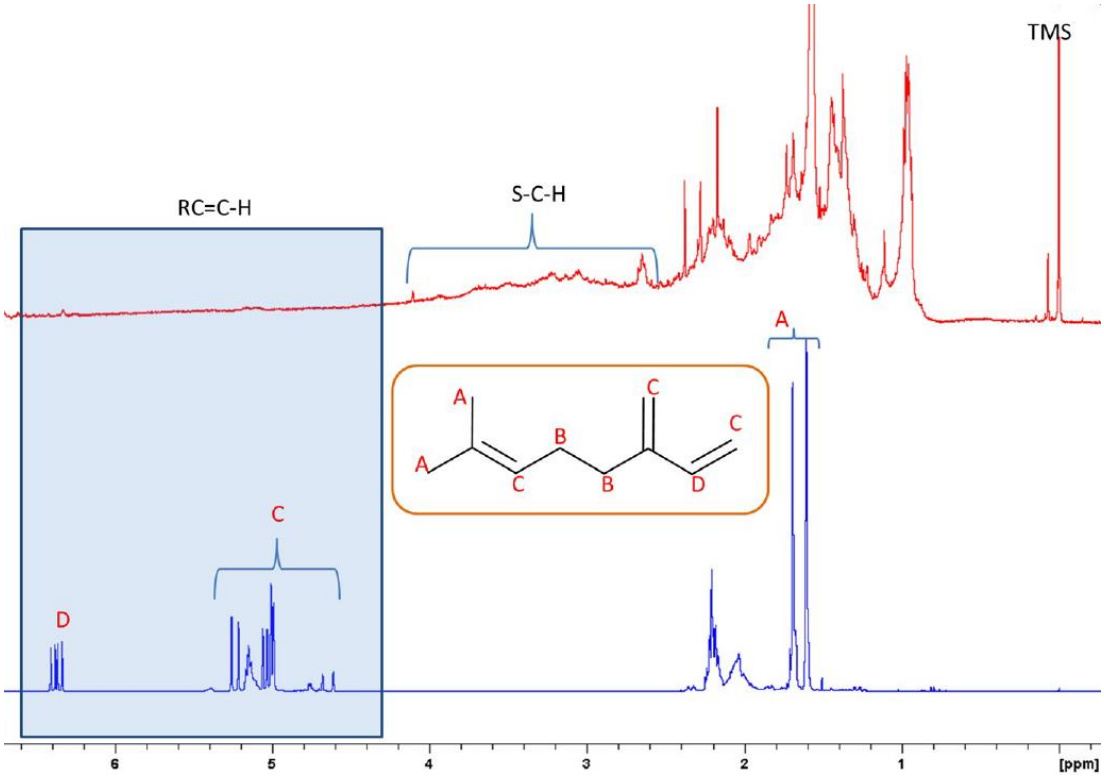

Figure 3.3.1 Stacked ^{1}H NMR (400 MHz, $CDCl_3$) spectra of S-MYR (red) and monomer (blue)

Gel permeation chromatography (GPC) analysis was performed on 50 wt.% samples from S-DIB, S-LIM, S-MYR, S-FSOL and S-FAR. Despite leaving these samples to agitate in the GPC solvent (chloroform) for 24 hours both S-MYR and S-FSOL still had solid remaining. It was decided to run the GPC on these soluble fractions, despite being unable to obtain a true value for the entirety of these materials. From this, it can be deduced that the overall calculated molecular weights for both S-MYR and S-FSOL are far higher than their soluble fractions. GPC analysis was performed by Duncan Woods.

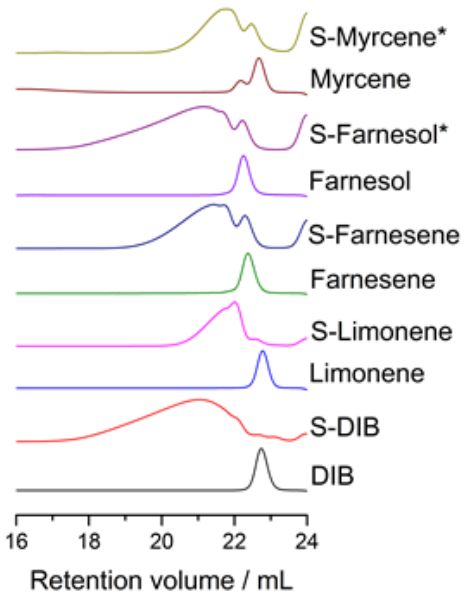

Polymer	M_w (g/mol)	M_n (g/mol)	PDI
S-DIB	8,450	882	9.58
	8,007	929	8.62
S-Limonene	904	493	1.83
	890	491	1.81
S-Farnesene	2,290	738	3.10
	2,298	745	3.08
S-Farnesol[*]	9,772	1,197	8.16
	10,118	1,195	8.47
S-Myrcene[*]	1,015	416	2.44
	962	401	2.40

Figure 3.3.2 Combined GPC traces and data for S-MYR, S-FSOL, S-FAR, S-LIM and S-DIB and their monomers. The asterisk denotes that the sample tested was from the soluble fraction of the copolymers

When comparing these copolymers, or their soluble fraction, with those copolymers previously reported (S-DIB and S-LIM) it is clear from the GPC traces (Figure 3.3.2) that they exhibit higher molecular weights than S-LIM and compare favourably with S-DIB. The higher molecular weight can be discerned from the retention volume, with larger molecular weight species passing through more quickly than smaller species. The GPC data also supports the results collected by DSC. These results show that copolymers which have a higher molecular weight than S-LIM also have a correspondingly higher T_g, this is likely caused by increased crosslinking between the sulfur chains and the monomer.

3.3.2 POLYMERIC TRENDS

Prior to preforming DSC analysis on polymeric samples, thermogravimetric analysis was undertaken on certain samples to ensure that these sample would be compatible with DSC analysis (*ie* they would not explosively decompose under heating). Samples from S-MYR, S-FSOL and S-FAR along with both

cured and uncured samples of the monomer were analysed via TGA under nitrogen up to 900 °C. Additional thermograms can be found in Appendix A5 and show a general trend across all inverse vulcanised copolymer samples, which shows that all samples start to decompose at ~ 200 °C and possess a single mass loss transition suggesting a slow but steady decomposition of the sample.

DSC analysis revealed several trends not only between different sulfur ratios using the same crosslinker, but also between the series of linear terpenoid crosslinking agents. Unsurprisingly, as the wt.% of the crosslinker increases in the copolymer blend, the T_g also increases. This is caused by increased bonding occurring between the sulfur chains and the terpenoid moiety creating a more fully crosslinked network. Similarly increasing the number of allylic groups present in the terpenoid structure (*ie* increasing the chain length) demonstrates a similar but slightly greater effect. One example of this would be the comparison between the 50 wt.% S-MYR and S-SQ, as show in Figure 3.3.3.

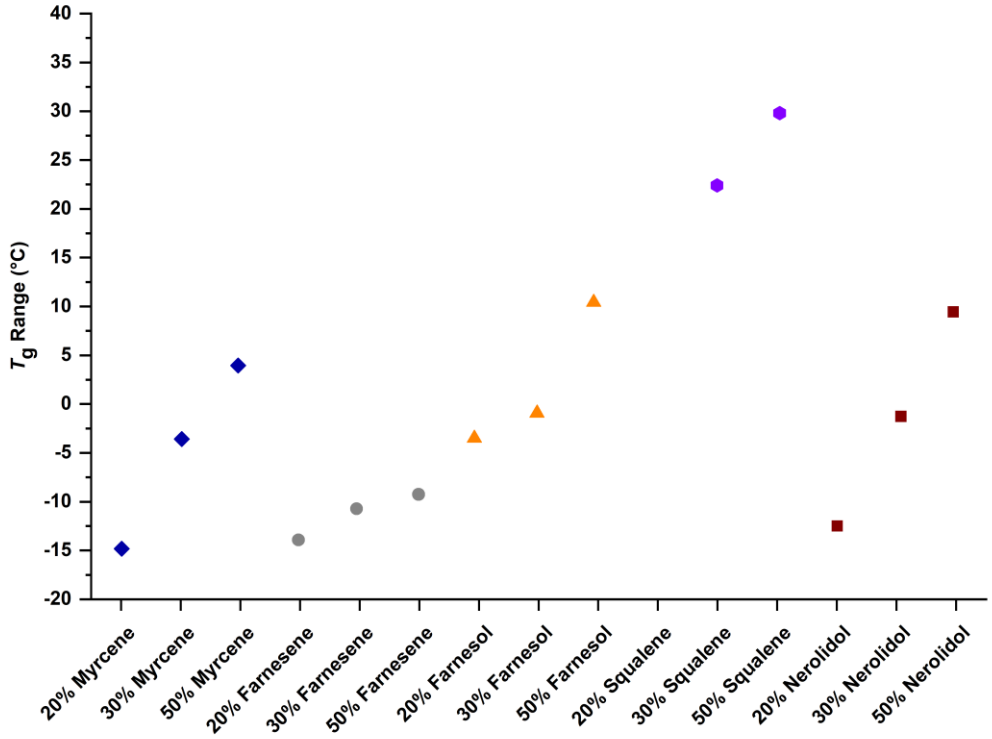

Figure 3.3.3 Comparison of glass transition temperatures and crosslinker content for S-MYR, S-FAR, S-FSOL, S-SQ and S-NER

One interesting result exhibited within this group of crosslinkers is the effect of functional group on the T_g of inverse vulcanised sulfur copolymers. Both S-FSOL and S-NER are sesquiterpene alcohols comprising three allylic groups, however S-FSOL contains a primary alcohol whereas S-NER contains a tertiary alcohol. This structural difference will be discussed later. As shown in Figure 3.3.3, across the range of copolymer compositions S-FSOL and S-NER both exhibit higher T_g than the similar copolymers derived from the monoterpene myrcene (which also contains three allylic groups) and fellow sesquiterpene farnesene.

When increasing the crosslinker length with additional allylic functional groups, as is the case between S-MYR and S-FAR, the T_g of the sulfur copolymer reduces. However the substitution of an allylic group for other functional groups, such as hydroxyls, markedly increases the T_g of the material (Figure 3.3.3). These findings suggest that the hydroxyl group plays a not

insignificant part in increasing the T_g of sulfur polymers, however there are differences between S-FSOL and S-NER. Although both exhibit similar T_g at 50 wt.%, there is a significant difference between the T_g at 20 and 30 wt.%. One possible explanation is that unlike nerolidol, farensol can undergo self-cyclisation as shown in Scheme 3.3.1.

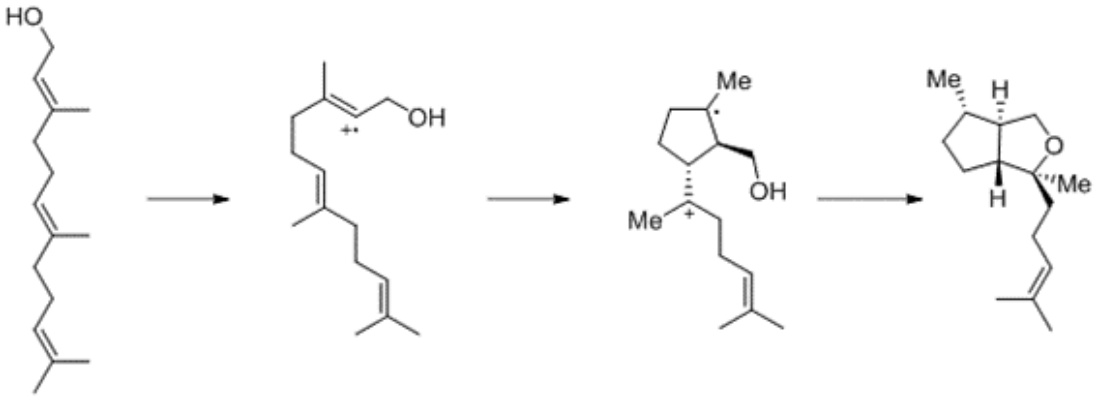

Scheme 3.3.1 Proposed scheme of the self-cyclisation of farnesol

Currently it is not fully understood why substituting the allylic group for a hydroxyl improves the T_g of the material or how the self-cyclisation of farnesol causes the T_g to differ greatly from nerolidol containing sulfur polymers. One possible theory is that as the farnesol undergoes a partial cyclisation with itself, the overall length of the crosslinker is shortened. This in turn makes a "denser" copolymer which, due to intermolecular forces acting between the elements of the copolymer, has a higher T_g than expected. There have been numerous publications on the self-polymerisation and cyclisation of general terpene,[42] myrcene,[43] and (E,E)-farnesol.[44] Shown in Scheme 3.3.1 is a possible reaction outlining how farnesol can self-cyclise.

Despite the wide variety of T_g recorded for differing copolymer compositions, the solubility of inverse vulcanised sulfur polymers derived from linear crosslinkers at 50 wt.% was remarkably consistent across the series apart from squaelene which proved to be insoluble across the series of solvents tested, as show in Table 3.3.2.

Table 3.3.2 Solubility data for S-MYR, S-FAR, S-FSOL, S-SQ and S-NER

Solvent	Solubility of sulfur copolymer (mg mL^{-1})				
	S-MYR	S-FAR	S-FSOL	S-SQ	S-NER
Acetone	Nil	Nil	Nil	Nil	Nil
Acetonitrile	Nil	Nil	Nil	Nil	Nil
Chloroform	9.70	≥ 10.0	≥ 10.0	Nil	≥10.0
Hexane	Nil	Nil	Nil	Nil	Nil
Methanol	Nil	Nil	Nil	Nil	Nil
THF	≥ 10.0	≥ 10.0	≥ 10.0	Nil	≥10.0
Toluene	≥ 10.0	≥ 10.0	≥ 10.0	Nil	≥10.0
Water	Nil	Nil	Nil	Nil	Nil

3.4 CONCLUSIONS

This chapter has shown that inverse vulcanised sulfur polymers synthesised from linear terpenoid derived crosslinking agents are possible and can exhibit a range of physiochemical properties. The linear nature of these crosslinkers allows a more hyper-branched network to form rather than a fully crosslinked polymeric network, although this can be overcome by using long chained linear terpenoids such as squalene. None of the copolymer compositions synthesised exhibited signs of translucency, such as those sulfur copolymers described in Chapter 2, however a range of colours was observed. Additionally all samples produced shape persistent materials that could be easily moulded when being cured, Figure 3.4.1.

Figure 3.4.1 Image of moulded linear sulfur copolymers (S-FAR and S-MYR), with a centimetre ruler for scale

The effect of varying the functional groups present in the crosslinker and its corresponding effect on the T_g of an inverse vulcanised copolymer is still not fully understood, although research presented in this chapter does suggest that it is possible to reduce the number of allylic groups present in the crosslinker and still improve the T_g, as observed between the sesquiterpene class of terpenoids.

3.5 REFERENCES

1. A. Behr and L. Johnen, *ChemSusChem*, 2009, **2**, 1072-1095.
2. M. B. Kolicheski, L. C. Cocco, D. A. Mitchell and M. Kaminski, *Journal of Analytical and Applied Pyrolysis*, 2007, **80**, 92-100.
3. E.-M. Kim, J.-H. Eom, Y. Um, Y. Kim and H. M. Woo, *Journal of Agricultural and Food Chemistry*, 2015, **63**, 4606-4612.
4. A. J. Johanson, F. L. McKennon and L. A. Goldblatt, *Industrial & Engineering Chemistry*, 1948, **40**, 500-502.
5. D. L. Trumbo, *Polymer Bulletin*, 1993, **31**, 629-636.
6. P. Sarkar and A. K. Bhowmick, *ACS Sustainable Chemistry & Engineering*, 2016, **4**, 2129-2141.
7. N. Bauer, J. Brunke and G. Kali, *ACS Sustainable Chemistry & Engineering*, 2017, **5**, 10084-10092.
8. F. E. Huelin and K. E. Murray, *Nature*, 1966, **210**, 1260-1261.
9. R. W. Gibson and J. A. Pickett, *Nature*, 1983, **302**, 608-609.
10. J. Šobotník, R. Hanus, B. Kalinová, R. Piskorski, J. Cvačka, T. Bourguignon and Y. Roisin, *Journal of Chemical Ecology*, 2008, **34**, 478-486.
11. K. Murray, *Australian Journal of Chemistry*, 1969, **22**, 197-204.
12. C. Wang, S.-H. Yoon, H.-J. Jang, Y.-R. Chung, J.-Y. Kim, E.-S. Choi and S.-W. Kim, *Metabolic Engineering*, 2011, **13**, 648-655.
13. P. P. Peralta-Yahya, M. Ouellet, R. Chan, A. Mukhopadhyay, J. D. Keasling and T. S. Lee, *Nature Communications*, 2011, **2**, 483.
14. C. Halfmann, L. Gu, W. Gibbons and R. Zhou, *Applied Microbiology and Biotechnology*, 2014, **98**, 9869-9877.
15. C. Cugini, M. W. Calfee, J. M. Farrow III, D. K. Morales, E. C. Pesci and D. A. Hogan, *Molecular Microbiology*, 2007, **65**, 896-906.
16. E. J. Corey, J. A. Katzenellenbogen and G. H. Posner, *Journal of the American Chemical Society*, 1967, **89**, 4245-4247.

17. J. M. Hornby and K. W. Nickerson, *Antimicrobial Agents and Chemotherapy*, 2004, **48**, 2305.

18. C. Wang, S.-H. Yoon, A. A. Shah, Y.-R. Chung, J.-Y. Kim, E.-S. Choi, J. D. Keasling and S.-W. Kim, *Biotechnology and Bioengineering*, 2010, **107**, 421-429.

19. J. E. Baldwin, R. E. Hackler and D. P. Kelly, *Journal of the American Chemical Society*, 1968, **90**, 4758-4759.

20. G. Teller, Y. Nakatani, G. Ourisson, M. Keller, D. Hafenbradl and K. O. Stetter, *Angewandte Chemie International Edition in English*, 1995, **34**, 1898-1900.

21. H. Koo, M. F. Hayacibara, B. D. Schobel, J. A. Cury, P. L. Rosalen, Y. K. Park, A. M. Vacca-Smith and W. H. Bowen, *Journal of Antimicrobial Chemotherapy*, 2003, **52**, 782-789.

22. M. A. Jabra-Rizk, T. F. Meiller, C. E. James and M. E. Shirtliff, *Antimicrobial Agents and Chemotherapy*, 2006, **50**, 1463.

23. M. Kuroda, S. Nagasaki, R. Ito and T. Ohta, *FEMS Microbiology Letters*, 2007, **273**, 28-34.

24. J. G. Jeon, S. Pandit, J. Xiao, S. Gregoire, M. L. Falsetta, M. I. Klein and H. Koo, *International Journal Of Oral Science*, 2011, **3**, 98.

25. M. Tsujimoto, *Journal of Industrial & Engineering Chemistry*, 1920, **12**, 63-72.

26. K. E. Bloch, *Critical Reviews in Biochemistry*, 1983, **14**, 47-92.

27. J.-J. Pan, J. O. Solbiati, G. Ramamoorthy, B. S. Hillerich, R. D. Seidel, J. E. Cronan, S. C. Almo and C. D. Poulter, *ACS Central Science*, 2015, **1**, 77-82.

28. P. Bhattacharjee, V. B. Shukla, R. S. Singhal and P. R. Kulkarni, *World Journal of Microbiology and Biotechnology*, 2001, **17**, 811-816.

29. X. Song, X. Wang, Y. Tan, Y. Feng, W. Li and Q. Cui, *Journal of Agricultural and Food Chemistry*, 2015, **63**, 8445-8451.

30. H. Thoms and A. Biltz, in *Arbeiten aus dem Pharmazeutischen Institut der Universität Berlin: Zweiter Band: Umfassend die Arbeiten des Jahres 1904*, ed. H. Thoms, Springer, Berlin, Heidelberg, 1905, ch. Über die Bestandteile des weißen Perubalsams, pp. 127-131.

31. J. K. Thum, *The Journal of the American Pharmaceutical Association (1912)*, 1915, **4**, 1496-1498.

32. W.-K. Chan, L. T.-H. Tan, K.-G. Chan, L.-H. Lee and B.-H. Goh, *Molecules*, 2016, **21**, 529.

33. M. C. de Freitas, K. C. B. de Oliveira, A. de Camargo Faria, E. N. dos Santos and E. V. Gusevskaya, *Catalysis Science & Technology*, 2014, **4**, 1954-1959.

34. B. F. Brehm-Stecher and E. A. Johnson, *Antimicrobial Agents and Chemotherapy*, 2003, **47**, 3357.

35. D. C. Arruda, F. L. Alexandri, A. M. Katzin and S. R. B. Uliana, *Antimicrobial Agents and Chemotherapy*, 2005, **49**, 1679.

36. F. M. Ferreira, C. M. Palmeira, M. M. Oliveira, D. Santos, A. M. Simões, S. M. Rocha, M. A. Coimbra and F. Peixoto, *Toxicology in Vitro*, 2012, **26**, 189-196.

37. M. Arslan, B. Kiskan and Y. Yagci, *Macromolecules*, 2016, **49**, 767-773.

38. Y. Zhang, J. J. Griebel, P. T. Dirlam, N. A. Nguyen, R. S. Glass, M. E. Mackay, K. Char and J. Pyun, *Journal of Polymer Science Part A: Polymer Chemistry*, 2017, **55**, 107-116.

39. L. Bateman and A. Natural Rubber Producers' Research, *The chemistry and physics of rubber-like substances; studies of the Natural Rubber Producers' Research Association*, Maclaren; Wiley, London; New York, 1963.

40. D. Dondi, A. Buttafava, A. Zeffiro, C. Palamini, A. Lostritto, L. Giannini and A. Faucitano, *European Polymer Journal*, 2015, **62**, 222-235.

41. R. S. Glass, *Topics in Current Chemistry*, 2018, **376**, 22.

42. K. Satoh, *Polymer Journal*, 2015, **47**, 527-536.

43. J. Raynaud, J. Y. Wu and T. Ritter, *Angewandte Chemie International Edition*, 2012, **51**, 11805-11808.

44. H. Weng, C. Scarlata and H. D. Roth, *Journal of the American Chemical Society*, 1996, **118**, 10947-10953.

Chapter 4: Applications for Heavy Metal Remediation

Contents

4.1 INTRODUCTION

As discussed previously in Chapter 1 there is a rapid and growing need to tackle the issues caused by heavy metal pollution in our environment. In addition there is also a need to develop a method for quick, cheap and efficient remediation of pre-existing toxic metals present in the environment. Similarly with the increasing demand for both consumer and industrial electronics, there is an increased demand for precious metals such as gold to be extracted in greater quantities.

By utilising inverse-vulcanised polymers and the inherent properties of sulfur with its ability to bind with metals, coupled to finding a method of optimising the surface area, it is possible to tailor the material properties of the inverse vulcanised polymers to maximise their potential uptake capacity. Current methods rely heavily on the physisorption process and highly porous materials to make efficient use of this process, however these materials are extremely energy intensive and consume a large quantity of raw materials. By introducing the chemisorption abilities of a high sulfur content polymer, similar uptake capacities can be achieved when compared to traditional materials but with a lower overall surface area and reduced raw material cost.

This chapter will first explore multiple different methods of inducing porosity into inverse vulcanised sulfur polymers before proceeding to dicuss how these materials were evaluated and the subsequent *in situ* heavy metal testing that followed.

4.2 SURFACE AREA OPTIMISATION

In order to improve the uptake of metals onto the polymer, it is important to maximise the surface area present as this allows increased efficiency of the material. This chapter primarily focuses on four different methods of

increasing/optimising the surface area (mechanical grinding, supercritical CO_2 foaming, carbonisation and coated solid supports) of different inverse vulcanised polymers synthesised.

4.2.1 MECHANICAL GRINDING

The simplest method of increasing the surface area of a given material that has intrinsically low porosity is to break it into smaller pieces, thus increasing the surface area per mass of material used. Grinding samples can be extremely quick and particle size can easily be controlled by sifting the ground/powdered material through a set of mesh sieves. However the mechanical grinding process produces heat which means that polymers with a low T_g may not be suitable unless the process can be run at a low temperature whilst grinding is carried out. Additionally, even with the use of mesh sieves, particle size distribution can vary slightly between batches causing a degree of error which is unacceptable should repeat batches be needed for testing.

Mechanical grinding was used primarily as a screening tool to quickly provide metal uptake results, due to its rapid ability to process numerous samples. This allowed the materials tested to be compared and certain copolymer compositions to be picked for further study. All samples were ground using either a pestle and mortar or an electric grinder before being sieved through a series of mesh sieves (35 and 60 Mesh respectively) resulting in a powder with a particle size between 250 and 500 μm.

4.2.2 SUPERCRITICAL CO_2 FOAMING

By turning a polymeric block into a powder, its surface area is dramatically increased. However a powder is intrinsically material inefficient as only the surface of the particle is exposed, whereas a larger porous particle would have a greater overall surface area available. In addition, the use of powders as

sorbents in flow systems is extremely difficult, due to the back-pressure generated being inversely proportional to the square of the particle size.[1] This ultimately diminishes the utility of fine powders as a filtration medium and therefore an alternative means was sought to increase the available surface area.

It was decided that supercritical carbon dioxide ($scCO_2$) would be used in an attempt to foam several inverse vulcanised polymers, and thus introduce an element of porosity to their structure. Carbon dioxide has low toxicity, is non-combustible, is a waste by-product and is considered as an environmentally benign foaming agent.[2, 3] Under ambient laboratory conditions, CO_2 is a gas and can therefore easily be removed from the reactor once the foaming process has completed without leaving residual solvent on the material. Outside these ambient conditions and above its critical point (31.06 °C and 7.38 MPa), CO_2 turns supercritical leaving the fluid with zero surface tension and tuneable density.[4] Once in its supercritical state CO_2 acts in a similar way to many other solvents in respect to interaction with a polymer: making it swell and acting as a plasticiser. On releasing the pressure in the reactor vessel, the dissolved $scCO_2$ rapidly expands as it reverts back to CO_2 gas foaming the polymer in the process.[5, 6]

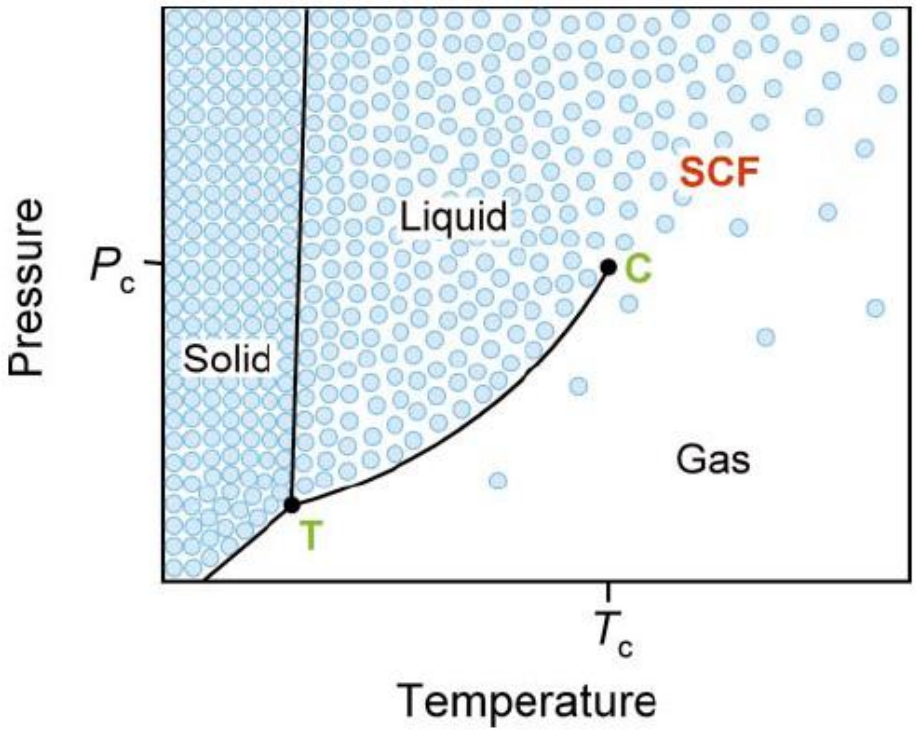

Figure 4.2.1 Illustration of the phase diagram for carbon dioxide, taken from[2] Shown on the diagram are the Triple Point (T) and Critical Point (C). The blue circles represent the density of CO_2 in the diagram with the supercritical fluid (SCF) region labelled. The critical temperature (T_c) and pressure (P_c) are also shown.

Four inverse-vulcanised sulfur polymers were chosen for $scCO_2$ foaming treatment; DIB, DCPD, myrcene and farnesol copolymers. All copolymer compositions used were of a 50:50 sulfur to crosslinker ratio, with the exception of the sulfur –DIB copolymer which was additionally synthesised in a 70:30 sulfur to crosslinker ratio. The five sulfur copolymers were freshly synthesised prior to foaming. In order to establish the optimal reaction parameters to foam the various copolymer compositions, the sulfur-DIB copolymer was chosen. Several reaction parameters were chosen to be altered including the autoclave temperature and pressure. Temperatures of 40, 60 and 80 °C, along with autoclave pressures of 10, 20 and 28 MPa were investigated. Figure 4.2.2 shows the effect of increasing temperature and time on the diffusion of CO_2 in to the copolymer. After 30 minutes of soaking $scCO_2$ had not fully penetrated the copolymer samples "core" (samples b – d) and

therefore it was decided that a soak time in excess of 30 minutes would achieve this (sample e was soaked for 180 minutes).

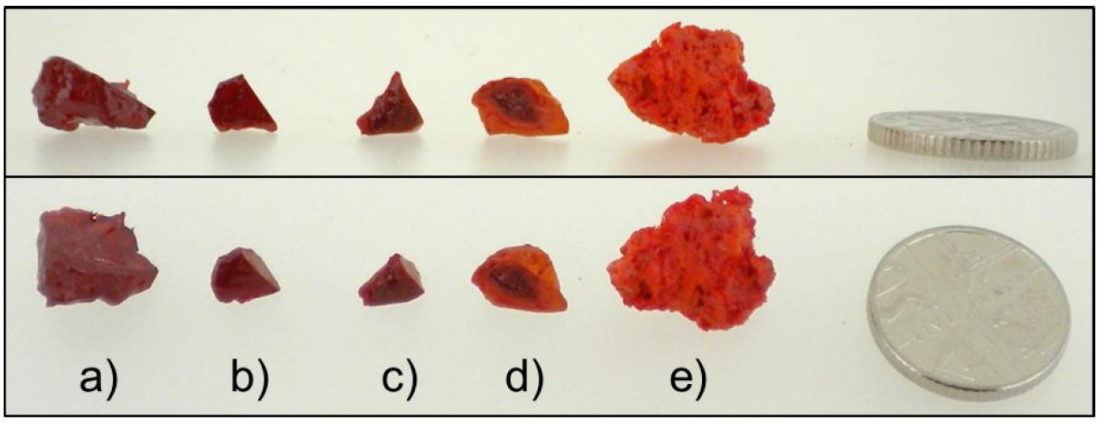

Figure 4.2.2 Photographed cross sections of 70:30 S-DIB copolymer. a) Before $scCO_2$ processing. b) 40 °C soak for 30 minutes. c) 60 °C soak for 30 minutes. d) 80 °C soak for 30 minutes. e) 80 °C soak for 180 minutes. A five pence piece is shown for scale.

After determining that reaction conditions of 80 °C and a soak time of 180 minutes produced a fully foamed copolymer, the effect of varying the pressure of $scCO_2$ in the autoclave was tested. Several samples from the same batch of 50:50 S-DIB copolymer were placed in the autoclave which was pressurised to 10, 20 or 28 MPa and heated to 80 °C for 180 minutes. As shown by the micrographs in Figure 4.2.3, increasing the pressure in the autoclave has a correlative effect on the density and size of the pores generated during the foaming process. This correlative effect is attributed to the increased homonucleation caused at higher pressures, due to the increased quantity of CO_2 dissolved in the swollen polymer and is in accordance with the findings of Tsivintzelis *et al*.[7]

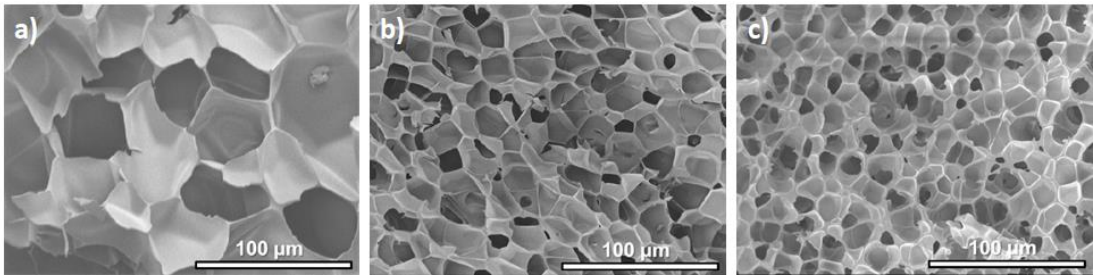

Figure 4.2.3 Scanning electron micrographs of 50:50 S-DIB copolymers. Copolymers were foamed at 80 °C, 180 minutes and variable pressures showing decreasing void size with increasing $scCO_2$ pressure. a) Sample at 10 MPa. b) Sample at 20 MPa. c) Sample at 28 MPa.

4.2.3 COATED SOLID SUPPORTS

4.2.3.1 POTENTIAL SOLID SUPPORTS

Certain inverse vulcanised copolymers proved to be more soluble in organic solvents compared with others. As discussed in Chapters 2 and 3, this is likely caused by a combination of factors but primarily the more oligomeric rather than fully hyper-branched or crosslinked structure of certain inverse vulcanised copolymers. Although these copolymers may exhibit poorer physical properties (for example lack of shape persistence and lower T_g) and therefore might seem undesirable for some applications, the ease with which they can be dissolved into a solution allows these copolymers to be readily applied as a coating to various supports and substrates. With regard to the adsorption of metal ions, decoupling the functionality of the copolymer from the requirements of maximising its surface area allows both factors to be independently tailored for the required task.

Applying polymer coatings to surfaces and substrates to either enhance the properties of the material or to protect the underlying structure is not a new concept and there are multiple methods of achieving this.[8-10] The copolymers chosen were soluble in organic solvents, such as toluene and tetrahydrofuran (THF), and a method of wet impregnation was investigated as a rapid means to coat the copolymer compositions onto a solid support. The four solid

supports investigated were kaolinite, mordenite, dried lycopodium spores and fumed silica. Kaolinite is an aluminosilicate clay with a low iron content found in many deposits worldwide and is the bulk constituent of china clay. It is low cost and although having a low cation exchange capacity, it has been studied previously as an adsorbent for heavy metals.[11-13] A naturally occurring zeolite, mordenite is widely used in catalysis and as a sorbent due to its uniform pore structure. It can be extracted from multiple deposits globally and due to its well understood MOR framework, can be synthesised easily for commercial applications also.[14, 15] The genus *Lycopodium* comprises a large family of clubmosses, of which *Lycopodium clavatum* is a member and due to its wide availability its spores have been investigated for numerous applications.[16-18] The spores of *Lycopodium clavatum* contain the extremely chemically inert biopolymer sporopollin.[19] Fumed silica, also known as pyrogenic silica, is synthesised by introducing either a silica precursor (usually some form of silane or siloxane) or quartz into a high temperature flame (≥ 1000 °C) which fuses together these discrete particles into small agglomerated masses.[20, 21] Although fumed silicas are not porous, due to their non-conformal chainlike structures they do possess surface areas in the hundreds of metres squared per gram range.[22, 23] The four solid supports chosen were readily available from numerous suppliers and were compatible with the wet impregnation method.

Initial results from trialling the wet impregnation method on fumed silica were conducted with catalysed S-LIM copolymers. The catalysed S-LIM copolymers were chosen as their increased T_g, when compared to non-catalysed S-LIM copolymers, led to less polymer creep and improved shape persistency whilst still having a lower molecular weight (M_w) than other inverse vulcanised copolymers. This reduced M_w meant that the catalysed S-LIM copolymers were more readily soluble than other potential sulfur

copolymers and therefore were more easily coated onto fumed silica supports. An arbitrary 10 wt.% loading of S-LIM copolymers was chosen with copolymers synthesised with either 0, 1 or 5 wt.% catalyst loading present and coated onto fumed silica. The copolymers were coated onto the fumed silica by first dissolving 500 mg of the chosen catalysed S-LIM copolymer in 50 mL of THF in a round bottom flask. Once dissolved, 5.0 grams of fumed silica was added to the polymer/solvent solution, the flask was then capped and agitated on a vortex shaker for 5 minutes before transferring the flask to a rotary evaporator equipped with a dry ice condenser. The water bath of the rotary evaporator was set to 35 °C and the THF was removed under low vacuum conditions, yielding a free flowing yellow powder. Once fully dry the powders were transferred to clean, capped glass vials.

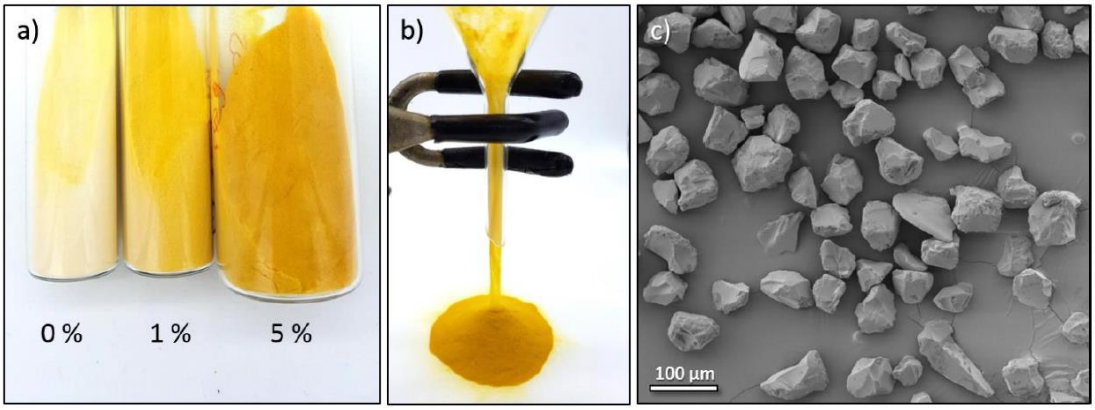

Figure 4.2.4 a) Photograph of fumed silica coated with a 10 wt.% loading of S-LIM copolymer synthesized using 0 wt.% (left), 1 wt.% (middle), and 5 wt.% catalyst (right). b) Photograph of the polymer coated fumed silica flowing through a funnel as a free flowing powder. c) SEM micrograph of the particles after coating with polymer.

Figure 4.2.4 shows that all three types of copolymer coated onto the fumed silica produced free flowing powders (although the polymers darkened with catalyst loading) with the small particle size of fumed silica retained and no agglomeration or aggregation of particles. Results were positive, with capacities of 17.9 mg and 38.8 mg per gram of coated sorbent reported for mercury and gold capture respectively. Detailed information relating to the

testing protocol and metal salts used in these tests can be found in section 5.4.3 This translated to a capacity of 716 mg of mercury per gram of polymer used and a control test between uncoated fumed silica and 5 wt.% catalysed S-LIM showed that silica itself has negligible capacity for the remediation of mercury from solution (Figure 4.2.5).[24] It was therefore desirable to conduct a full study on the effects of different solid supports, polymer composition and polymer loading on the uptake of heavy metal contaminants.

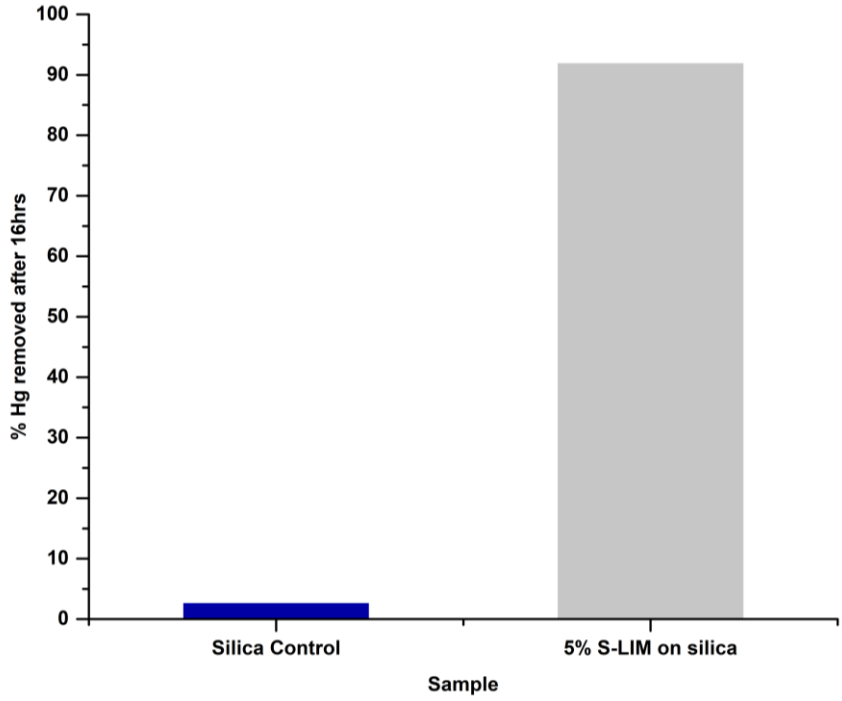

Figure 4.2.5 Comparison between the uncoated silica support and a sample of silica loaded with 5% catalysed S-LIM

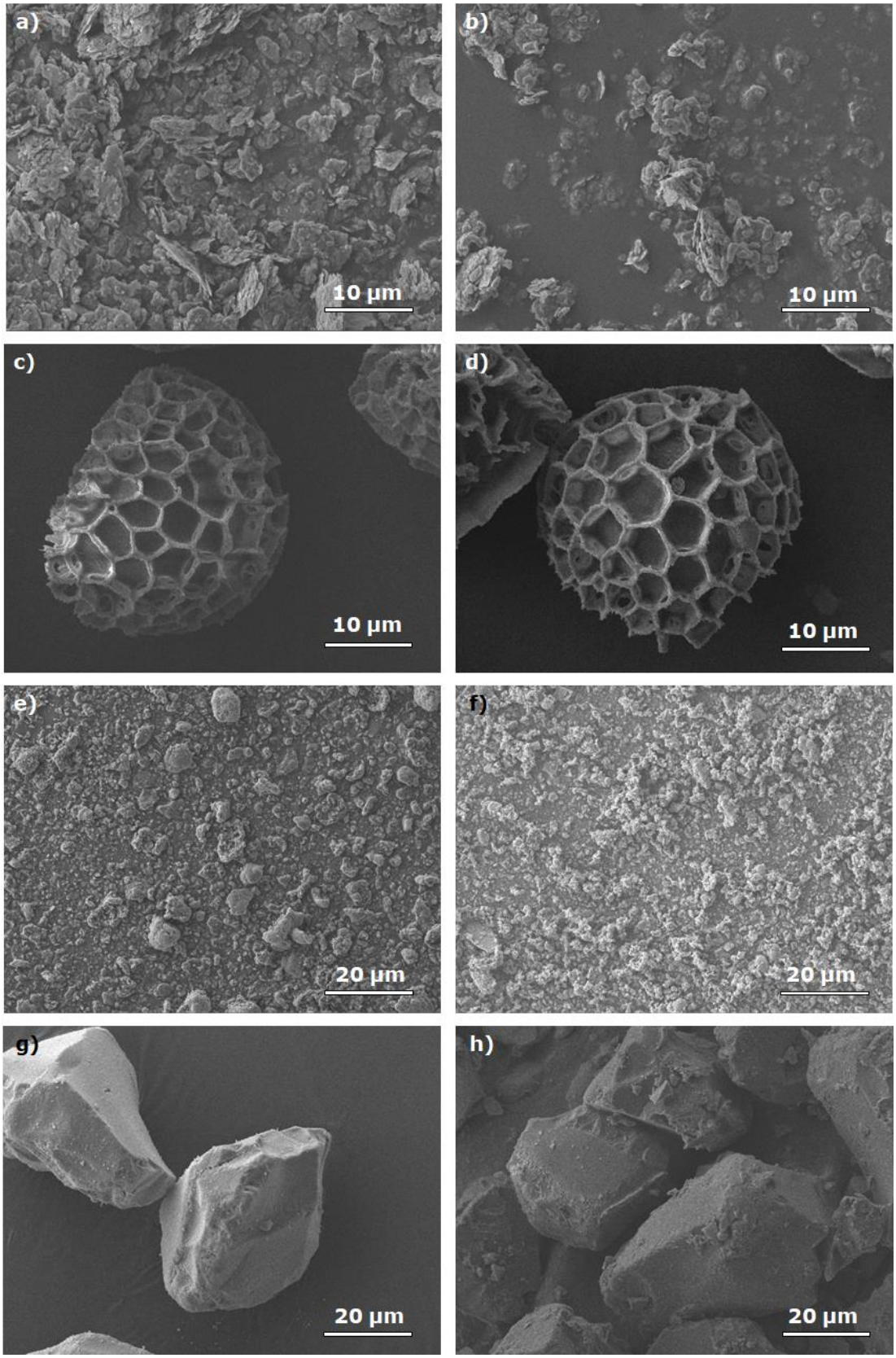

Figure 4.2.6 Scanning electron micrographs of the solid supports pre and post coating with S-HOP copolymer. a) Kaolinite. b) Kaolinite coated. c) Lycopodium. d) Lycopodium coated. e) Mordenite. f) Mordenite coated. g) Fumed silica. h) Fumed silica coated.

Samples were initially coated with a 50:50 sulfur-HOP copolymer at a 10 wt.% loading. This was achieved by dissolving 500 mg of copolymer in 50 mL of THF in a round bottom flask, to which 5.0 grams of solid support was added and the flask stoppered. The resultant slurry was agitated for 10 minutes using a vortex mixer. The round bottom flask was then transferred to a rotary evaporator (water bath set to 35 °C), where the THF was removed under low vacuum. As can be seen from the micrographs shown in Figure 4.2.6, the surface morphologies do not appear to drastically change when coated with 50:50 sulfur-HOP copolymer. However to fully understand the effects of coating on the solid supports, nitrogen sorption was conducted to determine the effects of coating on the pore structure and surface area of the solid supports after coating. Table 4.2.1 shows the calculated Brunauer – Emmett – Teller (BET) surface area measurements, calculated from nitrogen sorption studies conducted at 77 K, of the solid supports before and after wet impregnation with sulfur-HOP copolymer.

Table 4.2.1 Surface area data for solid supports before and after coating.

	Surface Area		
	Before ($m^2 g^{-1}$)	After ($m^2 g^{-1}$)	% Reduction
Kaolinite	15.15	8.26	45.48
Mordenite	264.32	8.41	96.82
Lycopodium	7.25	5.37	25.93
Fumed Silica	451.09	344.74	23.58

It is interesting to note that although all of the solid supports saw a reduction in the available surface area after coating, which would be expected, the available surface area of the mordenite solid supported sample reduced by ≥ 96.5 %. Mordenite was specifically chosen as a comparative to fumed silica as commercially available mordenite can have surface areas in excess of 500 $m^2 g^{-1}$.[25] The most likely explanation for the extremely low surface area reported

with respect to the mordenite solid support is due to the ability of mordenite to act as a molecular sieve. Since the impregnation step was not conducted under dry conditions the mordenite simply removed any water present in the solution and therefore the coating was primarily applied to the exterior surface of the particles only.

By contrast the coated silica solid support only lost approximately 23% of its available surface area post impregnation with the S-HOP copolymer. The majority of surface area lost was in the microporous and small mesoporous region with larger mesopores still available, as show in Figure 4.2.7.

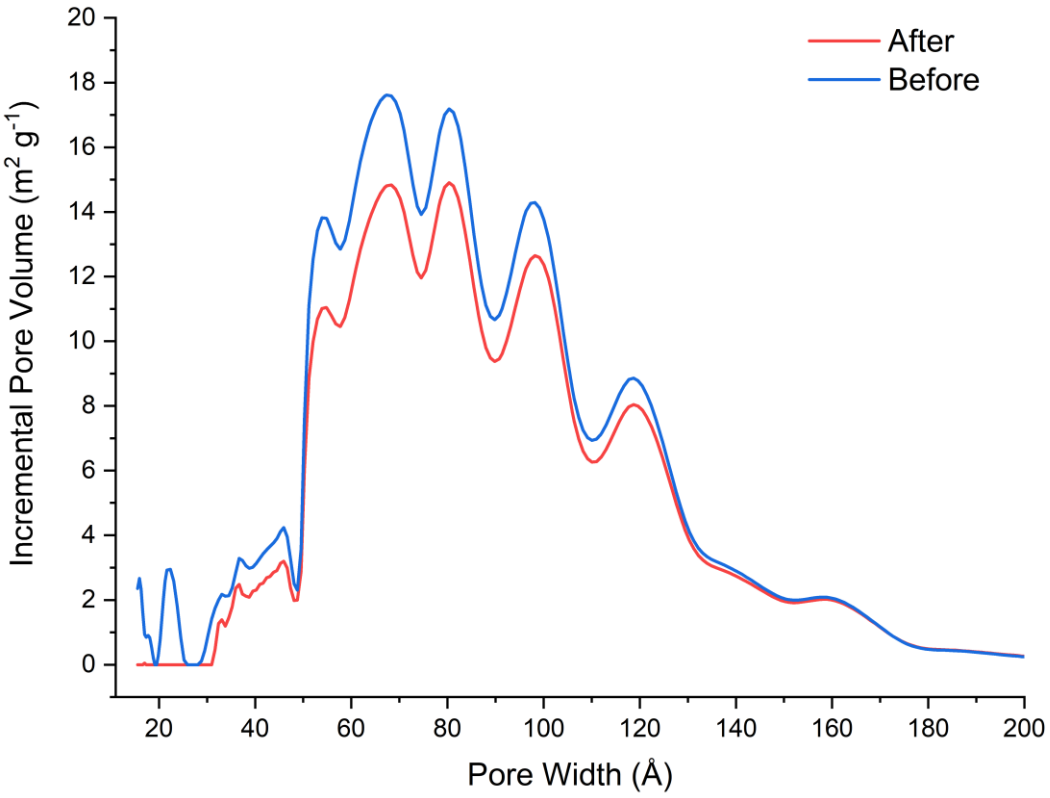

Figure 4.2.7 Overlaid plots of incremental surface area vs. pore size for silica before (blue) and after coating (red) calculated from nitrogen sorption isotherms at 77 K.

4.2.3.2 POLYMER LOADINGS AND COPOLYMER COMPOSITIONS

To optimise the polymer coatings two criteria have to be met, first is the determination of the optimal polymer loading and secondly the effect of the

sulfur content of the copolymer on uptake capacity. To find the optimum polymer loading for the solid supports fumed silica was coated at four different wt.% loadings, a fifth sample was left uncoated to determine what effect fumed silica had on capacity, and 120 mg of each was exposed to a 2000 ppm mercury solution for 16 hours using the standard testing protocol in 5.4.3.2. As can be seen from the results shown in Figure 4.2.8 there is a correlation between polymer loading and how it affects both total sorbent capacity and the polymer capacity.

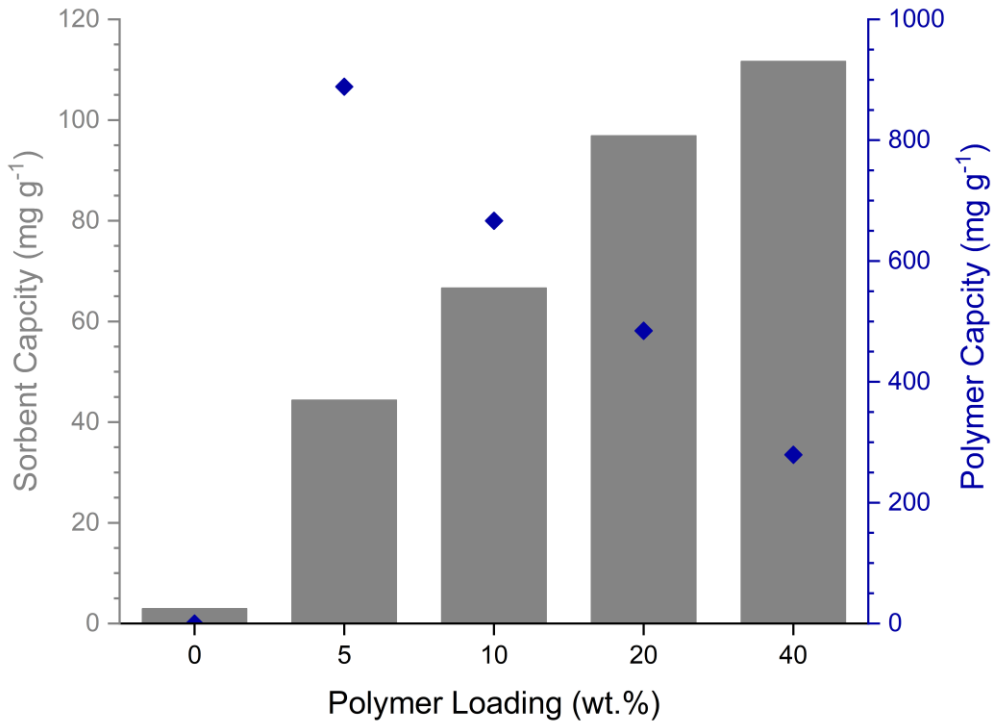

Figure 4.2.8 Graph showing the effect of polymer loading on sorbent capacity (grey) and polymer capacity (blue).

The total sorbent capacity (Q_s) is given by first calculating the amount of mercury removed, by comparing the test solution (C_{test}) to the control sample (C_{con}) and then dividing the result by the mass of sorbent (M_s) present in the test. This result is then multiplied by 1000 to yield the results in mg of mercury per gram of sorbent. The same formula is used to calculate the capacity of the

polymer (Qp) by substituting the total sorbent mass (M_s) for that of the mass of the sulfur copolymer (M_p) coated on to the silica.

Equation 4.2.1 Formulae for calculating total sorbent capacity (Q_s) and polymer capacity (Q_p) of solid supported sulfur copolymers.

$$Q_s = \frac{C_{con} - C_{test}}{M_s} \times 1000 \qquad Q_p = \frac{C_{con} - C_{test}}{M_p} \times 1000$$

These quick formulae allow a rapid assessment of how an inverse vulcanised sulfur copolymer coated solid support performs for a given test. However in order to get a full understanding of the potential of a material as a sorbent and to accurately calculate its overall capacity, then a series of isothermal tests needs to be conducted. Once conducted these data sets can be plotted and fitted to a Freundlich - Langmuir adsorption isotherm (Equation 4.2.2) to calculate a Q_{sat} value for capacity of the material. However since the tests in this section were used to rapidly determine an optimised set of conditions for further tests it was felt that a full Freundlich - Langmuir analysis and the subsequent number of experiments needed was not required at this stage.

Equation 4.2.2 The Freundlich - Langmuir adsorption isotherm, where Q_{sat} is the maximum capacity (mg g^{-1}), q_a is the mg of adsorbate per g of adsorbent, K is the adsorption parameter (L mg^{-1}) and Ce is the equilibrium concentration (mg L^{-1}).

$$q_a = \frac{K \times C_e \times Q_{sat}}{1 + K \times C_e}$$

Overall sorbent capacity increased with polymer loading which is unsurprising since pure fumed silica does not adsorb mercury from solution: therefore with increasing polymer coating content the greater volume of functionalised surface is available for sorption to take place. However by increasing the wt.% of polymer coating present on the silica, the polymer capacity for mercury capture is decreased as the coating present is likely to be thicker resulting in only the surface of the inverse vulcanised copolymer being exposed to the test solution. The results in Figure 4.2.8 suggested that a loading of approximately 15 wt.% would allow for a suitable compromise

between the total sorbent capacity and polymer capacity, however due to the time constraints present in a PhD program it was decided to slightly favour sorbent capacity for further tests over polymer capacity and therefore a polymer loading of 20 wt.% was chosen for all future solid support tests.

After deciding on the optimal polymer loading for the solid supports, the effect of polymer composition and therefore the effect of sulfur on the total uptake capacity of the sorbent was tested. These tests were conducted by coating fumed silica at a 20 wt.% loading with three different ratios of the same sulfur copolymer. 50:50, 60:40 and 70:30 ratios of sulfur to hop oil were chosen and were coated using the same method described in 4.2.3.1 Attempts were made to solubilise the 80:20 S-Hop copolymer in THF for coating, however the high sulfur content prevented the copolymer from fully dissolving.

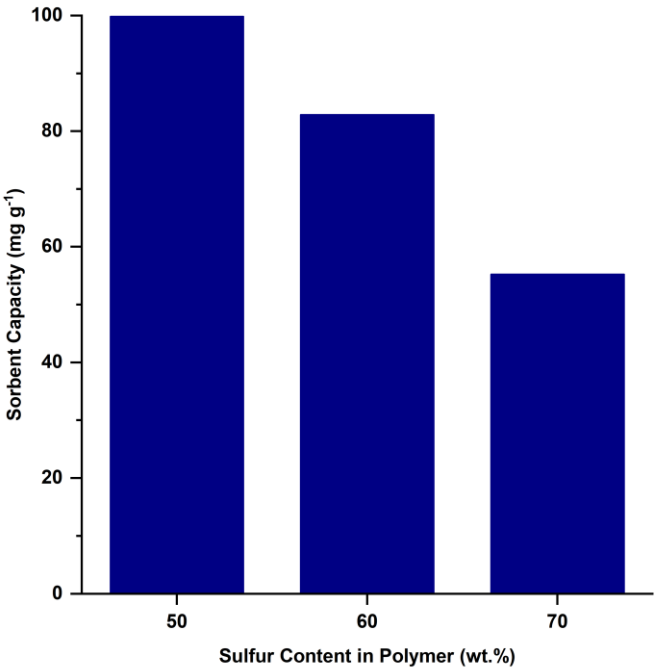

Figure 4.2.9 Bar chart showing the effect of sulfur content on sorbent capacity of S-HOP copolymers coated onto silica solid supports

Figure 4.2.9 shows that as the content of sulfur present in the copolymer increases, the total sorbent capacity decreases. This result was unexpected since it was believed that a higher sulfur content polymer would be able to

sequester more mercury from solution. The most logical explanation for this unexpected result is that as the sulfur content in the copolymer increases it becomes increasingly difficult to solubilise for coating. This in turn may have led to an uneven coating being applied to the fumed silica which could introduce an element of pore blocking, reducing the overall surface area available.

4.2.4 CARBONISATION

An alternative method for producing microporous filtration media from inverse vulcanised sulfur polymers is to carbonise them, if necessary in the presence of a chemical to aid the activation and generation of pores. To first understand the process of carbonisation, it is important to understand how this process differs from the other commonly used scientific term, pyrolysis. Pyrolysis, derived from the roots *-pyro* (fire) and *-lysis* (separation), is the thermal decomposition process of a material under high temperature in an inert atmosphere.[26] Carbonisation, however, is only achieved by heating the material at a much higher temperatures of between 800 to 1500 °C (Figure 4.2.10) therefore carbonisation is considered to be extreme pyrolysis.[27] At these high temperatures the majority of the material has been volatilised with carbon primarily left as a residue.

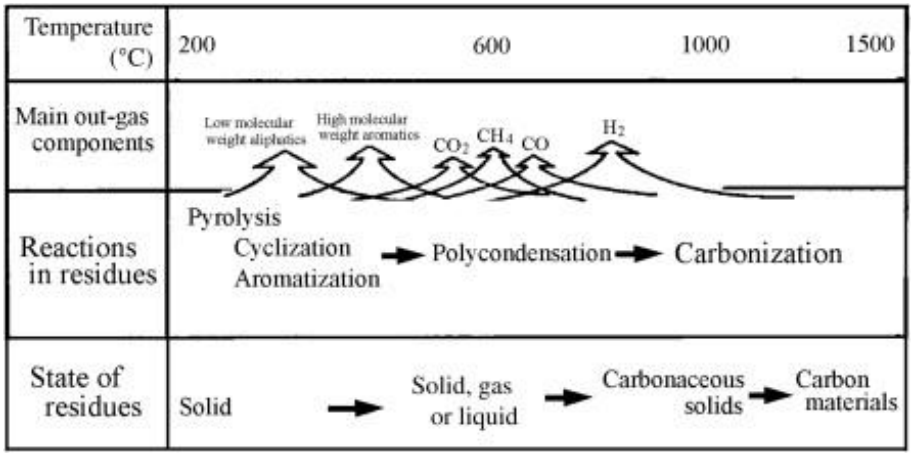

Figure 4.2.10 The carbonisation process, reproduced from[27]

In the case of carbonising inverse vulcanised sulfur polymers, the pore structure is generated through the formation of void spaces caused by the bulk removal of sulfur from the copolymer. Under carbonaceous conditions the sulfur copolymer precursor losses most of its sulfur content, as sulfur-sulfur bonds are weaker than carbon-sulfur or carbon-carbon bonds, therefore forming a "functionalised" activated carbon due to the carbon residue containing a layer of sulfur/sulfur copolymer at its surface.

Due to the need for a copolymer with a high T_g, sulfur-DCPD was chosen for carbonisation experiments. Porous sulfur-DCPD samples were prepared by either the "direct" or "activated" methods by Jet-Sing M. Lee of the Cooper Group.[28] Briefly the synthesis of the porous materials was achieved by taking 50:50 sulfur-DCPD copolymer, as synthesised in 5.2.2.1, and placing a ground portion of the copolymer in a ceramic boat within a tube furnace purged with N_2 and heated to the specified temperature at 5 °C min^{-1} and held for a desired time. The same method was used to synthesise the "activated" microporous materials by incorporating potassium hydroxide (KOH) with the sulfur-DCPD copolymer as it was ground in a pestle and mortar. After carbonisation the samples were washed with DI to remove any residual KOH and dried under vacuum. To aid the formation of high surface area carbonised sulfur copolymers, KOH was used as a chemical activating agent. One of several chemical activating agents, KOH has previously been reported as a known aid to porosity generation due to the following reaction.[29]

$$6KOH + 2C \rightarrow 2K + 3H_2 + 2K_2CO_3$$

The formation of potassium carbonate (K_2CO_3) further generates porosity through the production of CO_2, due to the decomposition of K_2CO_3 at high temperature. The addition of KOH slightly reduced the sulfur content remaining in the carbonised sulfur copolymers. It was instead the effect of increasing temperature that significantly reduced the sulfur content, although

increasing the weight equivalence of KOH did have a direct effect on the yield (Table 4.2.2).

Table 4.2.2 Carbonisation yields and elemental analysis results for S-doped porous carbon products.

Sample	Yield (%)	Elemental Analysis		
		C	H	S
S-DCPD-750	35	77.25	0.63	17.67
S-DCPD-850	32	81.86	0.50	11.89
0.5K-S-DCPD-750	23	74.91	0.35	13.54
1K-S-DCPD-750	34	74.14	0.55	13.27
2K-S-DCPD-750	14	78.37	0.95	12.77
4K-S-DCPD-750	16	77.98	0.55	12.73
1K-S-DCPD-850	34	69.40	0.87	9.55

When assessing the effect on pore volume and surface area of carbonised inverse vulcanised polymers by carbonisation with KOH, Table 4.2.3 shows the optimum reaction conditions required. To maximise micropore formation whilst having the highest calculated BET surface area the addition of KOH in a 1:1 stoichiometric ratio with respect to the mass of the sulfur copolymer is required, with the carbonisation process being conducted at 750 °C.

Table 4.2.3 Physical properties of KOH activated S–DCPD carbons. [a]Calculated by single point pore volume. [b]Total pore volume at P/P_0 = 0.99.

Sample	Surface Area ($m^2\ g^{-1}$)		Pore Volume[a] ($cm^3\ g^{-1}$)	
	BET	Langmuir	Micropore	Total pore[b]
0.5K-S-DCPD-750	1792	2379	0.51	1.00
1K-S-DCPD-750	2216	2976	0.80	1.09
2K-S-DCPD-750	2197	3015	0.68	1.21
4K-S-DCPD-750	1520	1995	0.26	0.92
1K-S-DCPD-850	1599	2226	0.48	0.84

With the addition of KOH to the carbonisation process, the materials went from a wholly microporous structure to one which contained both mesopores and micropores. This hierarchal porous structure enables a surface area greater than 2200 $m^2 g^{-1}$ to be formed, comparing extremely favourably to traditional activated carbons.[30]

4.3 RESULTS AND DISCUSSION

4.3.1.1 INORGANIC AND ORGANIC MERCURY

As established in Chapter 1.3.1 mercury in both its inorganic and organic forms are extremely toxic compounds that can ultimately be fatal to living organisms. Even though the Minamata Convention has been effective since August 2017 mercury is still used in multiple industrial process.[31] Due to its persistence and ability to bioaccumulate, there is a clear need for a cheap and efficient means to remediate mercury from the environment. Due to the extremely high sulfur content of inverse vulcanised copolymers, these materials should make ideal candidates for effective mercury remediation.

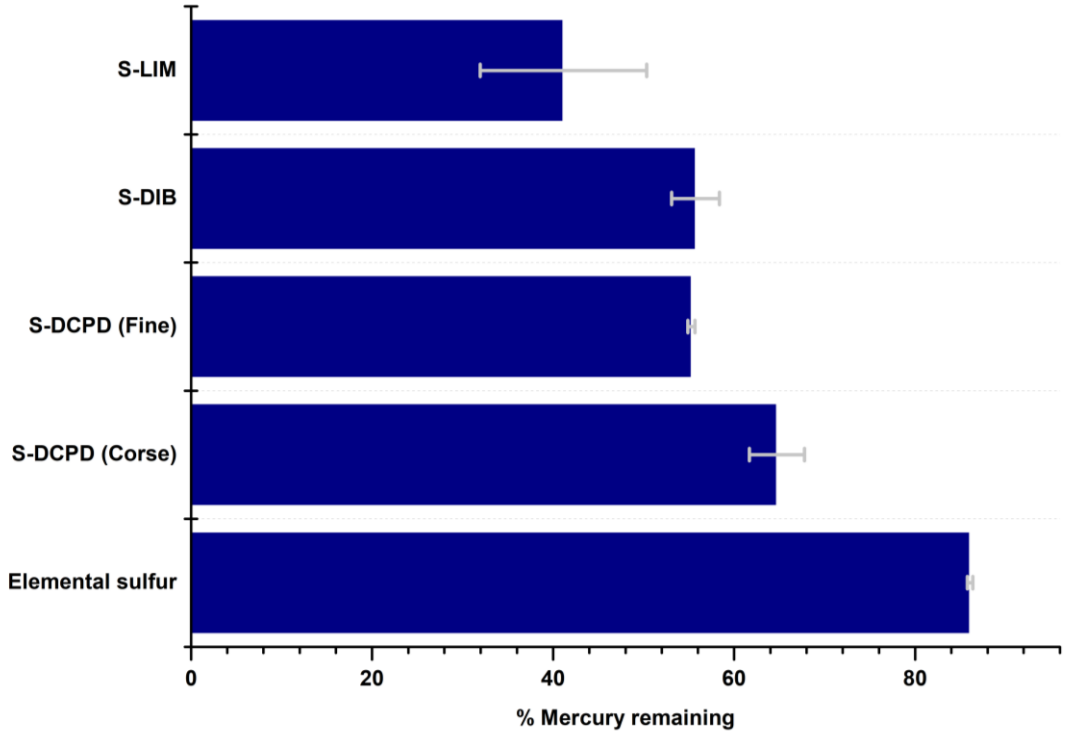

Figure 4.3.1 Mercury chloride removed from a 2 ppm aqueous solution using various inverse vulcanised sulfur polymers

Previous research published by Chalker *et al*. had shown that S-LIM could successfully be used for the remediation of mercury at low concentrations,[32] and in doing so proved the theory that high sulfur content polymers could be used as a successful sorbent. Therefore initial studies were conducted on inverse vulcanised sulfur polymers that had already be published; S-LIM copolymer,[32] and S-DIB.[33] This was deemed necessary in order to develop a reliable testing protocol using known materials.

The data from these first tests was encouraging with good reductions in mercury chloride content when compared to elemental sulfur alone. It was therefore felt that the next logical step would be to conduct triplicate tests to determine the repeatability of the test protocol and to experiment with the newly synthesised S-DCPD copolymer. The results from these tests are shown in Figure 4.3.1. From this it was ascertained that the repeatability of the 2 ppm mercury uptake tests was extremely good for all samples apart from the S-LIM, which had a much larger spread of results. This is attributed to the

physical characteristics of the S-LIM polymer, which due to its low T_g is in a sticky tar-like state at room temperature. This meant that unlike the other samples that could freely move around in the solution as small particles, the S-LIM mostly stuck to the side of the glass vial for the duration of the experiment and the differing uptake values differed depending on how much of the polymer was "spread" along wall of the vial. The results also show little difference between the coarsely ground and finely ground DCPD samples, indicating that a better method for increasing the polymer surface area was required.

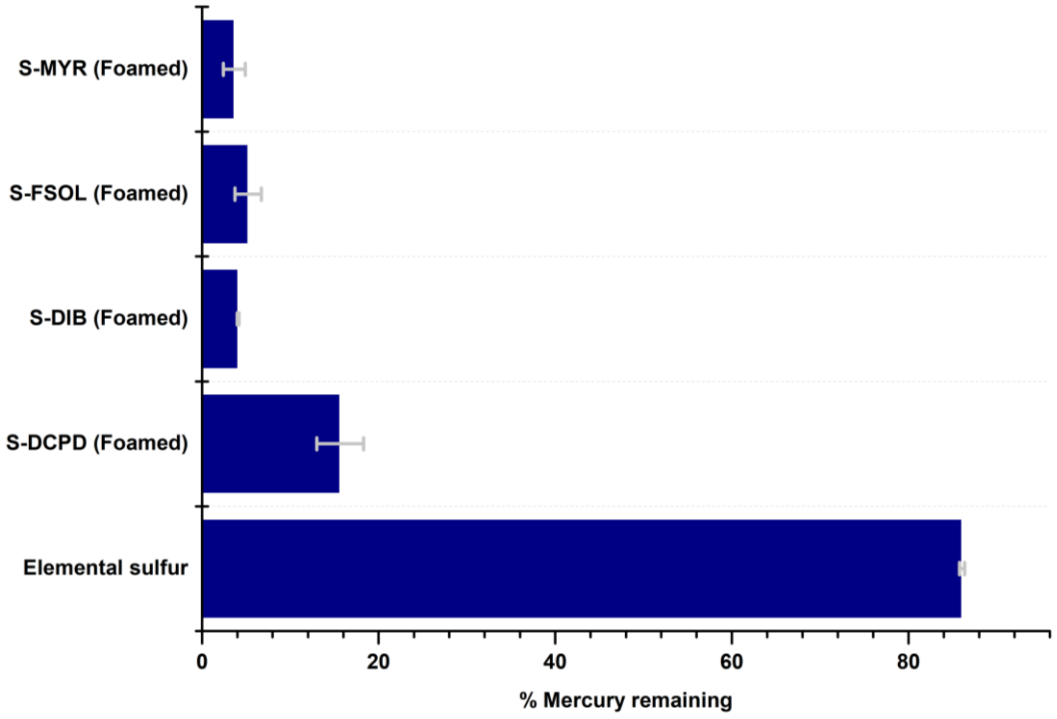

Figure 4.3.2 Comparison of $scCO_2$ foamed sulfur polymers and elemental sulfur, showing the amount of mercury remaining from a 2 ppm solution

Once additional sulfur copolymers, containing myrcene and farnesol as crosslinking agents, had be synthesised and foamed using $scCO_2$ to increase the available surface area, the 2 ppm mercury uptake test were repeated. These results (Figure 4.3.2) were plotted against those of the previous test shown in Figure 4.3.1 and the results were startling in their differences. Once foamed with $scCO_2$, S-DCPD showed a three-fold increase in the amount of

mercury adsorbed compared with untreated ground samples of the same copolymer. Equally impressive were the results for foamed S-MYR and S-FSOL copolymers which removed almost all of the mercury present in the test sample with good repeatability. Figure 4.3.2 clearly showed that to fully understand and maximise their potential, tests would need to be conducted using higher concentrations and with samples of sulfur copolymers which had measurably large surface areas.

Following on from the foaming experiments, samples of S-DCPD were successfully carbonised to yield a highly functionalised activated carbon, containing less than 14 wt.% of sulfur these activated carbons proved extremely good at remediating mercury chloride from solutions (Figure 4.3.3).

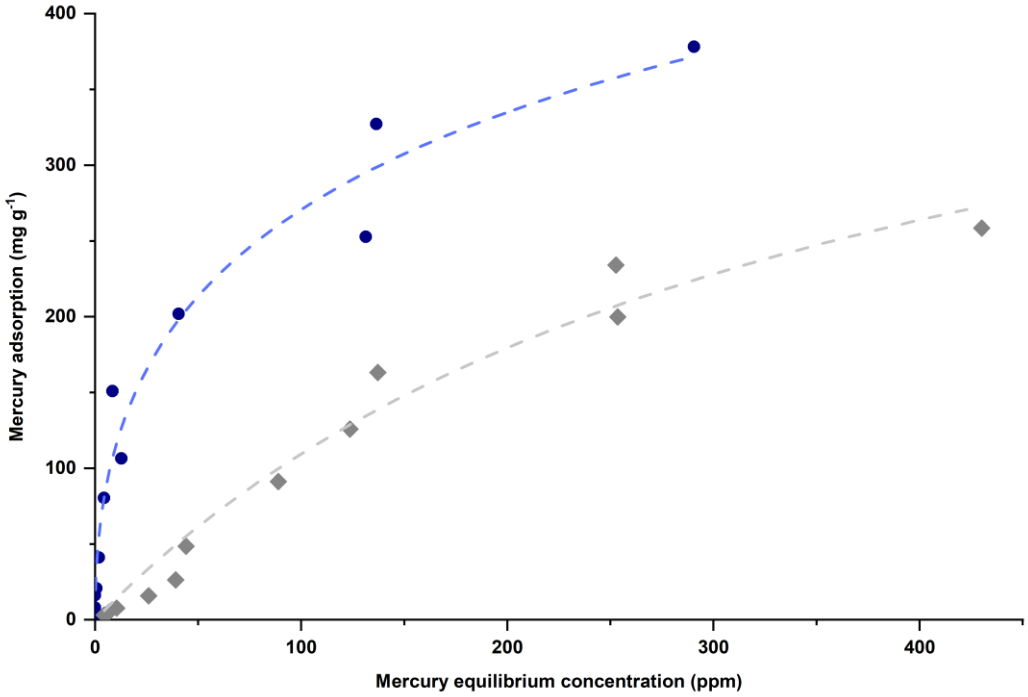

Figure 4.3.3 The adsorption isotherm of mercury (as aqueous $HgCl_2$) into samples of carbonised S-DCPD copolymer (blue circles) and conventional activated carbon (grey diamonds), with Langmuir isotherm fitting shown (dotted lines).

From the adsorption isotherms plotted in Figure 4.3.3 an uptake capacity for the carbonised S-DCPD was calculated. Once fitted to a Langmuir-Freundlich isotherm a capacity of 850 mg g^{-1} was calculated, compared to just 498 mg g^{-1}

for the industry standard activated charcoal. When compared to carbonised S-DCPD other reported carbonaceous materials perform equally poorly with a series of other activated carbons, some of which had surface treatments. The maximum capacities obtained for these materials were in the range of 50 to 700 mg g^{-1} with the majority failing to exceed the 500 mg g^{-1}.[34] These results additionally show that starting with a high sulfur content copolymer, rather than post treatment impregnation with sulfur or sulfur contain species is the preferred method as there is an almost three-fold increase in capacity using S-DCPD (850 mg g^{-1}) compared with sulfur impregnated activated carbon (294 mg g^{-1}).[35]

It is also important to note the difference in steepness of the fitted mercury uptake isotherms between the carbonised S-DCPD and activated carbon samples (Figure 4.3.3). The steepness of the carbonised sulfur copolymer samples directly relates to the uptake kinetics and shows that S-DCPD has a far higher specificity for mercury, even at low levels, compared to commercially sourced activated carbon. When compared at a low equilibrium concentration of 10 ppm, the carbonised S-DCPD had a sorption capacity that was over 19 times greater than that of activated carbon (151 mg g^{-1} *versus* 7.8 mg g^{-1}). This is especially relevant for "real world" applications since the concentration of mercury in the environment is mostly found in low levels. Governmental limits on the maximum amount of mercury allowed to be present in drinking water are extremely low, for example the US Environmental Protection Agency (EPA) sets a limit for safe drinking water of 2.0 μg L^{-1}.[36, 37]

Initial studies conducted with catalysed S-LIM coated onto a silica solid support revealed similar trends to those observed with carbonised S-DCPD samples, although the surface area between the two types of material varied

by approximately a factor of four, giving good uptake values for the coated silica when compared against commercially obtained activated carbon.

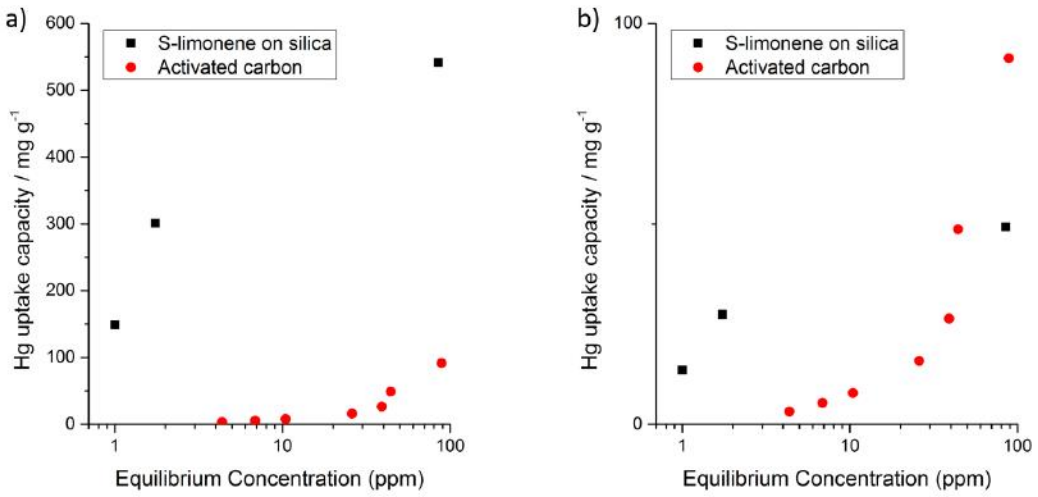

Figure 4.3.4 Mercury uptake isotherms, from aqueous solutions of $HgCl_2$, by S-LIM copolymers coated onto fumed silica compared to commercial activated carbon. a) Hg uptake into S-LIM coated on fumed silica calculated from the mass of copolymer only. b) Hg uptake into S-LIM coated on fumed silica gel calculated from the total mass of sorbent (copolymer and silica).

As is show in Figure 4.3.4, the S-LIM copolymer coated on fumed silica has a much higher affinity than activated carbon for inorganic mercury at industrially relevant low concentrations. It is only at higher concentrations (≥ 40 ppm) that activated carbon starts to exhibit a greater uptake capacity for mercury. One major advantage of using coated solid supports is that not only can the capacity for the total sorbent be calculated but also that of the polymer applied. If we were to consider just the polymer rather than the whole sorbent then catalysed sulfur-LIM has an uptake capacity in excess of 500 mg g^{-1}, which is five times greater than activated carbon. This compares extremely favourably to other sulfur polymers investigated as inorganic mercury sorbents. Theato *et al*. published work on electrospun high sulfur content fibres as sorbents for mercury remediation and reported a maximum uptake capacity of 440 mg g^{-1} for the fibres.[38] Electrospinning fibres is a low yield, time consuming and costly process compared with coating sulfur copolymers onto solid supports, resulting in a sub-optimal solution for mercury

remediation when taking into consideration the uptake capacity per gram of polymer used.

Although there have been several reported instances of inverse vulcanised sulfur polymers for use as inorganic mercury sorbents, there has been very little work on the remediation for much more toxic organomercury compounds. The exception being a study into the effectiveness of a porous sulfur-canola oil copolymer in the remediation of a methoxyethyl mercury chloride based pesticide.[39] As established in Chapter 1, organomercury compounds are far more toxic to humans than inorganic mercury due in part to the ease with which these compounds can be absorbed into the body. Since inorganic mercury waste left in the environment can convert to orgonmercury compounds it was felt that tests should be conducted using methylmercury chloride.

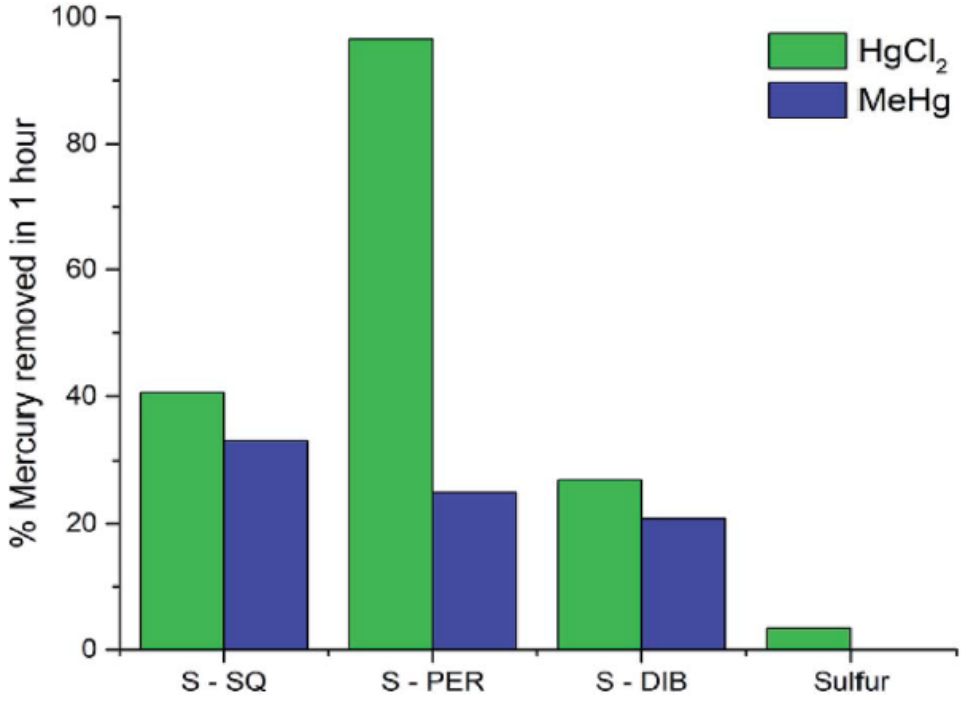

Figure 4.3.5 Mercury uptake results for mercury chloride and methylmercury chloride from 2.5 ppm aqueous solutions after 1 hour.

Initial tests were conducted on sulfur-squalene (S-SQ), sulfur-perillyl alcohol (S-PER), S-DIB and elemental sulfur to determine the effectiveness of sulfur

polymers to adsorb such a comparatively small organomercury compound, shown in Figure 4.3.5. Interestingly, unlike previous tests with inorganic mercury, elemental sulfur does not appear to interact at all with methylmercury. Despite the low concentration of methylmercury used in the tests, all sulfur copolymer successfully removed between 20 – 30% of the methylmercury present in one hour with S-SQ preforming the best. Further tests were conducted using S-PER and S-HOP coated onto fumed silica as a solid support, with the concentration of methylmercury in the test solutions increased by 80 times. Results from these tests indicate that S-HOP coated onto fumed silica outperformed the previously published porous sulfur-canola oil by an order of magnitude, with the S-HOP coated silica having a calculated methylmercury capacity of 25.6 mg g^{-1} of sorbent used and the copolymer itself having a calculated capacity of 128 mg g^{-1}.

4.3.1.2 GOLD

Gold is a precious, rare earth metal that is increasingly in demand and therefore the ability to sequester gold using a low cost sulfur copolymer is of significant interest to those in the mining, electronic and catalysts sectors.[40] In the mining sector there is a drive towards using hydrometallurgical extraction methods as a more environmentally friendly route for the extraction of gold rather than the use of toxic cyanide based methods.[41]

Tests were conducted using both sulfur copolymer coated onto fumed silica and carbonised S-DCPD copolymer. Due to gold being in the same period as mercury it was anticipated that results would be broadly similar. However it appears that inverse vulcanised copolymers possess a far greater affinity for gold than first thought. As can be seen in Figure 4.3.6, the trends between samples for mercury and gold are similar. Initial tests used a 400 ppm solution for both gold and mercury tests. Over a 16 hour period the S-LIM coated silica

removed gold from solution to a level that was undetectable using ICP-OES and therefore the test had to be repeated at twice the concentration.

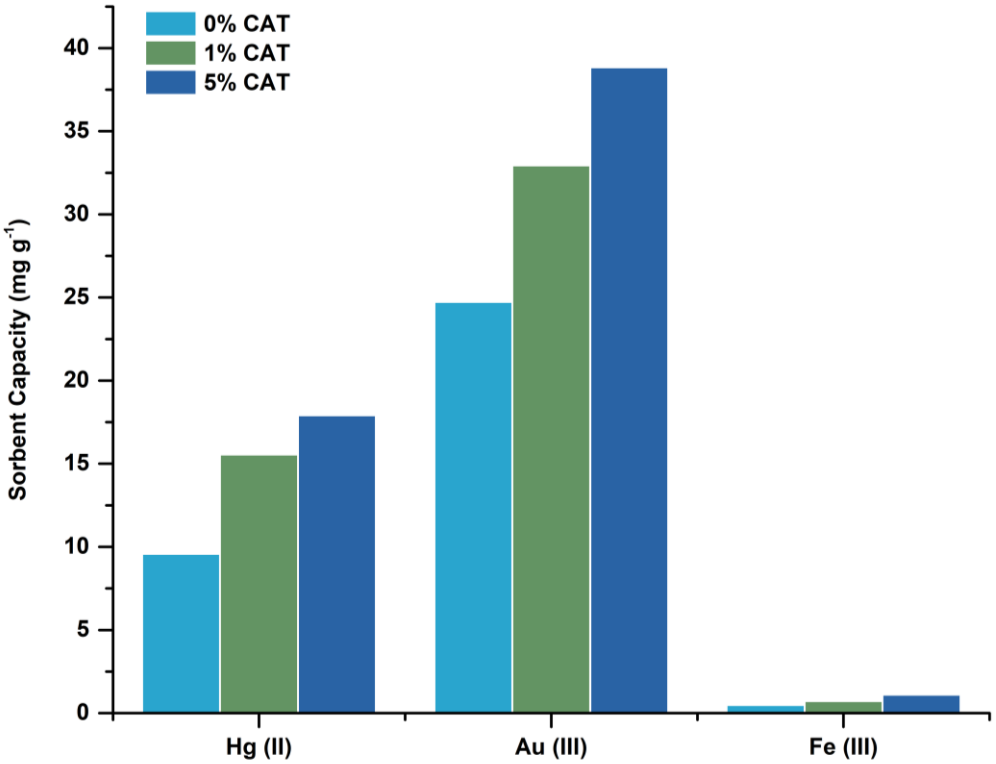

Figure 4.3.6 Metal uptake by S-LIM coated silica gel from 400 ppm aqueous solution of mercury chloride and iron chloride, and 800 ppm gold chloride, with varying $Zn(DTC)_2$ catalyst loading, after one hour. Experimental details found in 5.4.3

These results were extremely positive as it showed that inverse vulcanised based sorbents could potentially be used in hydrometallurgical extraction, due to their apparent high capacities. Therefore a capacity study was conducted between carbonised S-DCPD and commercially available activated carbon (since activated carbon is known as suitable sorbent for precious metals). Using 2000 ppm solutions and chloroaurcic acid ($HAuCl_4$) as the gold salt in solution, isothermal tests were conducted with the results shown in Figure 4.3.7. From the sharp curves present in the isotherms, it is clear that carbonised S-DCPD has a similar affinity for gold as activated carbon at low equilibrium ppm. However at equilibrium concentrations that exceed 200 ppm it is shown

that S-DCPD has a capacity that is three times greater than commercial activated carbon, with a maximum capacity of 1497 mg g^{-1}.

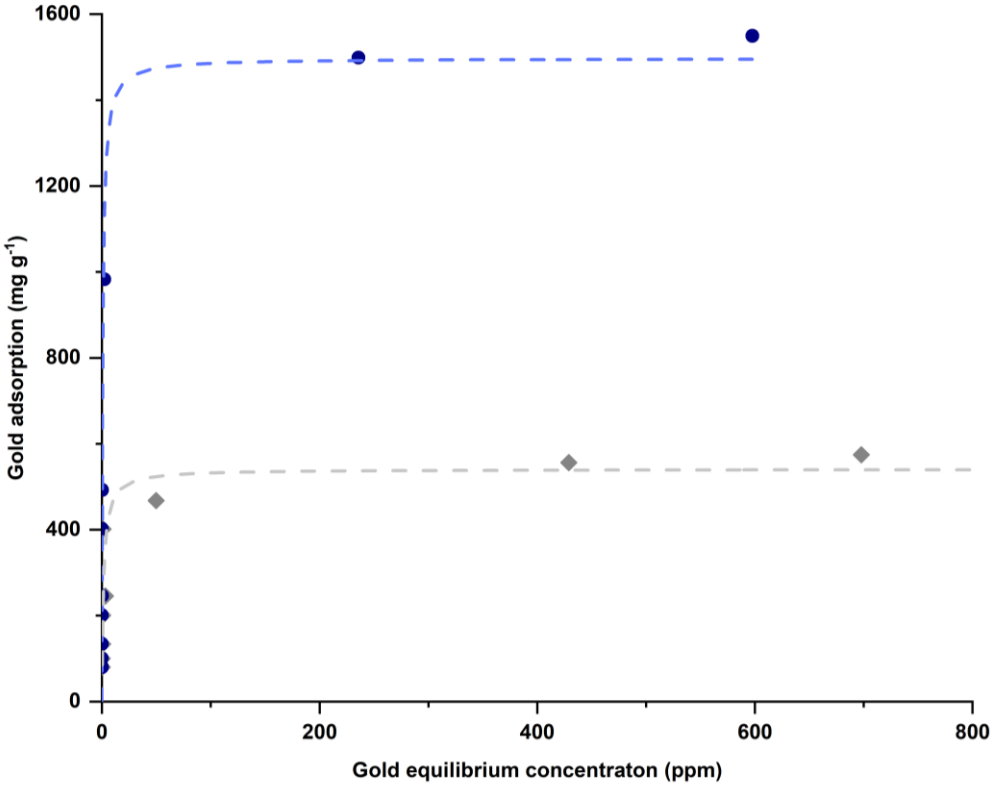

Figure 4.3.7 The adsorption isotherm of gold (as aqueous $HAuCl_4$) onto samples of carbonised sulfur polymer (blue circles) and conventional activated carbon (grey diamonds), with Langmuir isotherm fittings shown (dashed lines)

4.3.1.3 OTHER METALS

Although the primary focus for testing these inverse vulcanised copolymers involved gold and mercury salts, it was felt that additional tests should be conducted on a variety of other metals. Other metals chosen (cadmium, chromium, nickel and lead) are also extremely biopersistent and toxic, therefore it was felt that it was important to test these new inverse vulcanised materials for their potential to sequester other harmful metalloids. Relatively non-toxic first row transition metals such as copper and iron were also included to establish the specificity of these potential new sorbents.

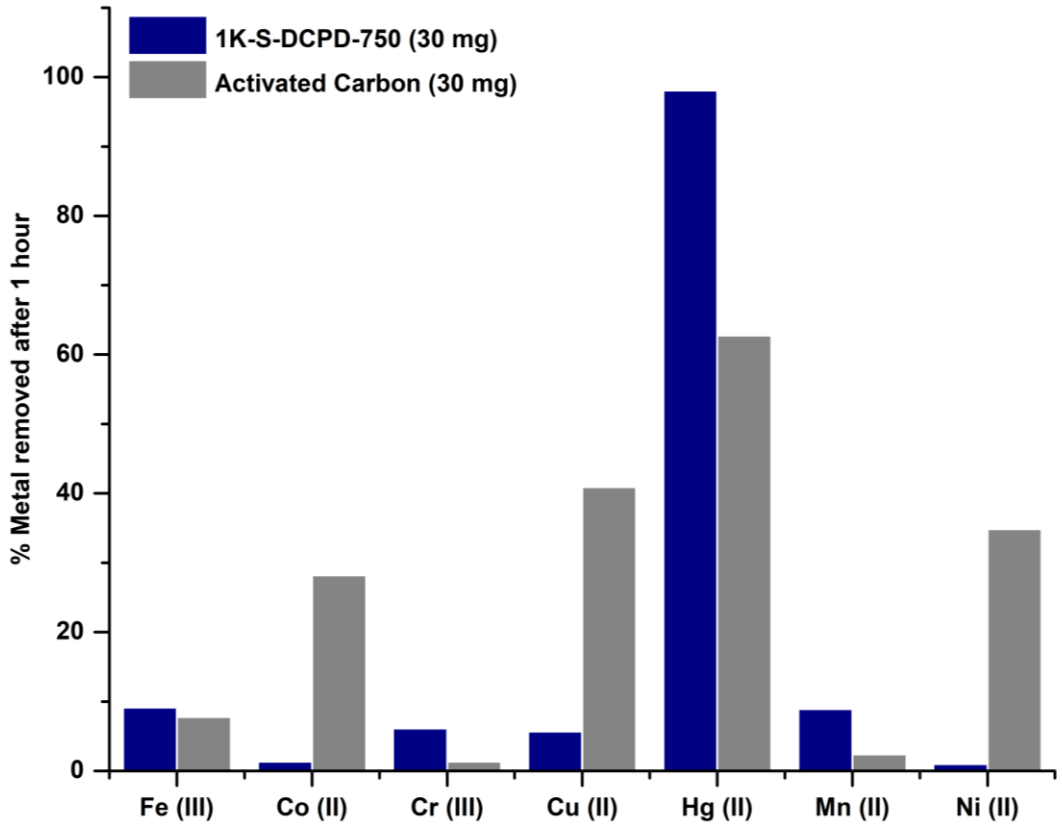

Figure 4.3.8 Metal uptake of 1K-S-DCPD-750 (blue) and activated carbon (grey) for a series of metal salts. Experimental details found in 5.4.3

In the testing of carbonised sulfur polymers, sample 1K-S-DCPD-750 was exposed to multiple metal salts, Figure 4.3.8. The carbonised sulfur copolymer, 1K-S-DCPD-750, was synthesised by carbonising S-DCPD in the presence of KOH at 1:1 wt. ratio at 750 °C for two hours. As can be seen from these results, activated carbon preforms poorly against known industrial pollutants chromium and manganese both of which are extremely toxic to humans in large doses or in prolonged exposures.[42-44] This effect cannot be wholly attributed to the increased surface area of 1K-S-DCPD when compared with activated carbon, since both materials performed comparably against iron and the activated carbon out preforms the carbonised S-DCPD copolymer when tested against copper and nickel. Therefore when trying to remediate certain toxic heavy metalloids a degree of chemisorption must be occurring between the inverse vulcanised sulfur polymer and the metal ions in solution.

With this hypothesis in mind it was decided to test against other known toxic heavy metal contaminants such as cadmium and lead. Additionally, the prevalence of data from previous tests suggesting that chemisorption must be also be occurring, led to the use of S-HOP copolymer coated on a silica solid support. Despite the solid supported S-HOP having a potential surface area six times lower than carbonised sulfur polymers, it was theorised that it would retain a greater proportion of polymeric material per gram and therefore would likely have better uptake potential.

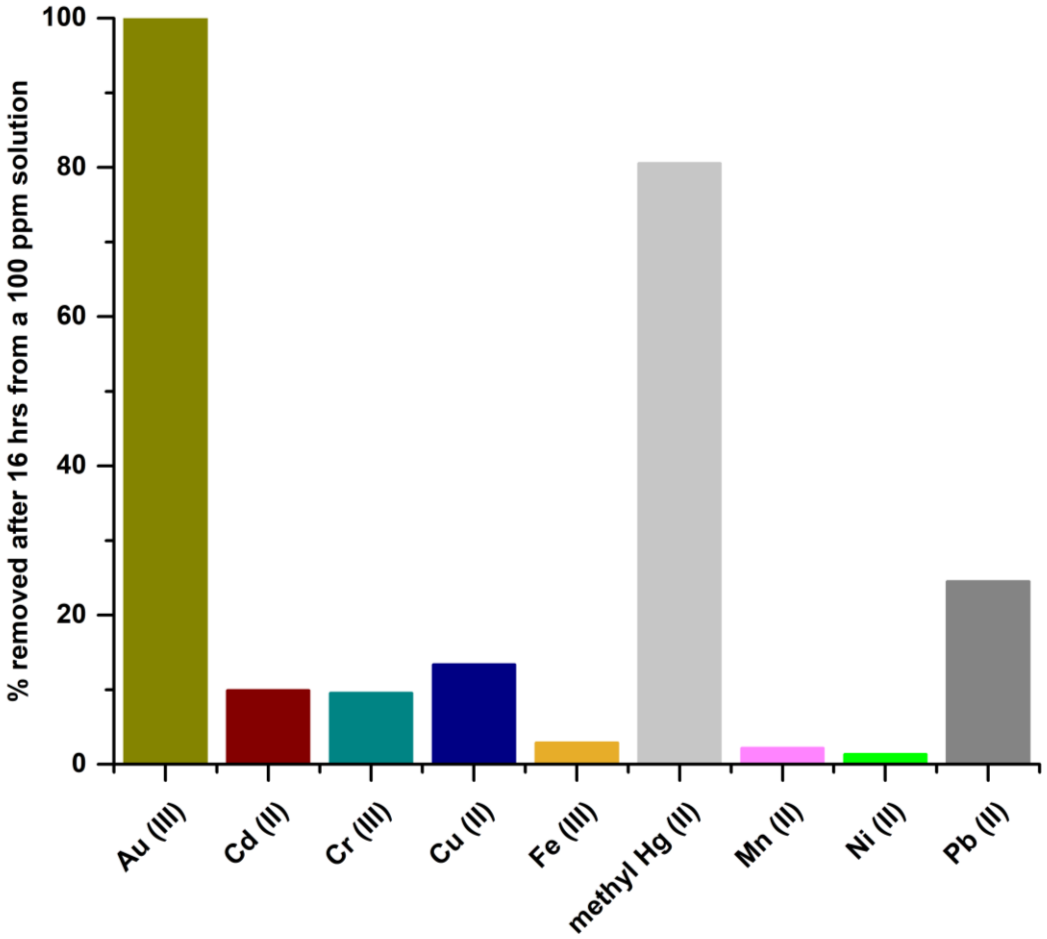

Figure 4.3.9 Uptake of various metals by S-LIM coated fumed silica solid support from 100 ppm aqueous solutions, after 16 hours. Experimental details found in 5.4.3

Similar results were noted between catalysed S-LIM (Figure 4.3.9) and carbonised S-DCPD (Figure 4.3.8) with respect to their affinities to certain metal ions and their uptake capacities calculated from 100 ppm solutions. Of

particular note are the similarities in uptake capacities of the first row transition metals. These were particularly comparable despite the large difference in surface area available, suggesting that the uptake capacity is directly related to the sulfur polymer content. This also confirms that sulfur polymers possess a greater affinity for "softer" heavy metals.

Although a higher concentration and a longer experimental duration were used in testing S-HOP coated silica solid support (Figure 4.3.10) parallels can be drawn between the sets of data as both show a similar, but unfortunately still low, uptake of chromium. The results for the cadmium and lead tests showed extremely good uptake levels after 16 hours with over a third of the cadmium removed and almost 80% of lead removed from solution. This gives a capacity of 19.23 mg g^{-1} and 35.37 mg g^{-1} for cadmium and lead respectively, which compares favourably with the inorganic mercury test conducted in parallel with these tests which demonstrated a capacity of 47.23 mg g^{-1}.

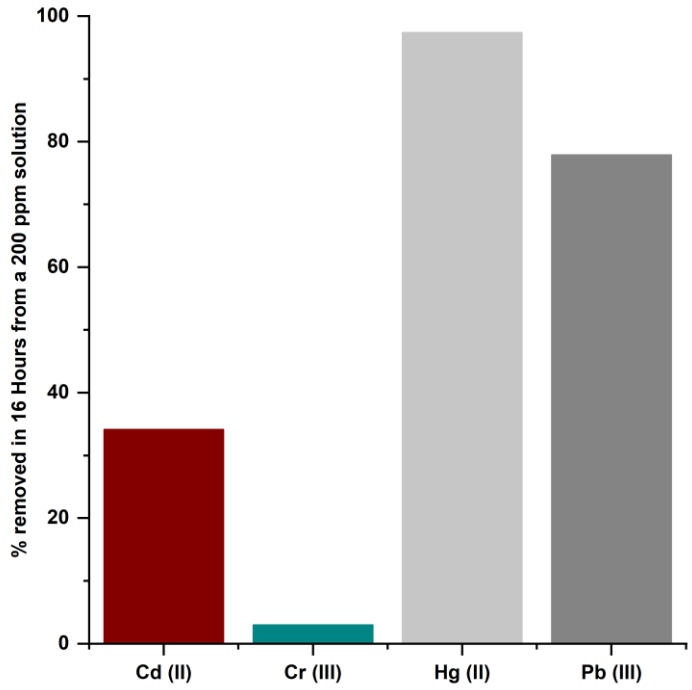

Figure 4.3.10 Reduction of metal ion concentration after 16 hours in the presence of S-Hop copolymer coated on fumed silica. Experimental details found in 5.4.3

Since previous tests have shown that the silica support has minimal impact on metal uptake (Figure 4.2.8), we can say with a great deal of certainty that the reduction of metal ions in solution after 16 hours is wholly due to the metal ions binding to the inverse vulcanised polymer deposited on the surface of the silica template. Therefore it can be inferred that the capacity of the polymer for the remediation of both cadmium and lead is an order of magnitude higher due to the copolymer loading on the silica being 20 wt.%, leading to actual capacities of 96.17 mg g^{-1} and 176.85 mg g^{-1} for both metals.

4.4 CONCLUSIONS

To summarise, factors such as crosslinker content, solubility of CO_2 in the copolymer and T_g all have varying effects on the final ability to foam an inverse vulcanised copolymer with $scCO_2$. The concentration and size of void spaces generated can be controlled to a degree by altering the autoclave pressure, temperature and soaking time, allowing a tailored structure to be produced. However $scCO_2$ tends to produce macroporous structures with mostly a closed pore structure, limiting the usefulness of $scCO_2$ as a method for producing higher surface area sorbents from inverse vulcanised sulfur polymers.

Solid support coated sorbents on the other hand, present a low-cost yet highly efficient means of maximising the surface area of inverse-vulcanised polymer synthesised. These supported copolymers may have a far lower surface area, compared with traditional filtration materials such as activated carbons, but their ability to undergo chemisorption allows these materials to possess capacities for mercury and other heavy metals into the hundreds of milligrams per gram of sorbent used. This far exceeds the ability of traditional activated carbon based filtration media. Additionally unlike activated carbons which are indiscriminate towards which metal ions they sequester from solution, it

has been shown that highly porous inverse vulcanised sulfur polymers specifically target toxic heavy metals such as mercury, lead, manganese, chromium and cadmium.

Both carbonised inverse vulcanised and solid support coated sulfur copolymers offer extremely high capacities and show great affinity for both gold and mercury salts, offering new methods to potentially remove these metals from aqueous streams. In the case of gold mining, using a sulfur polymer based method of extracting gold from solution could reduce the need to use harmful and toxic cyanide based lixiviants.[45] The low cost and high capacities of these materials makes these materials extremely attractive to industrial and bulk applications.

4.5 REFERENCES

1. P. R. Brown and E. Grushka, *Advances in Chromatography : Volume 41*, M. Dekker, New York, 2001.
2. A. I. Cooper, *Journal of Materials Chemistry*, 2000, **10**, 207-234.
3. L. J. M. Jacobs, M. F. Kemmere and J. T. F. Keurentjes, *Green Chemistry*, 2008, **10**, 731-738.
4. H. M. Woods, M. M. C. G. Silva, C. Nouvel, K. M. Shakesheff and S. M. Howdle, *Journal of Materials Chemistry*, 2004, **14**, 1663-1678.
5. T. Hasell, in *Nanocomposites*, 2013.
6. J. J. A. Barry, M. M. C. G. Silva, V. K. Popov, K. M. Shakesheff and S. M. Howdle, *Philosophical Transactions of the Royal Society A: Mathematical, Physical and Engineering Sciences*, 2006, **364**, 249-261.
7. I. Tsivintzelis, A. G. Angelopoulou and C. Panayiotou, *Polymer*, 2007, **48**, 5928-5939.
8. C. A. Bishop, in *Vacuum Deposition onto Webs, Films and Foils (Second Edition)*, ed. C. A. Bishop, William Andrew Publishing, Oxford, 2011, pp. 197-214.
9. L. F. Francis and C. C. Roberts, in *Materials Processing*, ed. L. F. Francis, Academic Press, Boston, 2016, pp. 415-512.
10. A. S. H. Makhlouf, in *Handbook of Smart Coatings for Materials Protection*, ed. A. S. H. Makhlouf, Woodhead Publishing, 2014, pp. 56-74.
11. M. K. Uddin, *Chemical Engineering Journal*, 2017, **308**, 438-462.
12. M.-q. Jiang, X.-y. Jin, X.-Q. Lu and Z.-l. Chen, *Desalination*, 2010, **252**, 33-39.
13. Ö. Yavuz, Y. Altunkaynak and F. Güzel, *Water Research*, 2003, **37**, 948-952.
14. O. Korkuna, R. Leboda, J. Skubiszewska-Zie¸ba, T. Vrublevs'ka, V. M. Gun'ko and J. Ryczkowski, *Microporous and Mesoporous Materials*, 2006, **87**, 243-254.
15. X. Li, R. Prins and J. A. van Bokhoven, *Journal of Catalysis*, 2009, **262**, 257-265.
16. R. C. Mundargi, M. G. Potroz, S. Park, J. H. Park, H. Shirahama, J. H. Lee, J. Seo and N.-J. Cho, *Advanced Functional Materials*, 2016, **26**, 487-497.
17. Z. Živcová, E. Gregorová and W. Pabst, *Journal of Materials Science*, 2007, **42**, 8760-8764.

18. G. Shaw, M. Sykes, R. W. Humble, G. Mackenzie, D. marsden and E. Pehlivan, *Reactive Polymers, Ion Exchangers, Sorbents*, 1988, **9**, 211-217.

19. C. H. Wellman, in *The Evolution of Plant Physiology*, eds. A. R. Hemsley and I. Poole, Academic Press, Oxford, 2004, pp. 43-63.

20. in *Ullmann's Encyclopedia of Industrial Chemistry*.

21. H. Zhang, D. R. Dunphy, X. Jiang, H. Meng, B. Sun, D. Tarn, M. Xue, X. Wang, S. Lin, Z. Ji, R. Li, F. L. Garcia, J. Yang, M. L. Kirk, T. Xia, J. I. Zink, A. Nel and C. J. Brinker, *Journal of the American Chemical Society*, 2012, **134**, 15790-15804.

22. R. Mueller, L. Mädler and S. E. Pratsinis, *Chemical Engineering Science*, 2003, **58**, 1969-1976.

23. H. Barthel, *Colloids and Surfaces A: Physicochemical and Engineering Aspects*, 1995, **101**, 217-226.

24. X. Wu, J. A. Smith, S. Petcher, B. Zhang, D. J. Parker, J. M. Griffin and T. Hasell, *Nature Communications*, 2019, **10**, 647.

25. H. Zhang, H. Zhang, P. Wang, Y. Zhao, Z. Shi, Y. Zhang and Y. Tang, *RSC Advances*, 2016, **6**, 47623-47631.

26. A. D. McNaught, A. Wilkinson, P. International Union of and C. Applied, *Compendium of chemical terminology : IUPAC recommendations*, Blackwell Science, Oxford, 2nd ed edn., 1997.

27. M. Inagaki and F. Kang, in *Materials Science and Engineering of Carbon: Fundamentals (Second Edition)*, eds. M. Inagaki and F. Kang, Butterworth-Heinemann, Oxford, 2014, pp. 17-217.

28. J.-S. Lee, D. J. Parker, A. I. Cooper and T. Hasell, *Journal of Materials Chemistry A*, 2017, **5**, 18603-18609.

29. S. J. Yang, H. Jung, T. Kim and C. R. Park, *Progress in Natural Science: Materials International*, 2012, **22**, 631-638.

30. F. Rodríguez-Reinoso, in *Encyclopedia of Materials: Science and Technology*, eds. K. H. J. Buschow, R. W. Cahn, M. C. Flemings, B. Ilschner, E. J. Kramer, S. Mahajan and P. Veyssière, Elsevier, Oxford, 2001, pp. 22-34.

31. H. Selin, S. E. Keane, S. Wang, N. E. Selin, K. Davis and D. Bally, *Ambio*, 2018, **47**, 198-215.

32. M. P. Crockett, A. M. Evans, M. J. H. Worthington, I. S. Albuquerque, A. D. Slattery, C. T. Gibson, J. A. Campbell, D. A. Lewis, G. J. L. Bernardes and J. M. Chalker, *Angewandte Chemie International Edition*, 2015, **55**, 1714-1718.

33. W. J. Chung, J. J. Griebel, E. T. Kim, H. Yoon, A. G. Simmonds, H. J. Ji, P. T. Dirlam, R. S. Glass, J. J. Wie, N. A. Nguyen, B. W. Guralnick, J. Park, SomogyiÁrpád, P. Theato, M. E. Mackay, Y.-E. Sung, K. Char and J. Pyun, *Nat Chem*, 2013, **5**, 518-524.

34. P. Hadi, M.-H. To, C.-W. Hui, C. S. K. Lin and G. McKay, *Water Research*, 2015, **73**, 37-55.

35. K. Rashid, K. Suresh Kumar Reddy, A. A. Shoaibi and C. Srinivasakannan, *Clean Technologies and Environmental Policy*, 2013, **15**, 1041-1048.

36. M. Otto and S. Bajpai, *Remediation Journal*, 2007, **18**, 21-28.

37. R. Ito, M. Kawaguchi, N. Sakui, H. Honda, N. Okanouchi, K. Saito and H. Nakazawa, *Journal of Chromatography A*, 2008, **1209**, 267-270.

38. M. W. Thielke, L. A. Bultema, D. D. Brauer, B. Richter, M. Fischer and P. Theato, *Polymers*, 2016, **8**, 266.

39. M. J. H. Worthington, R. L. Kucera, I. S. Albuquerque, C. T. Gibson, A. Sibley, A. D. Slattery, J. A. Campbell, S. F. K. Alboaiji, K. A. Muller, J. Young, N. Adamson, J. R. Gascooke, D. Jampaiah, Y. M. Sabri, S. K. Bhargava, S. J. Ippolito, D. A. Lewis, J. S. Quinton, A. V. Ellis, A. Johs, G. J. L. Bernardes and J. M. Chalker, *Chemistry – A European Journal*, 2017, **23**, 16219-16230.

40. S. I. Tsyganova, V. V. Patrushev and G. N. Bondarenko, *Russian Journal of Applied Chemistry*, 2013, **86**, 534-538.

41. S. Aktas, B. Gozuak, H. Acma, M. Reha Ozalp and E. Acma, *Environmental Chemistry Letters*, 2011, **9**, 47-53.

42. H. Sun, J. Brocato and M. Costa, *Current Environmental Health Reports*, 2015, **2**, 295-303.

43. D. G. Barceloux and D. Barceloux, *Journal of Toxicology: Clinical Toxicology*, 1999, **37**, 173-194.

44. S. L. O'Neal and W. Zheng, *Current Environmental Health Reports*, 2015, **2**, 315-328.

45. G. J. Sparrow and J. T. Woodcock, *Mineral Processing and Extractive Metallurgy Review*, 1995, **14**, 193-247.

CHAPTER 5: SYNTHESIS, CHARACTERISATION AND ANALYTICAL THEORY

CONTENTS

5.1 INTRODUCTION

Listed in this chapter are the experimental methods for all successfully synthesised and reported sulfur copolymers; methods and details pertaining to the material characterisation of the materials synthesised and their applications with respect to heavy metal remediation. Detailed discussion of the method development process and unsuccessful copolymerisation reactions can be found in Chapters 2 and 3.

5.2 SYNTHESIS

5.2.1 REAGENTS AND SUPPLIERS

Sulfur was supplied by both Sigma Aldrich (powder, 99.98% trace metals basis) and Brenntag UK & Ireland (S_8, sublimed powder, reagent grade, ≥99.5%). Limonene, myrcene (technical grade), farnesene (mixture of isomers), farnesol (≥95.0%, mixture of isomers), perillyl alcohol ((*S*)-(−)-perillyl alcohol, ≥95.0%, FG), nerolidol (98.0%, mixture of isomers) and squalene (≥98.0%, liquid) were supplied by Sigma Aldrich. Dicyclopentadiene was supplied by Sigma Aldrich (>96.0%) and Tokyo Chemical Industry UK Ltd (>97.0%, stabilised with BHT). 1,3-Diisopropenyl benzene was supplied by Tokyo Chemical Industry UK Ltd (>97.0%, stabilised with TBC). Perillartine (95.0%) was provided by Apollo Scientific Ltd. Hop oil was purchased from Hopsteiner. Acetone (GPR), acetonitrile (HPLC grade), chloroform (AR grade), hexane (HPLC grade), methanol (HPLC grade), toluene (AR grade), and tetrahydrofuran (HPLC grade) were provided by Fisher Scientific UK. All reagents were used as received, without additional purification.

5.2.2 EXPERIMENTAL METHOD

5.2.2.1 STANDARD SULFUR COPOLYMERS

The method to synthesise sulfur – limonene at 50 wt. % was derived from the work of Chalker *et al.*[1] Briefly this comprised taking sulfur (25.0 g, 97.50 mmol) and adding it to a 100 mL round bottom flask equipped with a stir bar. The flask was heated to 170 °C, using an oil bath under continuous stirring. After 30 minutes of heating, limonene (29.6 mL, 183.0 mmol) was added to the reaction over a period of five minutes with vigorous stirring. Once the addition was complete, the flask was then equipped with distillation head and condenser. After 60 minutes the temperature was increased (T = 180 °C) and any volatile material was removed by vacuum distillation (~ 66.5 mbar). Three hours later, the temperature was dropped to 100 °C and any non-volatile material remaining in the flask was dried further under high vacuum (< 1.3 mbar) overnight. After cooling to room temperature, the final product was obtained as a dark red/brown material.

The sulfur - diisopropenyl benzene 50 wt.% copolymer was synthesised by adapting the method established by Pyun *et al.*[2] The synthesis was conducted by charging a 40 mL glass vial with a magnetic stir bar and required mass of sulfur (2.50 g, 9.69 mmol). This was then placed in an oil bath or metal heating block and heated to 185 °C. Once the sulfur had liquefied the equivalent mass of 1,3-diisopropenyl benzene (2.50 g, 15.8 mmol) was added by pipette. The resulting mixture was stirred at (T = 185 °C) for 8 - 10 minutes, after which the resulting reaction media had vitrified into a translucent ruby red solid.

It is important to note that for all reactions reported in this thesis, the nominal temperature reported for these reactions being conducted is the temperature set on the hotplate and not an *in situ* temperature of the reaction as no *in situ* reaction monitoring was conducted.

5.2.2.2 SULFUR – MYRCENE COPOLYMERS

Sulfur – myrcene copolymers were synthesised by first heating (T = 160 °C) 40 mL glass vials (uncapped) in a metal heating block with the required amount of elemental sulfur, under constant stirring. Once the sulfur had liquefied, myrcene was added to the solution and continued to be stirred and heated at 160 °C for 15 minutes. After 15 minutes the temperature was increased to 175 °C and the reaction mixture was allowed to react for a further 45 minutes, at which point a solid black product had formed.

For samples that were moulded and cast the method proceeded as above, however once the temperature had been increased to 175 °C the reaction mixture was continually checked until a homogenous viscous solution had formed. Once at this stage the reaction mixture was transferred to a silicone mould and transferred to an oven to cure at 140 °C for 12 hours. Listed in Table 5.2.1 are the masses and moles used in the reactions.

Table 5.2.1 Reactant data for sulfur - myrcene copolymers

	Sulfur		Myrcene	
Content (wt.%)	Mass (g)	Moles (mmol)	Mass (g)	Moles (mmol)
50.0	5.00	19.49	5.00	36.70
60.0	6.00	23.39	4.00	29.36
70.0	7.00	27.29	3.00	22.02
80.0	8.00	31.19	2.00	14.68
90.0	9.00	35.08	1.00	7.34

5.2.2.3 SULFUR – FARNESENE COPOLYMERS

The synthesis of sulfur – farnesene copolymers was conducted by using the same method developed for the synthesis of sulfur – myrcene copolymers (5.2.2.2). Shown in the table below (Table 5.2.2) are the moles and masses of sulfur and farnesene used in the reactions.

Table 5.2.2 Reactant data for sulfur - farnesene copolymers

Content (wt.%)	Sulfur		Farnesene	
	Mass (g)	Moles (mmol)	Mass (g)	Moles (mmol)
50.0	5.00	19.49	5.00	24.47
60.0	6.00	23.39	4.00	19.57
70.0	7.00	27.29	3.00	14.68
80.0	8.00	31.19	2.00	9.79
90.0	9.00	35.08	1.00	4.89

5.2.2.4 SULFUR – FARNESOL COPOLYMERS

Sulfur – farnesol copolymers were synthesised using the same method as both sulfur – farnesene (5.2.2.3) and sulfur – myrcene (5.2.2.2). Shown in Table 5.2.3 are the moles and mass of reactants used in the polymerisation reactions.

Table 5.2.3 Reactant data for sulfur - farnesol copolymers

Content (wt.%)	Sulfur		Farnesol	
	Mass (g)	Moles (mmol)	Mass (g)	Moles (mmol)
50.0	5.00	19.49	5.00	22.49
60.0	6.00	23.39	4.00	17.99
70.0	7.00	27.29	3.00	13.49
80.0	8.00	31.19	2.00	8.99
90.0	9.00	35.08	1.00	4.49

5.2.2.5 SULFUR – SQUALENE COPOLYMERS

The synthesis of sulfur – squalene polymers was conducted by heating (T = 175 °C) a 100 mL round bottom flask containing the requisite amount of sulfur and allowing it to fully melt. Once melted the desired amount of squalene was added to the liquefied sulfur, with the resulting mixture being stirred for 15 to 25 minutes (depending on crosslinker ratio). Once the reaction had changed to a viscous dark brown homogenous solution the reactions were transferred

to a silicone mould and cured in an oven for 18 hours at 140 °C. Outlined below are the reaction masses and moles used.

Table 5.2.4 Reactant data for sulfur - squalene copolymers

	Sulfur		Squalene	
Content (wt.%)	Mass (g)	Moles (mmol)	Mass (g)	Moles (mmol)
50.0	7.50	29.24	7.50	18.26
60.0	9.00	35.08	6.00	14.61
70.0	10.5	40.93	4.50	10.96
80.0	12.0	46.78	3.00	7.30
90.0	13.5	52.63	1.20	3.65

5.2.2.6 SULFUR – PERILLYL ALCOHOL COPOLYMERS

Sulfur – perillyl alcohol copolymers were synthesised using the same method as outlined in 5.2.2.5 however the reaction times were greatly reduced with the reaction mixture being stirred for 5 to 12 minutes. Shown in Table 5.2.5 are the masses and moles used.

Table 5.2.5 Reactant data for sulfur - perillyl alcohol copolymers

	Sulfur		Perillyl Alcohol	
Content (wt.%)	Mass (g)	Moles (mmol)	Mass (g)	Moles (mmol)
50.0	7.50	29.24	7.50	49.26
60.0	9.00	35.08	6.00	39.41
70.0	10.5	40.93	4.50	29.59
80.0	12.0	46.78	3.00	19.71
90.0	13.5	52.63	1.20	9.85

5.2.2.7 SULFUR – PERILLARTINE COPOLYMERS

The sulfur – perillartine synthesis follows the same method as outlined in 5.2.2.2, however it is important to note that unlike most of the crosslinkers

used in this project perillartine is a solid at room temperature (soft, white crystals) and therefore takes longer to melt. Once the perillartine had liquefied, the reaction proceeded relatively quickly and reached a homogenous phase after 10 to 18 minutes. Once fully cured the copolymers were a dark red, almost matt black solid. Table 5.2.6 lists the masses and moles used in the synthesis.

Table 5.2.6 Reactant data for sulfur - perillartine copolymers

	Sulfur		Perillartine	
Content (wt.%)	Mass (g)	Moles (mmol)	Mass (g)	Moles (mmol)
50.0	7.50	29.24	7.50	45.39
60.0	9.00	35.08	6.00	36.31
70.0	10.5	40.93	4.50	27.23
80.0	12.0	46.78	3.00	18.16
90.0	13.5	52.63	1.20	9.09

5.2.2.8 SULFUR – NEROLIDOL COPOLYMERS

Sulfur – nerolidol copolymers were also synthesised using the same synthetic method as the sulfur - squalene copolymers (5.2.2.5). Reaction times, to a homogenous state, were comparable to the sulfur – perillartine copolymers (5.2.2.7), taking 10 to 20 minutes. After curing the copolymers were a black glossy solid. Outlined in Table 5.2.7 are masses and moles of the reactants used.

Table 5.2.7 Reactant data for sulfur - nerolidol copolymers

Content (wt.%)	Sulfur		Nerolidol	
	Mass (g)	Moles (mmol)	Mass (g)	Moles (mmol)
50.0	7.50	29.24	7.50	33.73
60.0	9.00	35.08	6.00	26.98
70.0	10.5	40.93	4.50	20.24
80.0	12.0	46.78	3.00	13.49
90.0	13.5	52.63	1.20	6.75

5.2.2.9 SULFUR – DICYCLOPENTADIENE COPOLYMERS

The synthesis of sulfur – dicyclopentadiene copolymers was conducted by first heating (T = 160 °C) a 100 mL round bottom flask in a metal heating block with the required amount of elemental sulfur, under constant stirring. On liquefaction of the sulfur, dicyclopentadiene was added to the solution and stirred for 15 minutes. After the addition of dicyclopentadiene and subsequent stirring for 15 minutes, the temperature was increased to 175 °C and the reaction mixture was allowed to react for a further 45 minutes, at which point a solid black product had formed.

If the copolymer needed to be moulded and cast then the same method discussed above was used, however once the temperature had been increased to 175 °C the copolymer mixture was checked until a homogenous dark brown solution had formed. Once at this stage the reaction mixture was transferred to a silicone mould and transferred to an oven to cure at 140 °C for 12 hours. Listed in Table 5.2.8 are the reactant details for the copolymer compositions.

Table 5.2.8 Reactant data for sulfur - dicyclopentadiene copolymers

Content (wt.%)	Sulfur		Dicyclopentadiene	
	Mass (g)	Moles (mmol)	Mass (g)	Moles (mmol)
50.0	7.50	29.24	7.50	37.82
60.0	9.00	35.08	6.00	30.26
70.0	10.5	40.93	4.50	22.69
80.0	12.0	46.78	3.00	15.13
90.0	13.5	52.63	1.20	7.56

5.2.2.10 SULFUR – HOP OIL COPOLYMERS

The synthesis of sulfur – hop oil copolymers, utilised a natural oil that has a complex mixture of components. The supplier was therefore unable to provide an exact molecular weight for the hop oil, although it is expected to be 110 to 150 $gmol^{-1}$ based on the molecular weights of the 3 largest components. Samples were synthesised using the method described in 5.2.2.6, with mass of sulfur ranging from 5.00 to 9.00 grams and the hop oil from 5.00 to 1.00 grams to produce copolymer compositions from 50 to 90 wt.%.

5.3 ANALYTICAL THEORY

5.3.1 DIFFERENTIAL SCANNING CALORIMETRY

The glass transition temperature (T_g) of a material or polymer is the temperature at which a reversible change occurs between a viscous or soft state to one that is hard or brittle.[3] Polymers can be used above or below their T_g, if the polymer is below its T_g then it is said to be in a glassy state or that it is a glassy polymer.[4] It is important to differentiate between the melting transition (T_m) and T_g of a potential material as they are two different types of thermal transition. Only amorphous regions would show a T_g, whereas crystalline or semi-crystalline materials can exhibit T_m and a crystallisation

transition, T_c. Due to semi-crystalline materials possessing areas in their structure that are amorphous in nature, it is these regions only that exhibit a T_g.[5] Therefore different materials can exhibit up to three different types of thermal transition; T_g, T_m and T_c (Figure 5.3.1).

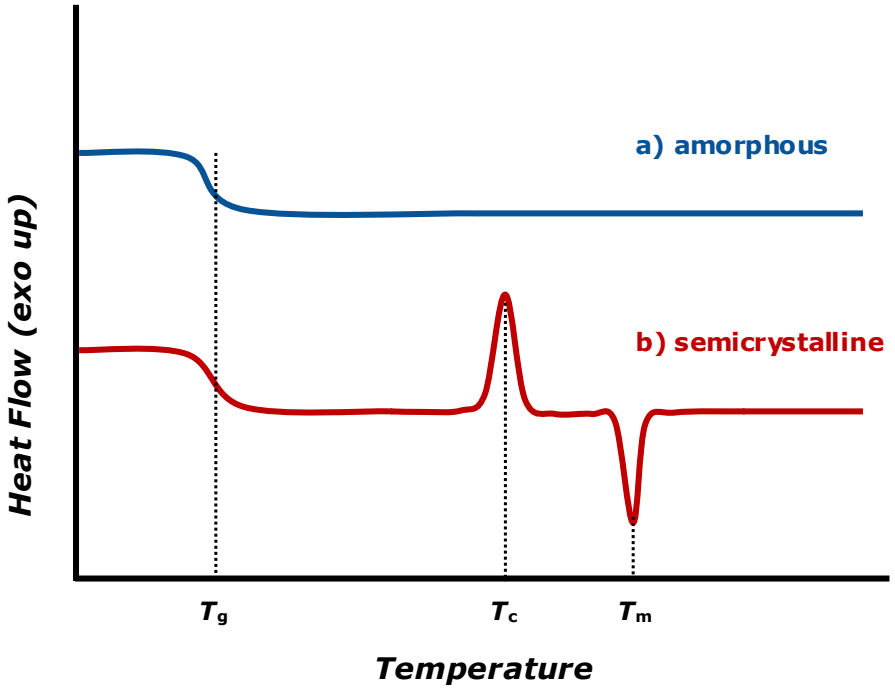

Figure 5.3.1 Simulated DSC traces for, a) An amorphous polymer and b) A semi-crystalline material. It is important to note that only the amorphous polymer and the amorphous regions in the semi-crystalline material exhibit a T_g. Only the semi-crystalline materials will possess a T_c and T_m

5.3.1.1 The Differential Scanning Calorimeter

The most common method of analysing T_g in materials is to use Differential Scanning Calorimetry (DSC). DSC works by continuously measuring the temperature of the sample and that of a reference, using a differential method to determine the heat flow into or out of the sample and to equalise this against the reference sample.[6] Shown if Figure 5.3.2 is a cross-sectional view through a DSC cell, illustrating the major components of the calorimeter. Both the heat flow and the heat capacity (C_p) of the system are monitored and recorded during a calorimetry experiment. The C_p is calculated by dividing the heat

flow by the heating rate. The equation for calculating the heat capacity of the system is given in Equation 5.3.1.

Equation 5.3.1 Equation for calculating Heat Capacity (C_p) of a system, where q is the difference in heat between the cells, t is time and ΔT is the change in temperature.

$$C_p = \frac{Heat\ Flow}{Heating\ Rate} = \frac{{}^{q}/_{t}}{{}^{\Delta T}/_{t}} = \frac{q}{\Delta T}$$

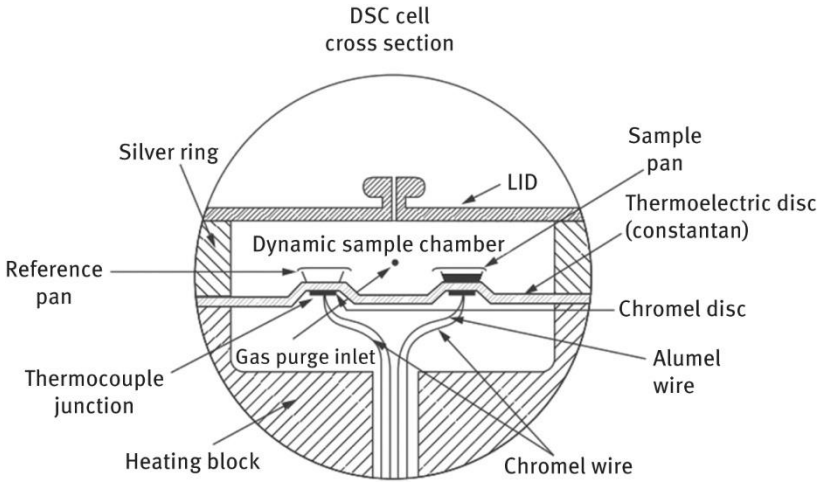

Figure 5.3.2 A cross-sectional view through a DSC cell, illustrating the major components present. Reproduced from[7]

5.3.1.2 THERMODYNAMIC THEORY AND THE DETERMINATION OF SULFUR STABILITY

Using classic thermodynamic theory it is also possible to predict the T_g for a specific copolymer composition as long as sufficient data has been collected; primarily the starting materials and several different compositions of the copolymer using DSC.[8] Analysis of T_g by DSC can reveal important material characteristics of polymers, such as the ability to determine whether a material is fully amorphous, crystalline or semi-crystalline.[9]

5.3.2 X-RAY DIFFRACTION AND CRYSTALLOGRAPHY

Derived from the Greek *crystallon* (cold or frozen drop) and *graphein*, (to write), crystallography is the study and determination of the crystal structure for a given material (*ie* the arrangement of atoms within that material). To determine the crystal structure a diffraction pattern first has to be generated and then analysed. Most commonly X-Rays are used for determination, however electrons and neutrons can be utilised to generate diffraction data. In the field of X-Ray crystallography there are two distinct forms of crystallographic analysis available to the analytical chemist: single crystal X-Ray Diffraction (scXRD) and powder X-Ray Diffraction (pXRD). If a single pure crystal can be grown and isolated then scXRD may be performed to fully characterise the structure of the substance being analysed, especially if other details such as an accurate elemental composition are known. If the sample to be studied is in bulk, a single crystal cannot be obtained or if other information is required (*ie* determination of structural defects or detection of polymorphs) then pXRD is the preferred method for characterisation.[10, 11]

5.3.2.1 BRAGG'S LAW

Underpinning X-Ray diffraction and crystallography is Bragg's Law. First proposed in 1913, it is an extremely simple formula that describes the interaction of the incident X-Rays and how they interact with the atoms in a crystalline system,[12] the law is also applicable to both neutron and electron diffraction.[13] In systems with a degree of long range order, the X-rays from the source will constructively interfere leading to the formation of peaks in the diffraction pattern. However in systems that contain no long range order, peaks would not be observed as the X-Rays would deconstructivity interfere.[14] Essentially Bragg's law allows calculation of the scattering angle (θ) at its peak constructive interference.[15]

Equation 5.3.2 The Bragg's Law equation, where d is the distance between lattice planes, n is a positive integer and λ is the wavelength of the incident wave.

$$2d \sin\theta = n\lambda$$

Figure 5.3.3 outlines the key elements to Bragg's Law, how the individual components interact with each other and ultimately how the equation is derived.

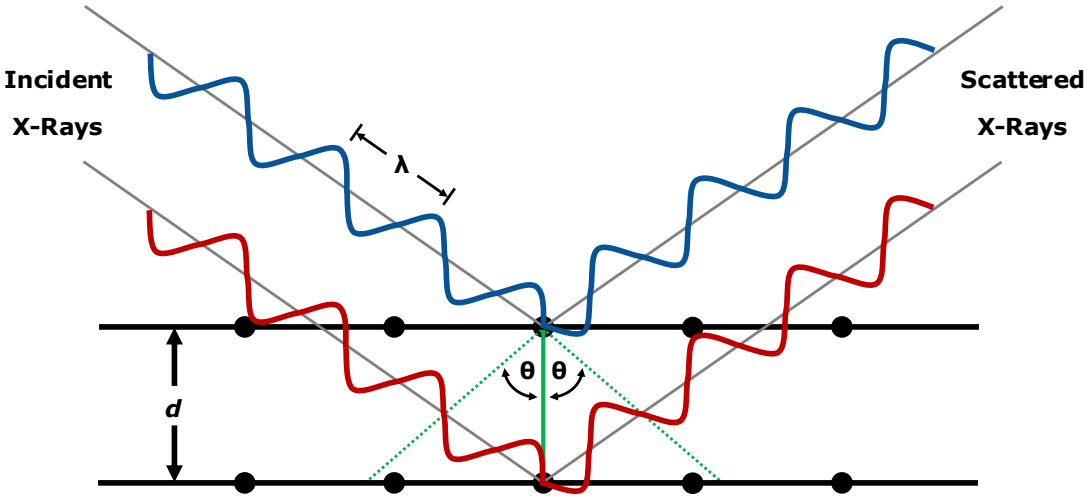

Figure 5.3.3 Diagrammatic view of Bragg's Law and its key elements

5.3.2.2 STRUCTURAL DETERMINATION AND CHARACTERISATION

The most common application for pXRD is that of phase identification, whereby the generated powder diffraction pattern is compared against known crystallographic databases such as the PDF (Powder Diffraction File),[16] or COD (Crystallography Open Database),[17] to ascertain if there is a match. In complex samples there may be multiple overlapping diffraction patterns present, however since all molecules have individual powder patterns not only can the constituents of the sample be determined but also their relative abundances in the sample. Additionally pXRD can also be used to study the crystallinity of a substance. As a general rule, the peaks present in the diffraction pattern are sharper and better resolvable if the sample is more crystalline and ordered. Conversely amorphous or low crystallinity materials tend to generate few peaks in their respective powder patterns and any that are observed are

usually very broad and ill-defined. Therefore by conducting mathematical analysis on the peaks generated in diffraction data, the crystallinity of a material can be established.[18]

5.3.3 BET SURFACE AREA ANALYSIS

Adsorption can be defined in terms of an increase in the concentration of a dissolved substance, be that of molecules, ions or atoms, at the interface of a layer due to surface forces.[19] When discussing adsorption it is important to define and characterise the two classes of adsorption that can occur; physical and chemical. Physical adsorption or physisorption is a phenomenon which can occur either in a solid/gaseous or solid/liquid system in which intermolecular forces (the van der Waals forces) bring the gas or liquid phase into contact with the solid phase.[20] By contrast, chemical adsorption or chemisorption is the process by which intermolecular forces have a strong interaction between the adsorbate and the surface leading to the formation of chemical bonds.[21] Gas sorption studies are used to characterise the pore structure of a given material. The relationship between the adsorbate and the equilibrium pressure at a given temperature produces a characteristic adsorption isotherm. The two main models used in the analysis of gas sorption studies are the Langmuir model,[22] and the Brunauer-Emmett-Teller (BET) model.[23]

5.3.3.1 LANGMUIR MODEL

First presented in 1916, the Langmuir model is the simpler of the two models primarily used in gas adsorption analysis and relies upon several assumptions. It is used primarily in the simplest of scenarios, for example where the adsorption of a specific adsorbate occurs at a series of equivalent

sites on the surface of a solid.[24] The Langmuir model is built upon five assumptions, which are:

I. The surface is a completely homogenous flat plane
II. The adsorbate is adsorbed into an immobile state
III. That all adsorption sites are equivalent
IV. Each adsorption site can hold a maximum of one molecule of adsorbate
V. There are no interactions between adsorbate molecules in adjacent sites

The Langmuir isotherm can be derived in terms of fractional occupancy (θ_{Ads}) of the adsorption sites, as shown in the equation below:

Equation 5.3.3 The Langmuir isotherm expressed in terms of fractional occupancy (θ_{Ads}), where K_{eq} is the equilibrium constant and P_A is the partial pressure of the adsorbate.

$$\theta_{Ads} = \frac{K_{eq}.p_A}{1 + K_{eq}.p_A}$$

5.3.3.2 BRUNAUER-EMMETT-TELLER (BET) MODEL

The BET theory is the more complex model used in gas adsorption analysis and builds upon the monolayer Langmuir theory by addressing the fact that adsorption can occur in multiple layers. The model makes three key assumptions:

I. The adsorbate molecules can adsorb on to a surface in an infinite number of layers
II. The adsorbate molecules only interact with the adjacent layers
III. The Langmuir theory can be applied to each layer

The BET equation is given as:

Equation 5.3.4 The BET equation, where v is the quantity of adsorbed gas, v_m is the quantity of adsorbed gas in the monolayer, p is equilibrium pressure, p_0 is the saturation pressure and c is the BET constant.

$$\frac{1}{v[(p_o/p) - 1]} = \frac{c - 1}{v_m.c}\left(\frac{p}{p_o}\right) + \frac{1}{v_m.c}$$

The BET constant is derived as follows:

Equation 5.3.5 The BET constant, where E_1 is the heat of adsorption for the first layer and E_L is the heat of adsorption for the second and subsequent layers

$$c = exp\left(\frac{E_1 - E_L}{RT}\right)$$

To avoid the effects of chemisorption, nitrogen is the most commonly used gas probe for BET adsorption analysis, although other gases can be used. However, since the specific surface area calculated via BET can depend on the cross section of the adsorbate, care needs to be taken in the selection of the adsorbate.[25]

5.3.3.3 ISOTHERM MODELS

Traditionally, results from gas adsorption studies had been classified by one of six different types of physisorption isotherms.[26] However recently IUPAC have refined these classifications into eight new physisorption isotherms to better fit with characteristic isotherms that have emerged in the past 30 years since the isotherms were last defined.[27] Shown in Figure 5.3.4 are the eight new physisorption isotherms; Type I(a), I(b), II, III, IV(a), IV(b), V and VI. A précis of all eight physisorption isotherms is provided.

Type I(a) & I(b) isotherms

Type I isotherms are reversible and are caused by microporous materials possessing relatively small external surfaces. The limited uptake is an effect of the acceptable micropore volume. Type I(a) isotherms are generated microporous materials with mainly narrow (< 1 nm) micropores in there structure, whereas Type I(b) are generated by materials containing a wider pore size distribution (although no larger than 2.5 nm).

Type II isotherms

The physisorption of a gas onto a nonporous or macroporous material leads to a reversible Type II isotherm. The gradual curvature of the isotherm (point B) in comparison to Type I isotherms is caused by the overlap of monolayers and the onset of multilayer adsorption.

Type III isotherms

Due to the absence of point B in Type III isotherms, it can be determined that there is little to no monolayer formation at the surface of the material with few adsorbate-adsorbent interactions occurring. The material is likely to be nonporous or macroporous.

Type IV(a) & IV(b) isotherms

Mesoporous materials tend to generate Type IV isotherms under gas adsorption analysis. The adsorption behaviour observed in Type IV isotherms by mesopores is caused by two factors; the adsorbate-adsorbent interactions and also the interactions between molecules in the condensed state. The hysteresis observed in Type IV(a) isotherms is due to capillary condensation of the sorbent. Hysteresis can start to be observed once pores begin to exceed 4 nm in width.[28-30] Type IV(b) isotherms are caused by the conical or cylindrical mesopores that are closed at one end. Both Type IV isotherms are reversible.

Type V isotherms

The similar shape of the Type V isotherm to that of the Type III isotherm is due to weak sorbent-sorbate interactions at low pressures, however an increase to a higher pressure does lead to pore filling.

Type VI isotherms

Type VI isotherms exhibit a reversible stepwise isotherm attributed to layer on layer adsorption onto a uniform nonporous surface. The step height shows the capacity for each layer, whereas the steepness of the step is determined by the temperature and the system.

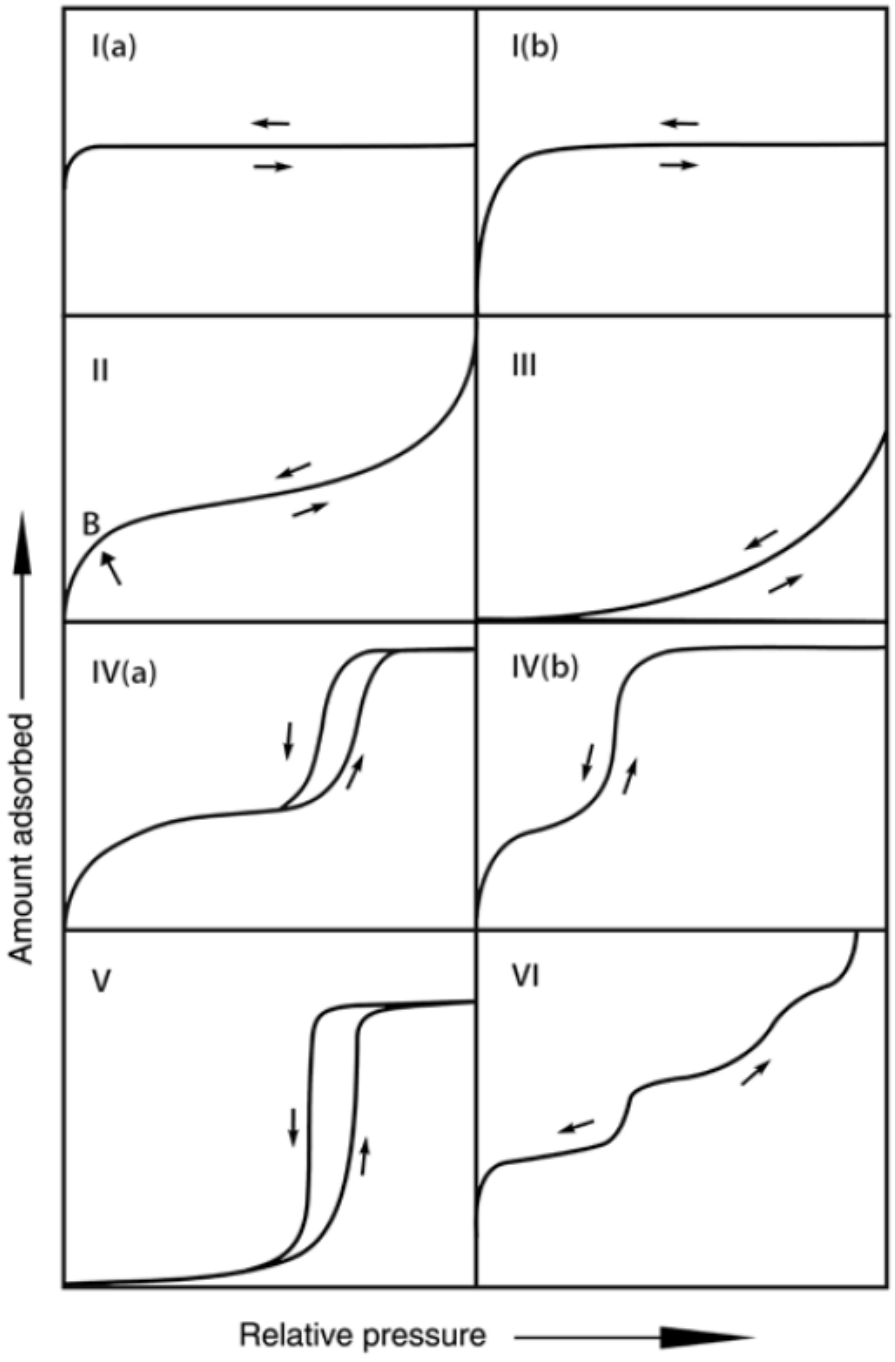

Figure 5.3.4 The eight physisorption isotherms as defined by IUPAC. Reproduced from[27]

5.3.4 ATOMIC/OPTICAL EMISSION SPECTROSCOPY

There are several different forms of Atomic Emission Spectroscopy (AES), also known as Optical Emission Spectroscopy or OES, available to the analytical chemist. In all instances of AES the basic principles remain the same and work by the emission of light caused by the relaxation of electrons from an excited state. There are three commonly used forms of AES employed in chemical analysis; arc/spark, flame and plasma emission spectroscopy.[31] All further discussion will be focused on plasma emission spectroscopy, as it is by far the most commonly used method of analysis.

5.3.4.1 PLASMA GENERATION

In plasma emission spectroscopic methods, the plasma is the excitation source for electrons present in the sample. Plasma is one of the four fundamental states of matter and is the state in which an ionised gaseous substance can become highly conductive where both long range electronic and magnetic fields can directly influence the behaviour of the matter present.[32, 33] The three most common methods for forming a stable plasma in AES are by: passing a DC current between electrodes (a plasma jet),[34] microwave field sources,[35] or by the induction of an electromagnetic field using high powered radio-frequency coils (inductively coupled plasma or ICP).[36]

5.3.4.2 EXCITATION AND DETECTION

The inductively coupled plasma through which the analyte is excited is produced in the torch of the instrument. Primarily composed of quartz the torch is a simple, although intricately designed device, with no movable parts (Figure 5.3.5). It comprises a central quartz tube tapering to a tip through which a nebulized mixture of analyte and argon gas flows, an outer quartz jacket through which more argon is flowed as a cooling gas and surrounding this in line with the tip of the central tube is a radio-frequency coil. A Tesla

coil generates a spark at the tip of the central tube that rapidly heats the argon/analyte mixture, the radio-frequency coil then induces an alternating electromagnetic field within this stream of heated nebulized gas and through the process of ohmic heating a plasma is maintained.[31, 37]

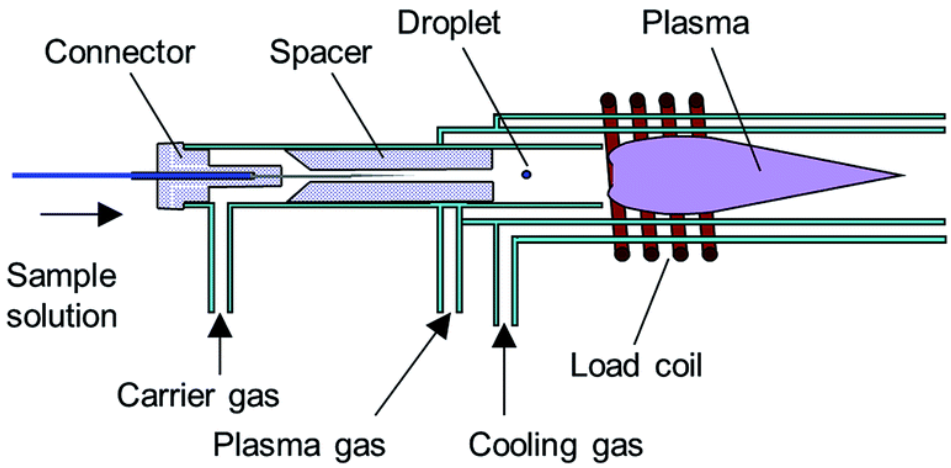

Figure 5.3.5 Diagram of an Inductively Coupled Plasma (ICP) torch, reproduced from[38]

After excitation via the torch, emission spectrum is recorded after first passing through various prisms and/or diffraction gratings to resolve the component wavelengths generated. The resolved spectral data generated is then passed through either a monochromator or polychromator, thus allowing the signal to be tuned for the elements desired, before being detected using a Charge Coupled Device (CCD).[31, 39, 40]

5.4 METHODS OF CHARACTERISATION

5.4.1 THERMAL ANALYSIS

5.4.1.1 THERMOGRAVIMETRIC ANALYSIS

Thermograms of polymeric samples were carried out using a TA instruments Q5000IR analyser with an automated vertical overhead thermobalance. Samples were run in platinum pans, up to 900 °C with a ramp rate of 10 °C per minute under a nitrogen atmosphere, then held at 900 °C whilst being run under air to combust any char products formed. Thermogravimetric analysis

was primarily used to analyse the polymer decomposition temperature and to check suitability for elemental analysis.

5.4.1.2 DIFFERENTIAL SCANNING CALORIMETRY

Differential Scanning Calorimetry (DSC) analysis was carried out using a TA instruments Q2000 and DSC 25, at a heating/cooling rate of 10 °C min^{-1}. Samples were cycled through a heat/cool/heat program under the following conditions; samples were heated from room temperature to 150 °C before cooling to -80 °C and heating back up to 150 °C.

5.4.2 STRUCTURAL DETERMINATION

5.4.2.1 INFRA-RED SPECTROMETRY

Fourier-transform infrared spectroscopy (FT-IR) was performed using a Thermo NICOLET IR200 or a Bruker TENSOR 27 FT-IR, between 400 cm^{-1} to 4000 cm^{-1} for 64 scans. The majority of samples were analysed neat using an attenuated total reflectance accessory, however several samples required analysis in transmission mode after pressing into a KBr pellet to obtain a satisfactory IR spectrum.

5.4.2.2 NUCLEAR MAGNETIC RESONANCE SPECTROMETRY

Nuclear Magnetic Resonance (NMR) experiments were used to check the formation of C-S bonds and the removal of allylic groups in the final product when compared to the crosslinker. For samples that could be solubilised in deuterated chloroform or benzene, solution NMR analysis was conducted using a Bruker Advance DRX (400 MHz) spectrometer. Proton (^{1}H) NMRs were run for 96 scans using the standard Zg30 pulse program and carbon (^{13}C) NMRs for 1024 scans, using the ZgPg30 pulse program. All solution experiments were carried out at ambient spectrometer temperature.

5.4.2.3 ELEMENTAL ANALYSIS

Elemental analysis of copolymer was provided to confirm carbon, sulfur and hydrogen ratios were within an acceptable margin from the calculated values. Samples were submitted to the departmental CHNS micro-analysis service and analysed on an Elementar Vario Micro Cube.

5.4.2.4 POWDER X-RAY DIFFRACTOMETRY

In order to determine whether there was any residual elemental sulfur remaining in the samples, powder diffraction patterns were measured using a PANalytical X'Pert PRO or a PANalytical Empyrean diffractometer. Both diffractometers used a CuKα radiation source (Kα1 = 1.54060 Å, Kα2 = 1.54443 Å) and the PANalytical Empyrean powder diffractometer was equipped with a PIXcel3D detector. Both diffractometers used well-plates to hold multiple samples and all experiments were run in transmission geometry.

Diffraction pattern data for two of the three sulfur polymorphs β[41] and γ[42] were obtained from the Inorganic Crystal Structure Database (ICSD) of the National Chemical Database Service.

5.4.2.5 SCANNING ELECTRON MICROSCOPY

Micrographs of copolymer samples were either imaged using a Hitachi S-4800 Cold Field Emission Scanning Electron Microscope (CFE-SEM) or a TESCAN S8000G Focused Ion Beam /Scanning Electron Microscope (FIB-SEM).

When using the Hitachi S-4800, dry samples were prepared by dispersing the copolymer powder directly onto carbon tabs. Imaging on the S-4800 was conducted at 3.0 kV and a working distance of ~ 8.0 mm. Dry samples for analysis on the TESCAN S800G were prepared by dispersing the sample directly onto carbon tabs. When using the TESCAN, imaging was conducted

at a range of acceleration voltages operating in UH-Resolution mode and a working distance of ~ 6.0 mm.

5.4.2.6 GAS SORPTION ANALYSIS

A Micromeretics ASAP 2040 volumetric adsorption analyser was used to measure nitrogen adsorption and desorption isotherms of porous samples. The samples were degassed by heating under dynamic vacuum (10^{-5} mbar) at a ramp rate of 10 °C per minute to a temperature of 60 – 100 °C, which was followed by holding for 15 hours.

5.4.2.7 GEL PERMEATION CHROMATOGRAPHY

Gel Permeation Chromatography (GPC) was used to determine the average molecular weight and number weight of the sulfur copolymers that were either soluble or had a soluble fraction. Analysis was carried out on either an Agilent or Viscotek system, using chloroform (AR grade) supplied by Fisher Scientific as the eluent. Calibration standards used were Agilent EasiVial PS-H and PS-2 EasiCal.

The Viscotek system comprised a GPCmax and a TDA302 detector array, with columns, 2x T6000M plus Tguard, provided by Malvern. System flow rate was 1.0 mL min^{-1}. All samples were stored and injected at room temperature with columns and detectors stabilised at 40 °C. Samples were analysed in duplicate.

The Agilent system comprised an Agilent 1260 Infinity II GPC/SEC single detection system, with two PLgel 5 μm MIXED-D columns, a PLgel 5 mm guard column and a refractive index (RI) detector. The eluent was kept at 40 °C and a flow-rate of 1.0 mL min^{-1}. Samples were analysed in duplicate.

5.4.3 HEAVY METAL TESTING

5.4.3.1 REAGENTS, SUPPLIERS AND STOCK SOLUTIONS

Chromium (III) nitrate, Cobalt (II) nitrate, Copper (II) nitrate, Gold (III) chloride (Au ≥ 64.4%), Lead (II) nitrate, Manganese (II) chloride, Mercury (II) chloride and Nickel (II) nitrate were supplied by Alfa Aesar. Cacodylic acid and Cadmium (II) chloride were supplied by Sigma Aldrich. Methylmercury chloride (1000 μg/mL in H_2O) was supplied by LGC Standards, LGC Ltd. Hafnium standard solution, 1000 ppm (μg/mL), was provided by Inorgnaic Ventures. All reagents were used as received without additional purification.

For heavy metal testing, stock solutions were prepared from the reagents listed above. All stock solutions were prepared in deionised water, stored unstabilised (no additional acid added to the solution) and refrigerated. Stock solutions were remade every four to six months, to ensure the concentration of the solutions. Outlined below are the details of the stock solutions prepared.

Cadmium: 101.80 mg of $CdCl_2$ was dissolved in 20.0 mL of DI H_2O and then made up to 100 mL in a volumetric flask, yielding a concentration of 500 ppm.

Chromium: 384.80 mg of $Cr(NO_3)_3 \cdot 9H_2O$ was dissolved in 40.0 mL of DI H_2O and then made up to 100 mL in a volumetric flask, resulting in a concentration of 500 ppm.

Cobalt: 617.24 mg of $Co(NO_3)_2 \cdot 6H_2O$ was dissolved in 100.0 mL of DI H_2O and then made up to 250 mL in a volumetric flask, yielding a concentration of 500 ppm.

Copper: 474.75 mg of $Cu(NO_3)_2 \cdot 3H_2O$ was dissolved in 100.0 mL of DI H_2O and then made up to 250 mL in a volumetric flask, yielding a concentration of 500 ppm.

Gold: 1600 mg of $AuCl_3$ was dissolved in 100.0 mL of DI H_2O and then made up to 500 mL in a volumetric flask, resulting in an approximate concentration of 2000 ppm (as the actual quantity of gold present in the salt is not accurately known, calculations were based on 64.4% gold content, ICP-OES was used to determine exact concentration).

Lead: 199.75 mg of $Pb(NO_3)_2$ was dissolved in 100.0 mL of DI H_2O and then made up to 250 mL in a volumetric flask, yielding a concentration of 500 ppm.

Manganese: 180.39 mg of $MnCl_2 \cdot 4H_20$ was dissolved in 40.0 mL of DI H_2O and then made up to 100 mL in a volumetric flask, resulting in a concentration of 500 ppm.

Mercury (Inorg): 1352.00 mg of $HgCl_2$ was dissolved in 100.0 mL of DI H_2O and then made up to 500 mL in a volumetric flask, yielding a concentration of 2000 ppm.

Mercury (Org): 2000 µL of CH_3HgCl was diluted in 40.0 mL of DI H_2O and then made up to 100 mL in a volumetric flask, resulting in a concentration of 200 ppm. Due to the highly toxic nature of organomercury compounds, this stock solution was prepared as needed.

Nickel: 619.13 mg of $Ni(NO_3)_2 \cdot 6H_2O$ was dissolved in 100.0 mL of DI H_2O and then made up to 250 mL in a volumetric flask, yielding a concentration of 500 ppm.

5.4.3.2 TESTING PROTOCOL

The following is the general method for conducting the heavy metal tests. The mass of sorbent used in the tests was largely kept constant, however when

conducting material capacity tests it became necessary to alter not only the concentrations of the test solutions but also the mass of sorbent used in order to generate enough data points whilst staying within the maximum concentration limits allowed for the test solutions.

Tests were conducted by placing the desired amount of sorbent (typically between 10 – 60 mg for most tests) in a 15 mL centrifuge tube, to which the required test solution was added. Concurrently with the preparation of the test sample, a parallel sample was prepared without the sorbent present for the control. Once the test solution had been prepared to the correct concentration, 12 mL was added to each centrifuge tube. The tubes were subsequently capped and agitated for 60 seconds before being placed on a tube roller for 16 hours. The standard time for a test was 16 hours however, other time points were used in certain tests to ascertain how quickly metals could be removed, 16 was chosen primarily to allow adequate time for the test solution to interact with the sorbent present whilst allowing multiple tests to be conducted in a short period of time.

After 16 hours the samples were removed from the tube roller and allowed to stand in a rack for five minutes before an aliquot was removed for testing. The aliquot removed was first filtered through a 0.22 or 0.45 μm nylon syringe filter to remove any suspended sorbent present. Different methods of filtration were tested to ensure that mercury, due to its "sticky" properties, would not bind to the filter material and artificially enhance the results. More traditional filtration materials such as glass fibre and cellulose acetate were rapidly eliminated, as were other syringe filters contacting polyethersulfone (PES) and polyvinyl difluoride (PVDF). Filtering a mercury solution with a nylon filter showed negligible effects on the result reported and therefore all tests were subsequently filtered using nylon syringe filters. Due to the varying concentrations of the test solutions, samples with starting concentrations

higher than 20 ppm were diluted by serial dilutions to be within a range of 2 – 20 ppm using DI and were made up to 10 mL. To ensure that results were accurate random samples prepared for ICP-OES analysis were spiked with 0.2 µL of a 1000 ppm hafnium solution as in internal standard. Hafnium was chosen due the limited interaction of its spectral bands with those of the heavy metals to be tested.

5.4.3.3 INDUCTIVELY COUPLED PLASMA OPTICAL EMISSION SPECTROMETRY

The concentration of metal ions remaining in solution after sorbent testing was determined by difference when compared with its corresponding control sample. ICP-OES tests were conducted on the same day as the samples were prepared and therefore samples were not stabilised with acid. All samples were analysed by an Agilent 5110 ICP-OES spectrometer with the following settings.

Table 5.4.1 Settings for ICP-OES Spectrometer

Read Time	15 seconds	**Nebulizer Flow**	0.70 L min^{-1}
RF Power	1.2 kW	**Plasma Flow**	12.0 L min^{-1}
Stabilisation Time	35 seconds	**Aux Flow**	1.00 L min^{-1}
Viewing Mode	Axial		

5.5 REFERENCES

1. M. P. Crockett, A. M. Evans, M. J. H. Worthington, I. S. Albuquerque, A. D. Slattery, C. T. Gibson, J. A. Campbell, D. A. Lewis, G. J. L. Bernardes and J. M. Chalker, *Angewandte Chemie International Edition*, 2015, **55**, 1714-1718.

2. W. J. Chung, J. J. Griebel, E. T. Kim, H. Yoon, A. G. Simmonds, H. J. Ji, P. T. Dirlam, R. S. Glass, J. J. Wie, N. A. Nguyen, B. W. Guralnick, J. Park, SomogyiÁrpád, P. Theato, M. E. Mackay, Y.-E. Sung, K. Char and J. Pyun, *Nat Chem*, 2013, **5**, 518-524.

3. B. Wunderlich, *The Nature of the Glass Transition and its Determination by Thermal Analysis*, ASTM International, West Conshohocken, PA, 1994.

4. V. Meille Stefano, G. Allegra, H. Geil Phillip, J. He, M. Hess, J.-I. Jin, P. Kratochvíl, W. Mormann and R. Stepto, *Journal*, 2011, **83**, 1831.

5. B. Wunderlich, in *Thermal Analysis of Polymeric Materials*, Springer Berlin Heidelberg, Berlin, Heidelberg, 2005, pp. 279-454.

6. P. Le Parlouër, in *Calorimetry and Thermal Methods in Catalysis*, ed. A. Auroux, Springer Berlin Heidelberg, Berlin, Heidelberg, 2013, pp. 51-101.

7. M. Abd-Elghany and M. Klapötke Thomas, *Journal*, 2018, **3**.

8. P. R. Couchman, *Macromolecules*, 1978, **11**, 1156-1161.

9. J. Rieger, *Polymer Testing*, 2001, **20**, 199-204.

10. D. Louër, in *Encyclopedia of Spectroscopy and Spectrometry*, ed. J. C. Lindon, Elsevier, Oxford, 1999, pp. 1865-1875.

11. G. Artioli, in *Encyclopedia of Spectroscopy and Spectrometry (Third Edition)*, eds. J. C. Lindon, G. E. Tranter and D. W. Koppenaal, Academic Press, Oxford, 2017, pp. 676-683.

12. W. H. Bragg and W. L. Bragg, *Proceedings of the Royal Society of London. Series A, Containing Papers of a Mathematical and Physical Character*, 1913, **88**, 428-438.

13. J. M. Cowley, *Diffraction physics*, Elsevier Science B.V, Amsterdam ; Oxford, 3rd rev. ed. edn., 1995.

14. B. Gu and D. J. Burgess, in *Natural and Synthetic Biomedical Polymers*, eds. S. G. Kumbar, C. T. Laurencin and M. Deng, Elsevier, Oxford, 2014, pp. 333-349.

15. H. P. Myers, *Introductory solid state physics*, Taylor & Francis, London, 1990.

16. J. Faber and T. Fawcett, *Acta Crystallographica Section B*, 2002, **58**, 325-332.

17. S. Gražulis, D. Chateigner, R. T. Downs, A. F. T. Yokochi, M. Quirós, L. Lutterotti, E. Manakova, J. Butkus, P. Moeck and A. Le Bail, *Journal of Applied Crystallography*, 2009, **42**, 726-729.

18. N. S. Murthy and H. Minor, *Polymer*, 1990, **31**, 996-1002.

19. A. D. McNaught, A. Wilkinson, P. International Union of and C. Applied, *Compendium of chemical terminology : IUPAC recommendations*, Blackwell Science, Oxford, 2nd ed edn., 1997.

20. M. C. Desjonquères and D. Spanjaard, *Concepts in surface physics*, Springer, Berlin ; London, 2nd ed. edn., 1996.

21. K. Oura, M. Katayama, A. V. Zotov, V. G. Lifshits and A. A. Saranin, in *Surface Science: An Introduction*, eds. K. Oura, M. Katayama, A. V. Zotov, V. G. Lifshits and A. A. Saranin, Springer Berlin Heidelberg, Berlin, Heidelberg, 2003, pp. 295-323.

22. I. Langmuir, *Journal of the American Chemical Society*, 1916, **38**, 2221-2295.

23. S. Brunauer, P. H. Emmett and E. Teller, *Journal of the American Chemical Society*, 1938, **60**, 309-319.

24. R. I. Masel, *Principles of adsorption and reaction on solid surfaces*, Wiley, New York ; Chichester, 1996.

25. D. A. H. Hanaor, M. Ghadiri, W. Chrzanowski and Y. Gan, *Langmuir*, 2014, **30**, 15143-15152.

26. K. S. W. Sing, *Journal*, 1985, **57**, 603.

27. M. Thommes, K. Kaneko, V. Neimark Alexander, P. Olivier James, F. Rodriguez-Reinoso, J. Rouquerol and S. W. Sing Kenneth, *Journal*, 2015, **87**, 1051.

28. S. Lowell, J. E. Shields, M. A. Thomas and M. Thommes, *Characterization of porous solids and powders : surface area, pore size, and density*, Kluwer Academic Publishers, Dordrecht ; Boston, 2004.

29. M. Thommes and K. A. Cychosz, *Adsorption*, 2014, **20**, 233-250.

30. J. Landers, G. Y. Gor and A. V. Neimark, *Colloids and Surfaces A: Physicochemical and Engineering Aspects*, 2013, **437**, 3-32.

31. S. Higson and S. Higson, *Analytical chemistry*, Oxford University Press, Oxford ; New York, 2003.

32. J. P. Freidberg, *Plasma physics and fusion energy*, Cambridge University Press, Cambridge, 2007.

33. F. F. Chen, *Introduction to plasma physics and controlled fusion*, Plenum Press, New York, 2nd ed. edn., 1984.

34. M. Margoshes and B. F. Scribner, *Spectrochimica Acta*, 1959, **15**, 138-145.

35. R. K. Skogerboe and G. N. Coleman, *Analytical Chemistry*, 1976, **48**, 611A-622.

36. A. Montaser, A. Montaser and D. W. Golightly, *Inductively coupled plasmas in analytical atomic spectrometry*, VCH Publishers, New York, NY, 1987.

37. R. Rezaaiyaan, G. M. Hieftje, H. Anderson, H. Kaiser and B. Meddings, *Applied Spectroscopy*, 1982, **36**, 627-631.

38. K. Shigeta, Y. Kaburaki, T. Iwai, H. Miyahara and A. Okino, *Journal of Analytical Atomic Spectrometry*, 2015, **30**, 1609-1616.

39. N. Wieberneit and P. Heitland, *Applied Spectroscopy*, 2001, **55**, 598-603.

40. P. W. J. M. Boumans and J. J. A. M. Vrakking, *Spectrochimica Acta Part B: Atomic Spectroscopy*, 1987, **42**, 553-579.

41. Y. Watanabe, *Acta Crystallographica Section B*, 1974, **30**, 1396-1401.

42. D. E. Sands, *Journal of the American Chemical Society*, 1965, **87**, 1395-1396.

Chapter 6: Conclusions and Future Work

Contents

6.1 CONCLUSIONS

6.1.1 INVERSE VULCANISED SULFUR POLYMERS

The research presented in this thesis demonstrates that inverse vulcanised sulfur polymers are a viable and commercially relevant set of materials. Being low cost and containing a large proportion of sulfur, with respect to total mass of the polymer, these materials possess tuneable physiochemical properties. By harnessing waste industrial by-products and biorenewable crosslinking agents with the utilisation of a solvent free "one pot" synthetic method, the sulfur copolymers synthesised are highly atom efficient, highlighting the green credentials of these materials. All crosslinking agents presented in this thesis are currently commercially available and relatively cheap, this coupled with the low cost of sulfur allows the potential scale up of inverse vulcanised polymers to a scale that is suitable for industrial needs.

By varying the position, number and additional functional groups present in a crosslinking agent and by modifying the ratio of sulfur to crosslinker, a range of sulfur copolymer composites can be synthesised with differing properties. Sulfur copolymers synthesised from linear crosslinkers with a high allylic bond content, such as squalene, or those with additional functional groups present (*eg* farnesol) had improved T_g values compared with other copolymers presented in this thesis. Additionally these polymers were either totally insoluble or sparingly soluble when tested against a range of common laboratory solvents, suggesting a higher level of crosslinking had occurred. Similarly DCPD produces insoluble glossy black copolymers with reported glass transition temperatures in excess of 100 °C under the right synthetic conditions.

The majority of inverse vulcanised sulfur copolymers synthesised in this thesis were brown to black in colour, with some producing glossy "glass like" surfaces. However, certain crosslinking agents such as perillyl alcohol and

DIB produced ruby red translucent copolymers at a 50 wt.% sulfur loading. The translucency of the S-PER varied with sulfur content of the copolymer, by increasing the sulfur loading the copolymer became more opaque. Despite the similarities between limonene and its derivatives (perillyl alcohol and perillartine) only S-PER copolymers produced red translucent materials.

6.1.2 SULFUR POLYMERS AS HEAVY METAL SORBENTS

It has been shown in this thesis that inverse vulcanised sulfur polymers possess great potential for use as heavy metal adsorbents for the remediation of pre-existing and future sources of both natural and anthropogenic sources of pollution. The ability to synthesise a material that can utilise both physisorption as well as chemisorption, allows sulfur copolymers to have capacities for heavy metal remediation that are several times higher than existing commercially available materials.[1]

There are several different routes for inducing porosity and therefore maximising the maximum surface area of the sulfur copolymer available for remediation. Although swelling with $scCO_2$ did produce a notable increase in the uptake capacity when compared to solid blocks of copolymer, the improvement yielded did not compare favourably to other methods such as carbonisation. When comparing the carbonisation of inverse vulcanised sulfur polymers to the coating of them onto solid supports it is interesting to note that both exhibited similar uptake capacities (2216 m^2, carbonisation, and 344.74 m^2, coated silica, per gram respectively) despite having a large difference in surface area. In both methods adsorption capacities for inorganic mercury (mercury chloride), have been noted for the carbonised sulfur copolymers (850 mg g^{-1}) and silica coated solid supports (≥ 500 mg g^{-1}), which are higher than other previously published sulfur copolymers.[2, 3]

6.2 FUTURE WORK

The next logical steps to continue this work would entail testing the successful candidates for their abilities to; sequester mercury in the gaseous phase, how these materials could be cycled and regenerated, the effect pH has on the absorption of heavy metals and assessing how inverse vulcanised sulfur polymers may be used in the remediation of radionuclides.

The effect of pH can have a noticeable impact on how a sorbent interacts with metal ions in solution.[4-6] Additionally there has been little in the way of recently published literature on the effect of acids or bases on sulfur-sulfur bonds, with the only review investigating these effects and other factors on the scission of sulfur-sulfur bonds published in 1959.[7] It would therefore be prudent to not only test how inverse vulcanised sulfur polymers reacted in basic and acid environments but also how that would impact their effectiveness as sorbents for heavy metal remediation.

As previously discussed in 1.3.1, both artisanal small gold mining operations and coal power fired power plants are significant contributors to mercury pollution and these emissions are predominantly in the gaseous form.[8, 9] The low cost polymers reported in this thesis have shown to be extremely capable in remediating mercury from the aqueous phase and would therefore be expected to perform similarly in gaseous tests providing that materials can handle the different temperatures and pressures required to work in these systems.

There are numerous sources of radionuclide soil and groundwater contamination, particularly from uranium and other actinides.[10] It is therefore imperative that we find ways to effectively remove this toxicological health risk from our environment. Studies have shown that either polysulfides or sulfur containing systems can be used to sequester uranium from

contaminated sources.[11-13] Considering the high sulfur content of inverse vulcanised polymers and their low cost to synthesise, studies into the ability to remediate actinides and in particular uranium salts should be investigated.

To maximise the usefulness of inverse vulcanised sulfur polymers to industry and for their applications as heavy metal sorbents research should be conducted on the ability of these materials to be cycled and regenerated. Most commercially available sorbents possess an ability to be cycled and regenerated a number of times before their capacities are reduced to a point at which they are no longer commercially viable. Investigating how sulfur polymers can be regenerated and cycled is important since their enhanced uptake capacities relies not only on physisorption but also chemisorption, unlike traditional activated carbons which rely on physisorption alone.

6.3 REFERENCES

1. J.-S. Lee, D. J. Parker, A. I. Cooper and T. Hasell, *Journal of Materials Chemistry A*, 2017, **5**, 18603-18609.

2. M. W. Thielke, L. A. Bultema, D. D. Brauer, B. Richter, M. Fischer and P. Theato, *Polymers*, 2016, **8**, 266.

3. A. Hoefling, Y. J. Lee and P. Theato, *Macromolecular Chemistry and Physics*, 2017, **218**, 1600303.

4. A. Walcarius and C. Delacôte, *Analytica Chimica Acta*, 2005, **547**, 3-13.

5. H.-T. Fan, J.-B. Wu, X.-L. Fan, D.-S. Zhang, Z.-J. Su, F. Yan and T. Sun, *Chemical Engineering Journal*, 2012, **198-199**, 355-363.

6. M. F. Yardim, T. Budinova, E. Ekinci, N. Petrov, M. Razvigorova and V. Minkova, *Chemosphere*, 2003, **52**, 835-841.

7. A. J. Parker and N. Kharasch, *Chemical Reviews*, 1959, **59**, 583-628.

8. H. Gibb and K. G. O'Leary, *Environmental Health Perspectives*, 2014, **122**, 667-672.

9. M. Rallo, M. A. Lopez-Anton, M. L. Contreras and M. M. Maroto-Valer, *Environmental Science and Pollution Research*, 2012, **19**, 1084-1096.

10. Q.-H. Hu, J.-Q. Weng and J.-S. Wang, *Journal of Environmental Radioactivity*, 2010, **101**, 426-437.

11. S. Ma, L. Huang, L. Ma, Y. Shim, S. M. Islam, P. Wang, L.-D. Zhao, S. Wang, G. Sun, X. Yang and M. G. Kanatzidis, *Journal of the American Chemical Society*, 2015, **137**, 3670-3677.

12. A. Luna-Velasco, R. Sierra-Alvarez, B. Castro and J. A. Field, *Biotechnology and Bioengineering*, 2010, **107**, 933-942.

13. P. Wersin, M. F. Hochella, P. Persson, G. Redden, J. O. Leckie and D. W. Harris, *Geochimica et Cosmochimica Acta*, 1994, **58**, 2829-2843.

APPENDICES

CONTENTS

APPENDIX A1: FT-IR SPECTRA

This appendix includes the FT-IR spectra for the following inverse vulcanised sulfur polymers:

I. S-MYR
II. S-FAR
III. S-FSOL
IV. S-PER
V. S-DCPD

I. Stacked FT-IR spectra for S-MYR at 50 wt.% and myrcene monomer

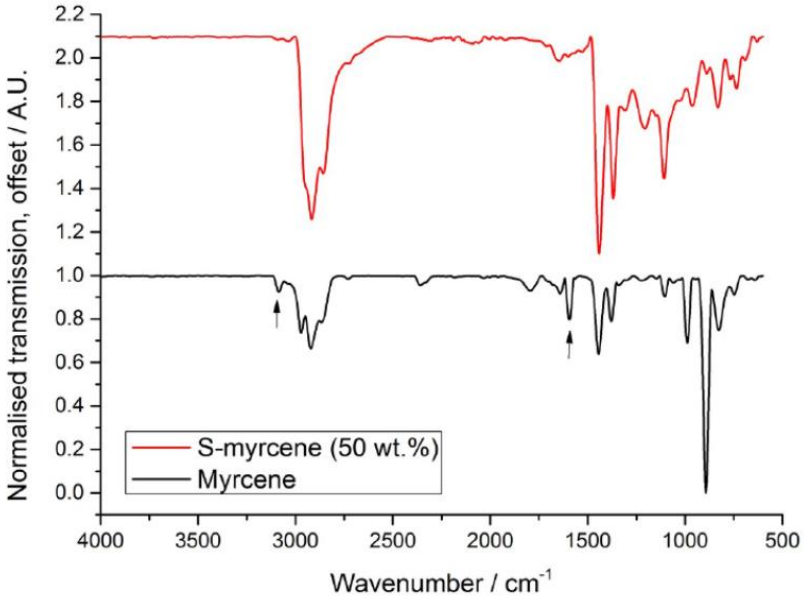

II. Stacked FT-IR spectra for S-FAR at 50 wt.% and farnesene monomer

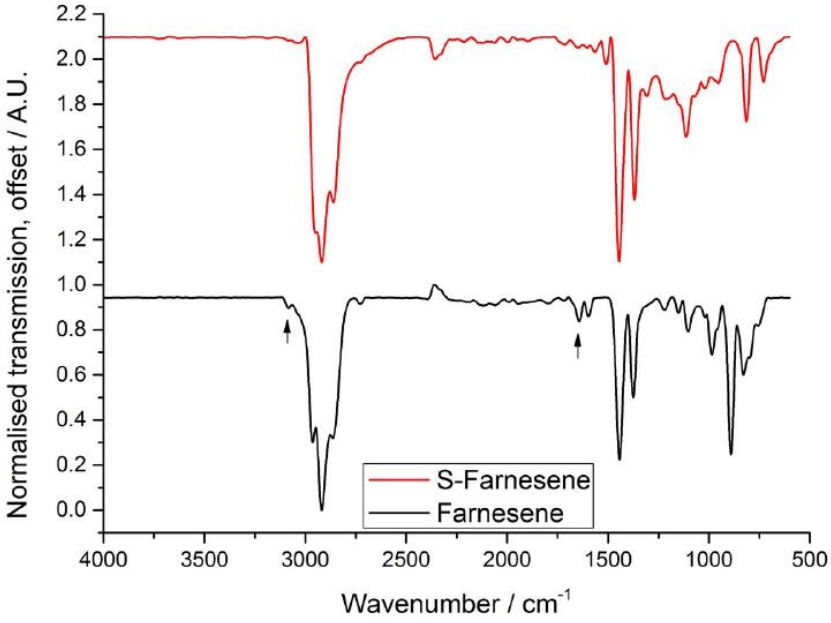

III. Stacked FT-IR spectra for S-FSOL at 50 wt.% and farnesol monomer

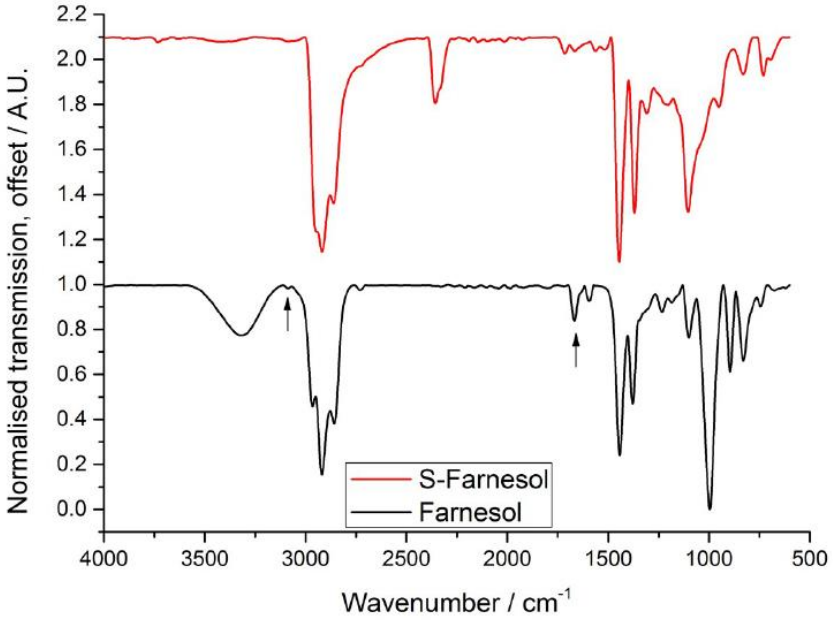

IV. Stacked FT-IR spectra for S-PER at 50, 60, 70 and 80 wt.% and perillyl alcohol monomer

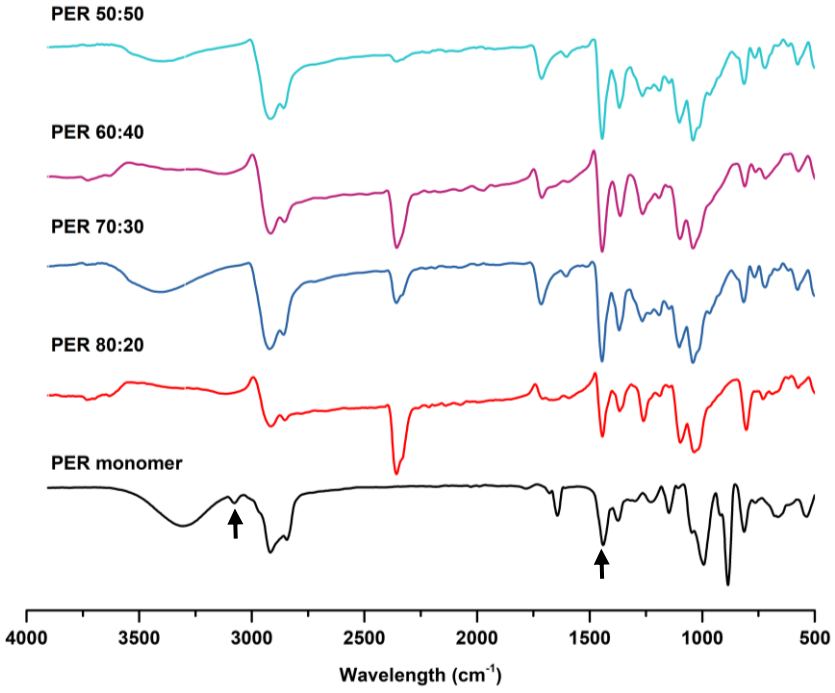

V. Stacked FT-IR spectra for S-DCPD at 50, 60, 70, 80, 90 wt.% and DCPD monomer

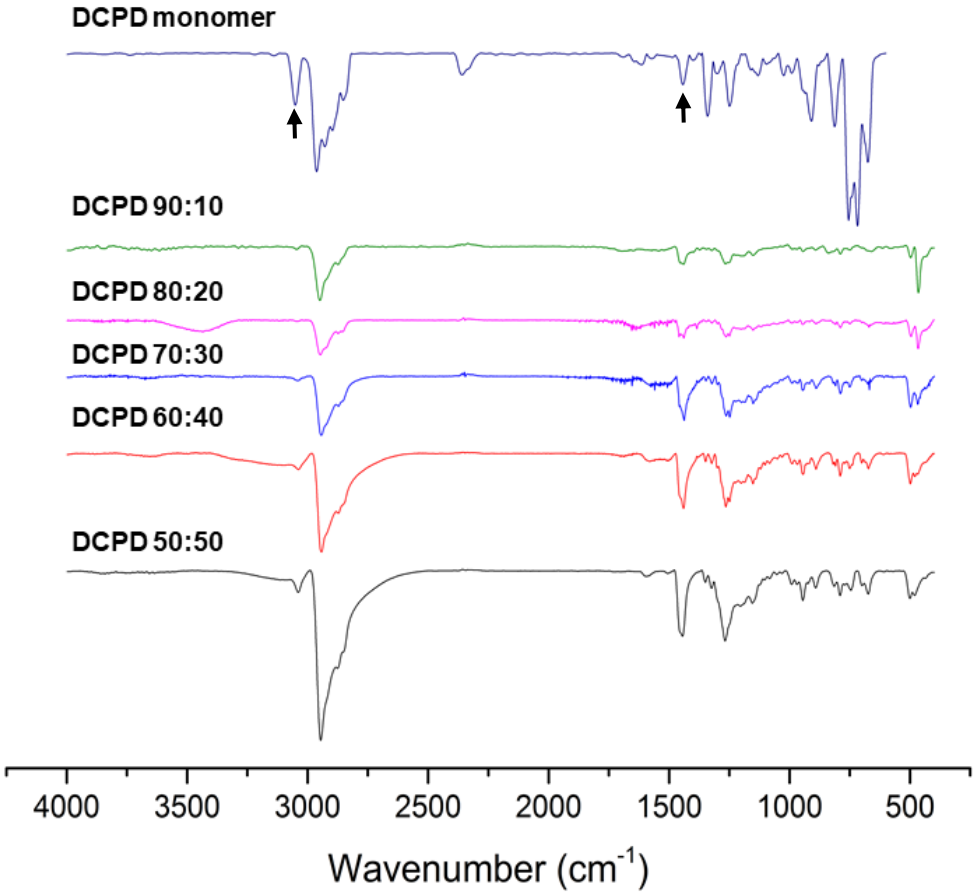

APPENDIX A2: X-RAY DIFFRACTION PATTERNS

This appendix includes the powder X-Ray diffraction patterns for the following inverse vulcanised sulfur polymers:

I. S-MYR
II. S-FSOL
III. S-FAR
IV. S-SQ
V. S-HOP
VI. S-PERT

I. Stacked pXRD patterns for S-MYR at 50, 70, 80 wt.% and elemental sulfur (80 wt.% = blue, 70 wt.% = green, 50 wt.% grey and S_8 = red)

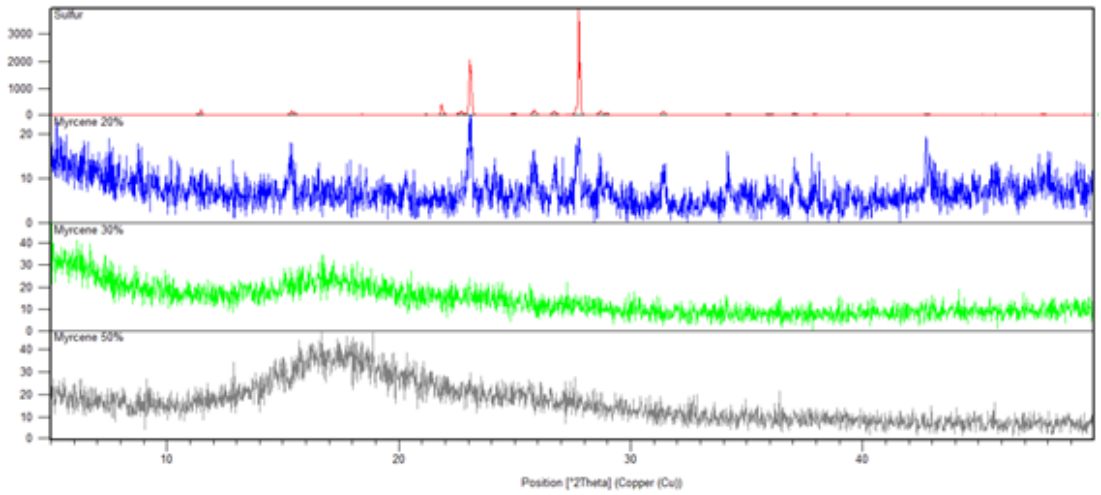

II. Stacked pXRD patterns for S-FSOL at 50, 70, 80 wt.% and elemental sulfur (80 wt.% = blue, 70 wt.% = green, 50 wt.% grey and S_8 = red)

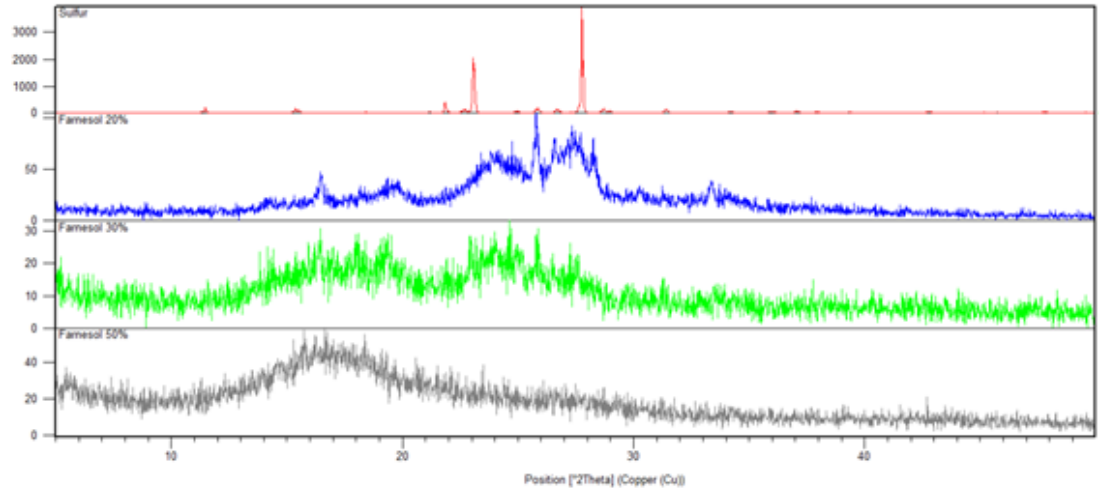

III. Stacked pXRD patterns for S-FAR at 50, 70, 80 wt.% and elemental sulfur (80 wt.% = blue, 70 wt.% = green, 50 wt.% grey and S_8 = red)

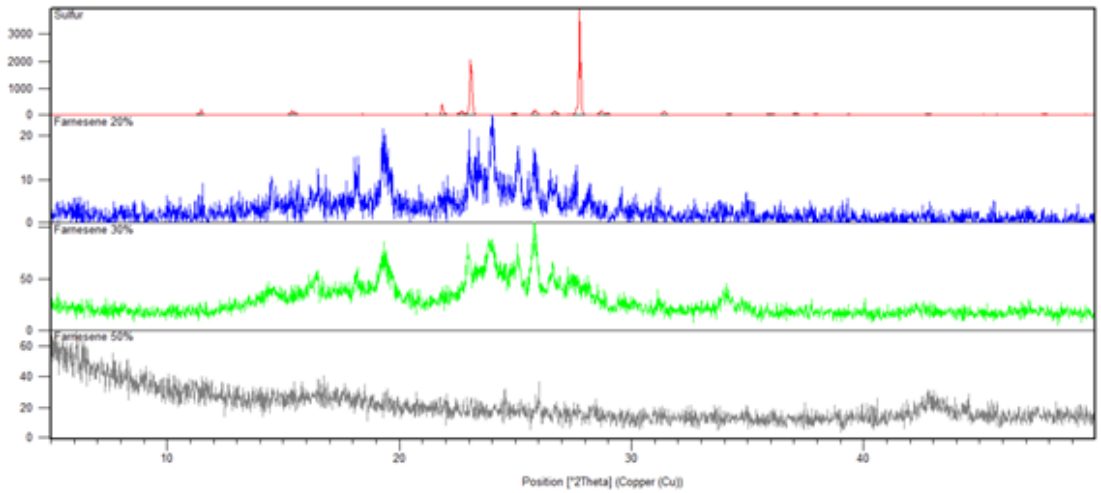

IV. Stacked pXRD patterns for S-SQ at 50, 60, 70, 80, 90 wt.% and both α and γ sulfur polymorphous. X-Ray data for the α and γ sulfur polymorphs was obtained from the ICSD

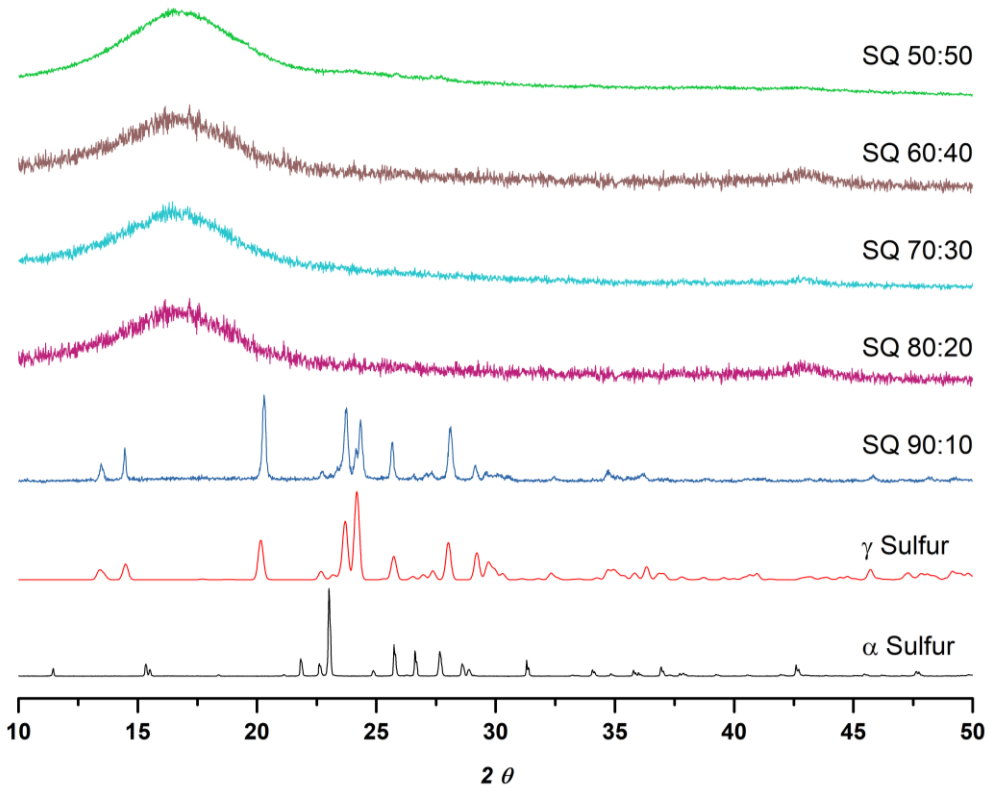

V. Stacked pXRD patterns for S-HOP at 50, 60, 70, 80 wt.% and elemental sulfur (50 wt.% = blue, 60 wt.% = green, 70 wt.% grey, 80 wt.% brown and S_8 = red)

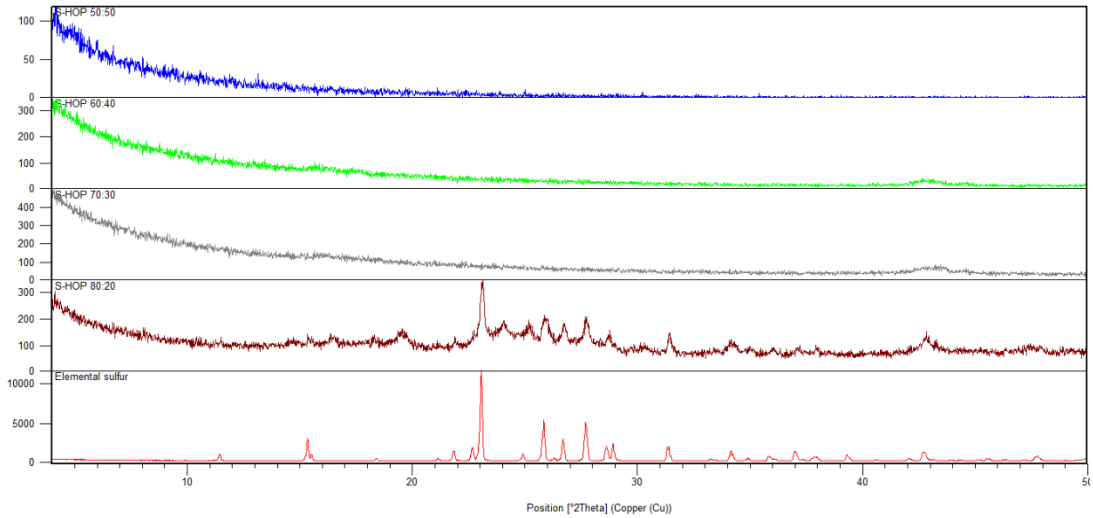

VI. Stacked pXRD patterns for S-PERT at 50, 70 wt.% and elemental sulfur (50 wt.% = blue, 70 wt.% green and S_8 = red)

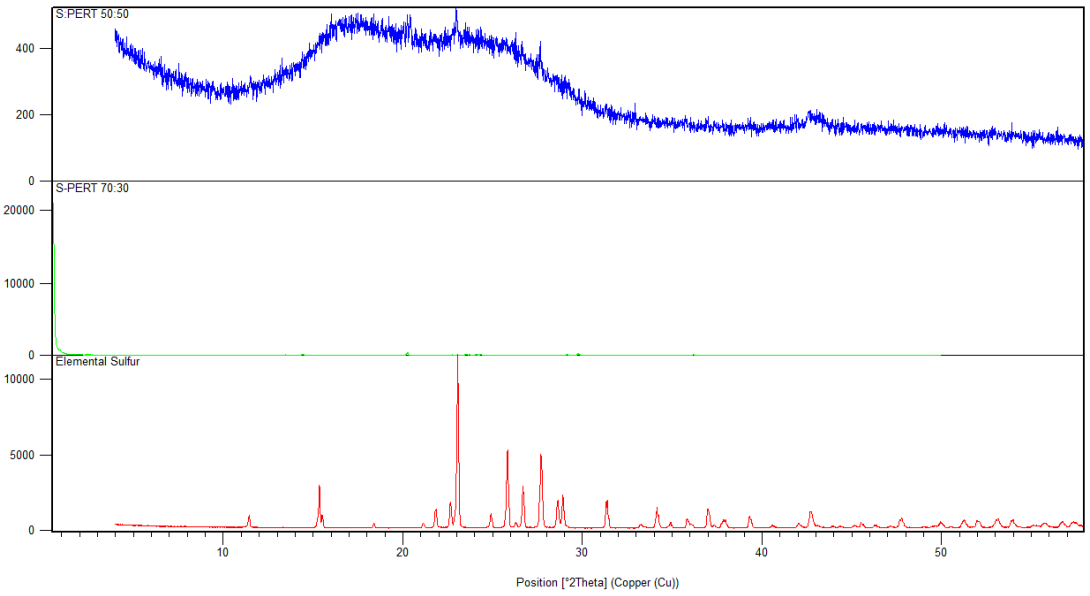

APPENDIX A3: ELEMENTAL (CHNS) ANALYSIS

This appendix includes the full elemental analysis results for the following inverse vulcanised sulfur polymers at their differing compositions:

I. S-MYR
II. S-FSOL
III. S-FAR
IV. S-SQ
V. S-PER

I. Elemental analysis results for 50, 60, 70 and 80 wt.% S-MYR copolymers

Sample	Calculated			Observed		
	C	H	S	C	H	S
S-MYR 50:50	44.08	5.92	50.00	37.31	4.53	57.28
S-MYR 60:40	35.26	4.74	60.00	32.25	4.12	63.45
S-MYR 70:30	26.45	3.55	70.00	23.84	2.94	74.09
S-MYR 80:20	17.63	2.37	80.00	14.73	1.74	85.47

II. Elemental analysis results for 50, 60, 70 and 80 wt.% S-FSOL copolymers

Sample	Calculated			Observed		
	C	H	S	C	H	S
S-FSOL 50:50	40.51	5.89	50.00	40.55	5.21	51.86
S-FSOL 60:40	34.84	4.72	60.00	34.64	3.95	60.79
S-FSOL 70:30	24.31	3.54	70.00	23.25	2.79	74.13
S-FSOL 80:20	16.20	2.36	80.00	14.67	1.75	84.13

III. Elemental analysis results for 50, 60, 70 and 80 wt.% S-FAR copolymers

Sample	Calculated			Observed		
	C	H	S	C	H	S
S-FAR 50:50	44.08	5.92	50.00	41.87	5.22	54.16
S-FAR 60:40	35.26	4.74	60.00	33.59	4.14	62.34
S-FAR 70:30	26.45	3.55	70.00	22.42	2.41	76.61
S-FAR 80:20	17.63	2.37	80.00	16.62	1.41	83.30

IV. Elemental analysis results for 50, 60, 70, 80 and 90 wt.% S-SQ copolymers

Sample	Calculated			Observed		
	C	H	S	C	H	S
S-SQ 50:50	43.87	6.13	50.00	43.57	5.91	50.52
S-SQ 60:40	35.09	4.91	60.00	33.92	4.63	61.35
S-SQ 70:30	26.32	3.68	70.00	20.68	2.75	76.47
S-SQ 80:20	17.55	2.45	80.00	13.20	1.51	84.93
S-SQ 90:10	8.77	1.23	90.00	8.38	0.90	91.18

V. Elemental analysis results for 50, 60, 70 and 80 wt.% S-PER copolymers

Sample	Calculated			Observed		
	C	H	S	C	H	S
S-PER 50:50	39.45	5.30	50.00	37.66	4.73	53.79
S-PER 60:40	31.56	4.24	60.00	32.25	3.97	60.51
S-PER 70:30	23.67	3.18	70.00	24.89	2.98	69.75
S-PER 80:20	15.78	2.19	80.00	15.88	1.85	80.04

APPENDIX A4: NMR SPECTRA

This appendix includes the ^{1}H spectra for the following inverse vulcanised sulfur polymers:

I. S-FAR
II. S-FSOL
III. S-PER

I. Stacked ^{1}H NMR (400 MHz, $CDCl_3$) for S-FAR and farnesene monomer

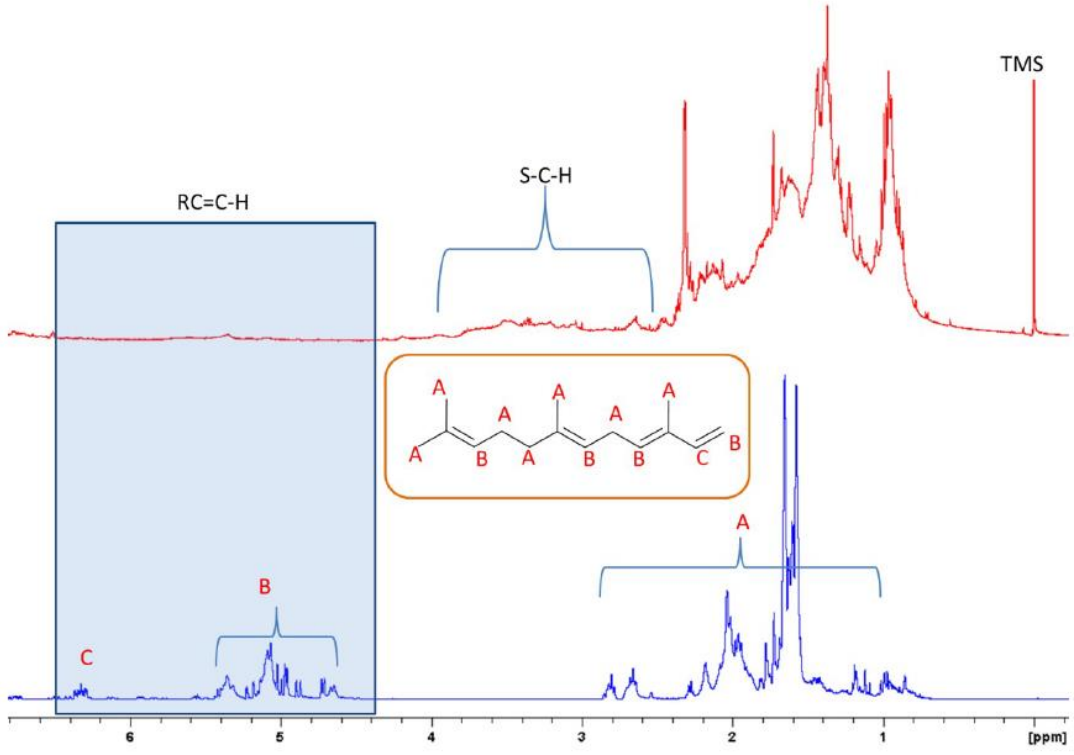

II. Stacked ^{1}H NMR (400 MHz, $CDCl_3$) for S-FSOL and farnesol monomer

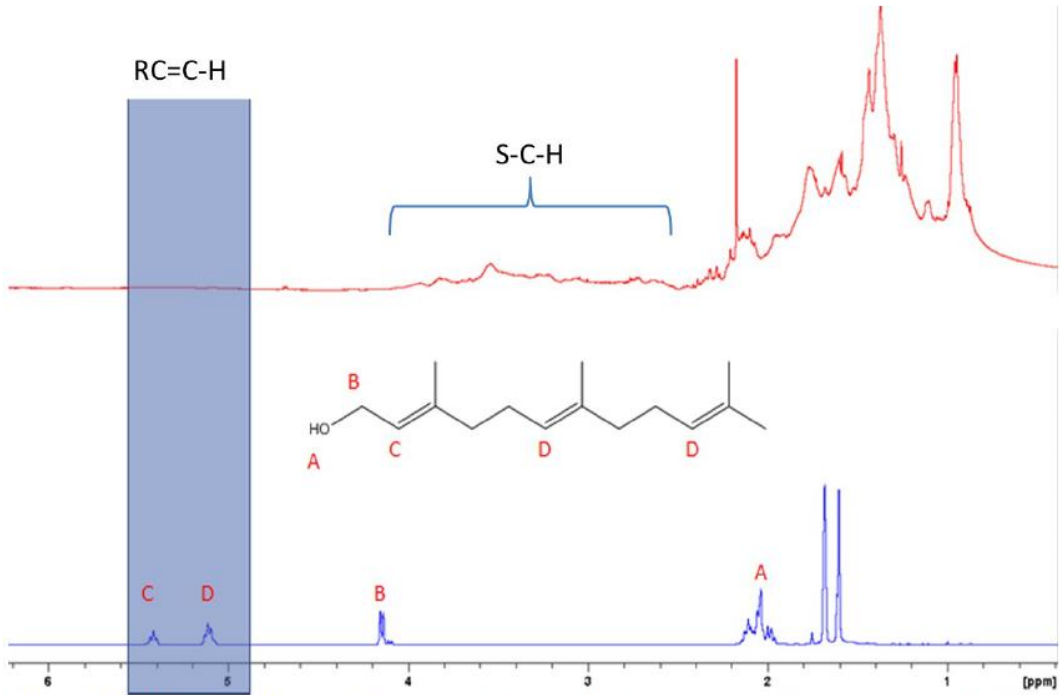

III. Stacked ^{1}H NMR (400 MHz, $CDCl_3$) for S-PER and perillyl alcohol monomer

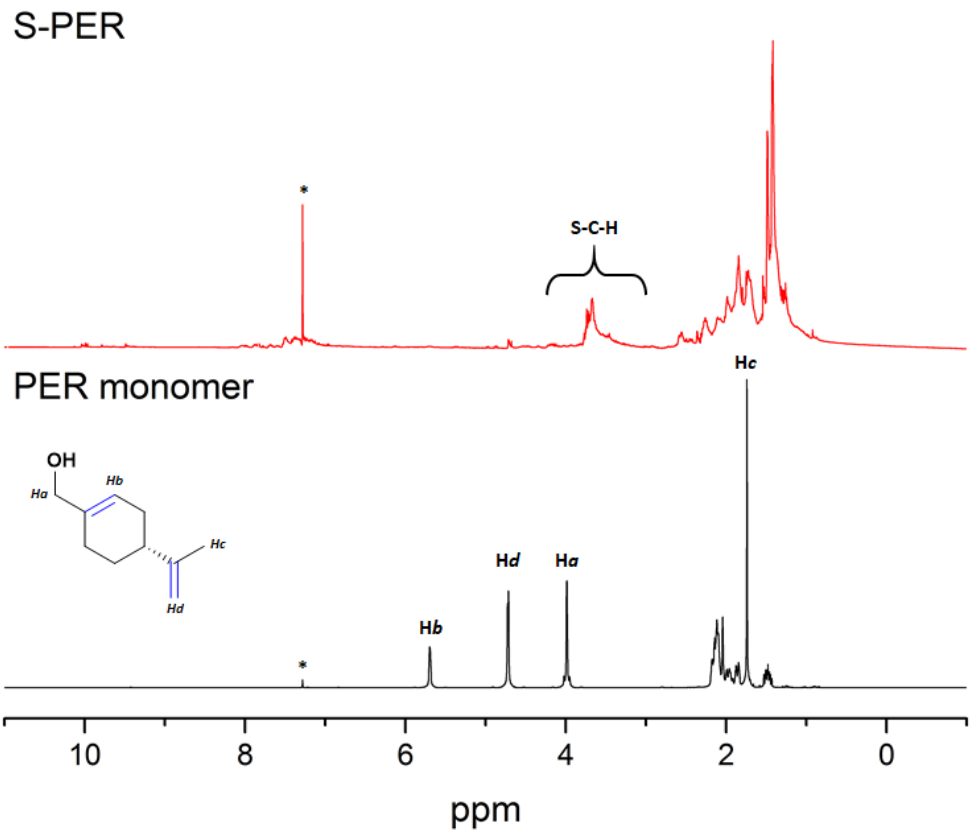

APPENDIX A5: THERMOGRAVIMETRIC ANALYSIS

This appendix includes the thermogravimetric analysis results for the following inverse vulcanised sulfur polymers:

I. S-MYR
II. S-FSOL
III. S-FAR

I. Stacked TGA thermograms for S-MYR at 50, 70 and 80 wt.% and both cured and uncured myrcene monomer

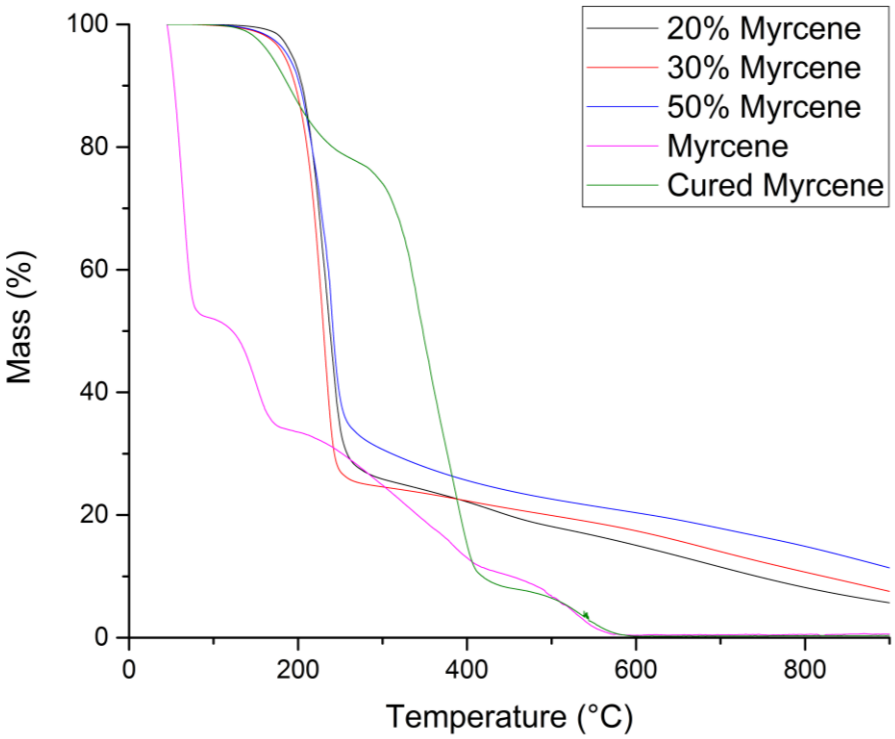

II. Stacked TGA thermograms for S-FSOL at 50, 70 and 80 wt.% and both cured and uncured farnesol monomer

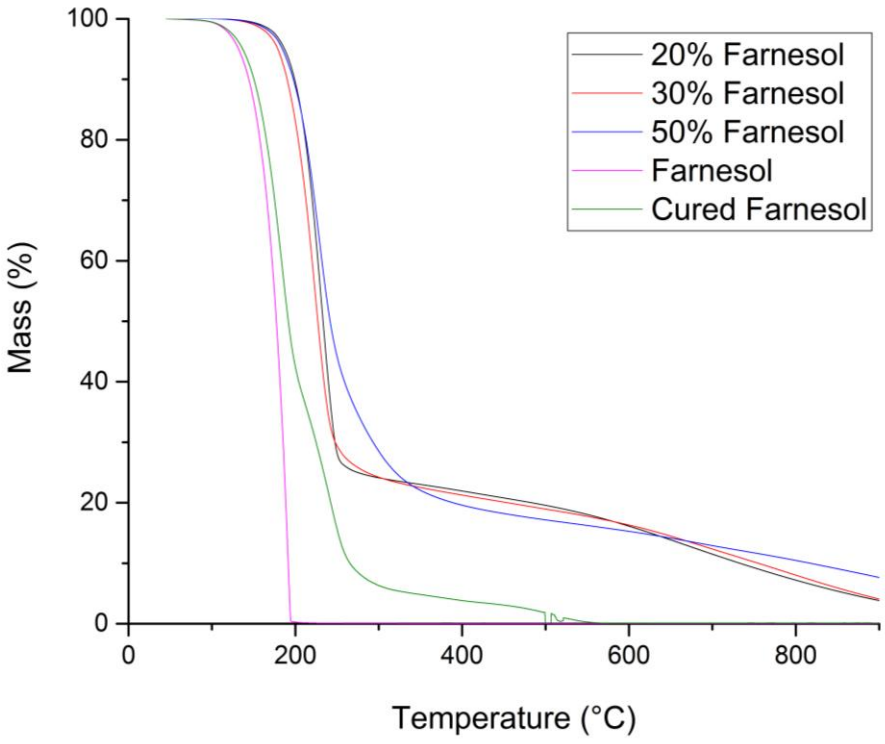

III. Stacked TGA thermograms for S-FAR at 50, 70 and 80 wt.% and both cured and uncured farnesene monomer

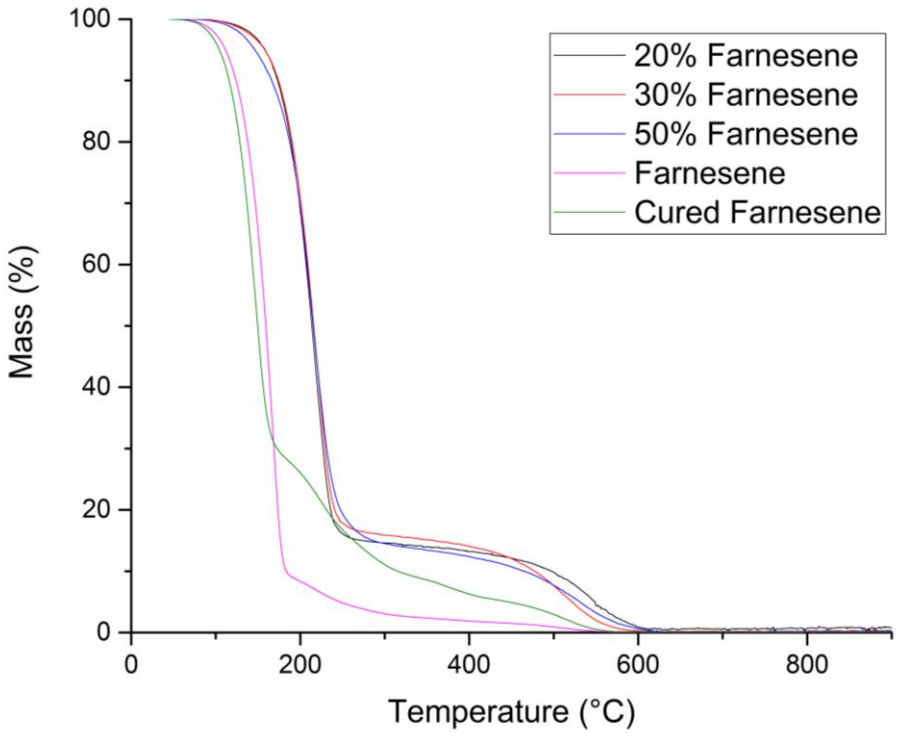

APPENDIX A6: GAS ADSORPTION

This appendix includes the nitrogen gas adsorption data collected for the following samples:

I. Kaolin nitrogen adsorption isotherm
II. Kaolin coated with S-HOP nitrogen adsorption isotherm
III. Lignin nitrogen adsorption isotherm
IV. Lignin coated with S-HOP nitrogen adsorption isotherm
V. Mordenite nitrogen adsorption isotherm
VI. Mordenite coated with S-HOP nitrogen adsorption isotherm
VII. Fumed silica nitrogen adsorption isotherm
VIII. Fumed silica coated with S-HOP nitrogen adsorption isotherm

I. Kaolin nitrogen adsorption isotherm and report summary

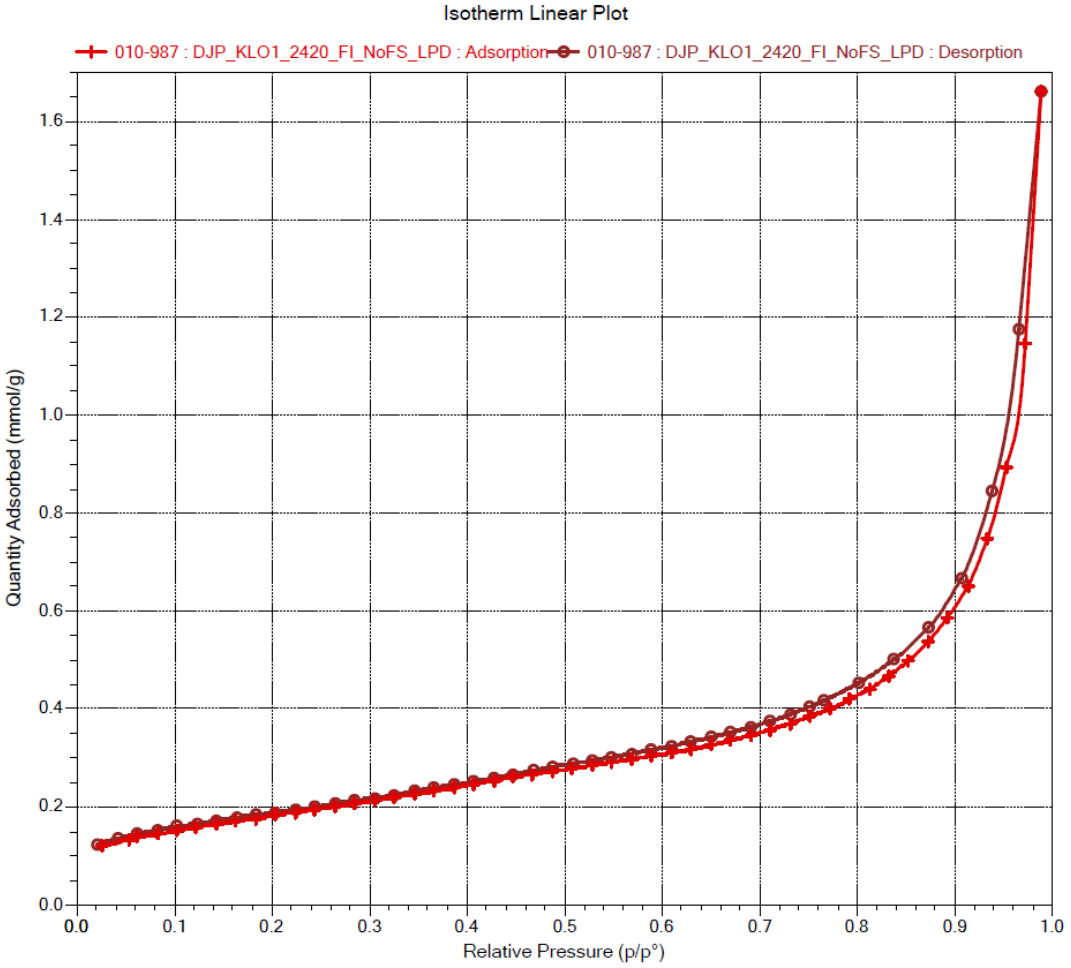

Surface Area		**Pore Volume**	
Single point at p/p^0 p/p^0 = 0.223982100	14.3324 m^2/g	**Maximum at p/p^0** p/p^0 = 0.142943786	0.005691 cm^3/g
BET	15.1457 m^2/g		
Langmuir	20.9225 m^2/g		

II. Kaolin coated with S-HOP nitrogen adsorption isotherm

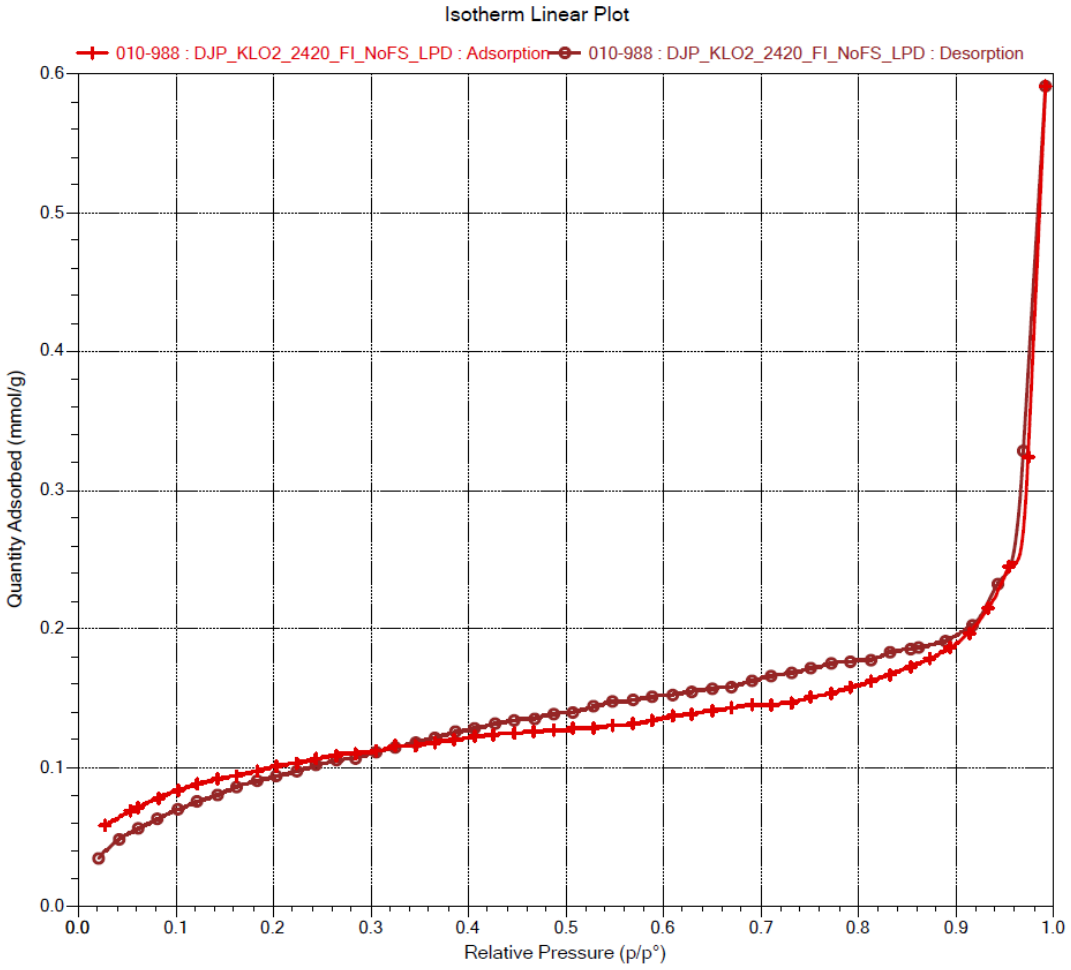

Surface Area		**Pore Volume**	
Single point at p/p^0 p/p^0 = 0.223982100	7.8527 m^2/g	**Maximum at p/p^0** p/p^0 = 0.143013269	0.003171 cm^3/g
BET	8.2698 m^2/g		
Langmuir	11.9871 m^2/g		

III. Lignin nitrogen adsorption isotherm

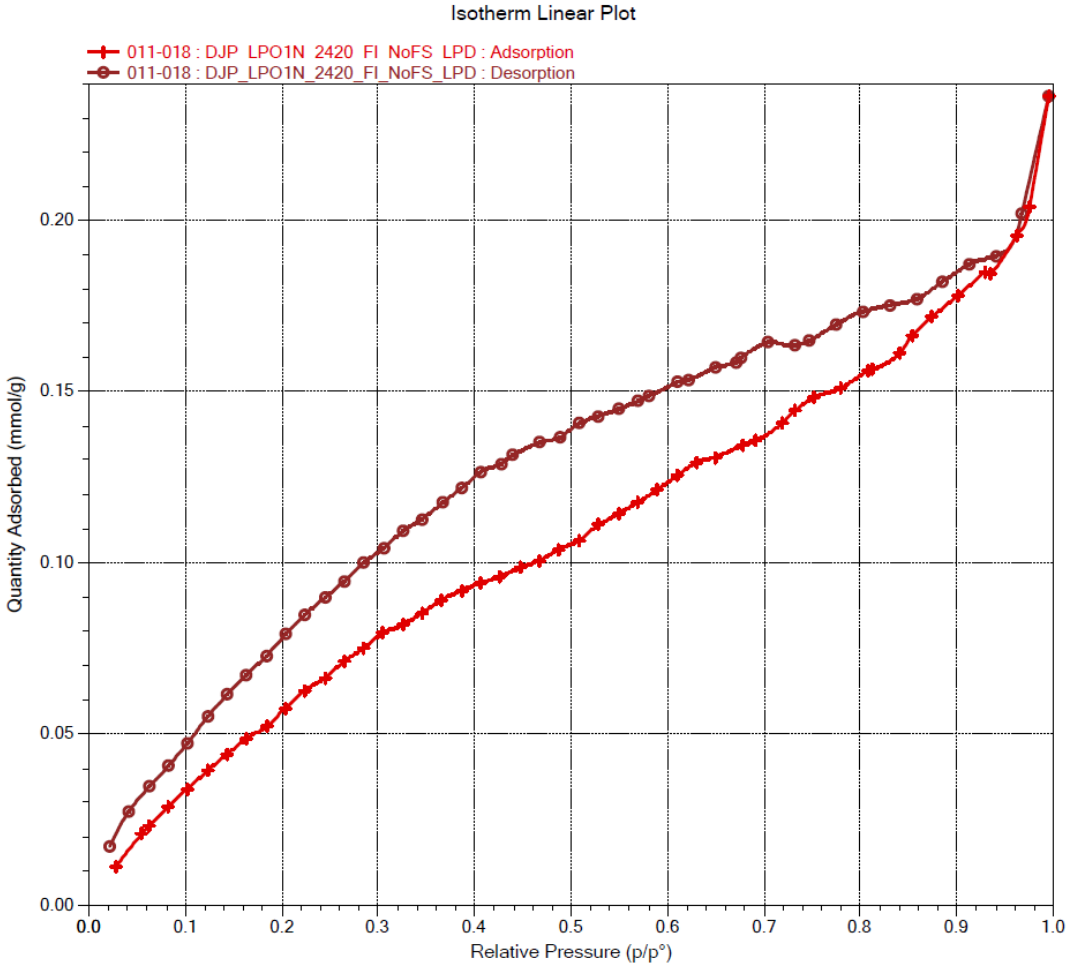

Surface Area		**Pore Volume**	
Single point at p/p^0 p/p^0 = 0.163409512	3.9747 m^2/g	**Maximum at p/p^0** p/p^0 = 0.143197078	0.001528 cm^3/g
BET	7.2548 m^2/g		
Langmuir	15.9444 m^2/g		

IV. Lignin coated with S-HOP nitrogen adsorption isotherm

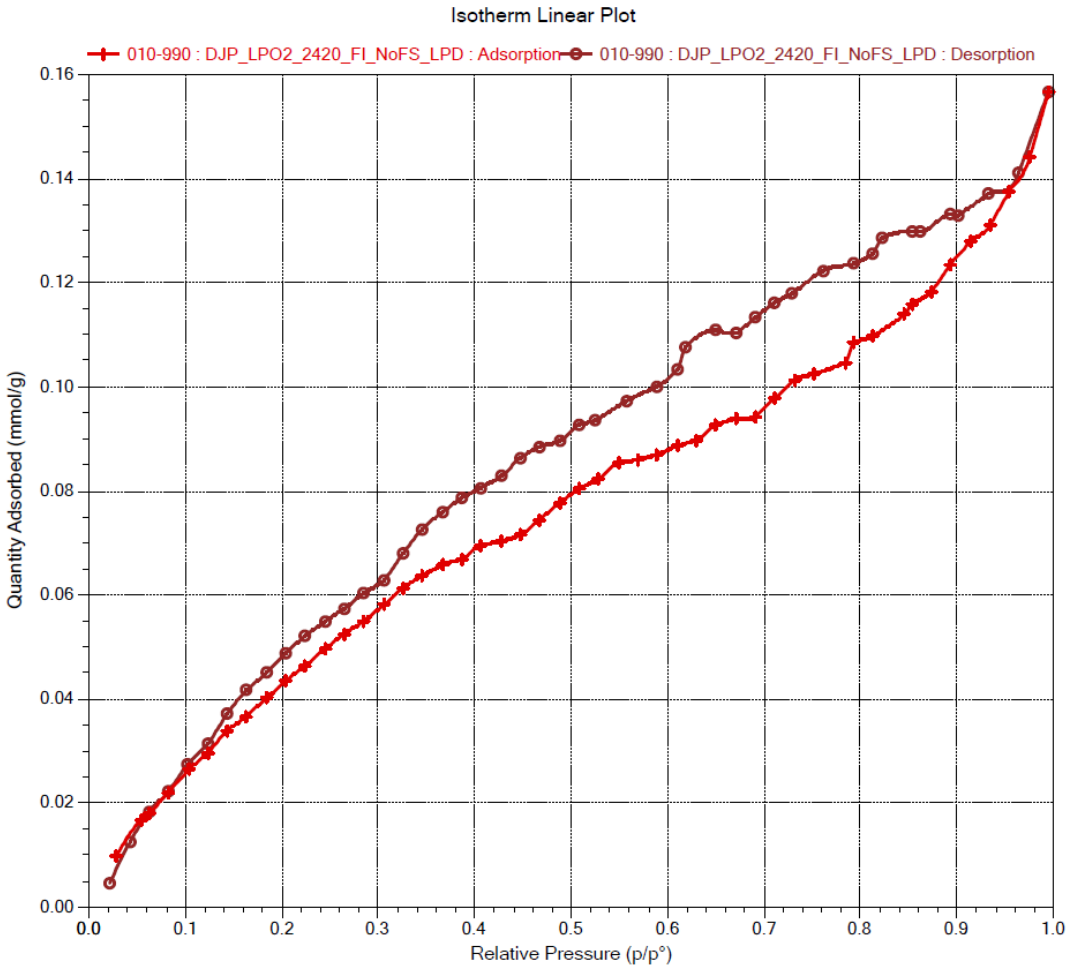

Surface Area		**Pore Volume**	
Single point at p/p^0 p/p^0 = 0.224393986	3.5031 m^2/g	**Maximum at p/p^0** p/p^0 = 0.143357948	0.001175 cm^3/g
BET	5.3684 m^2/g		
Langmuir	11.3675 m^2/g		

V. Mordenite nitrogen adsorption isotherm

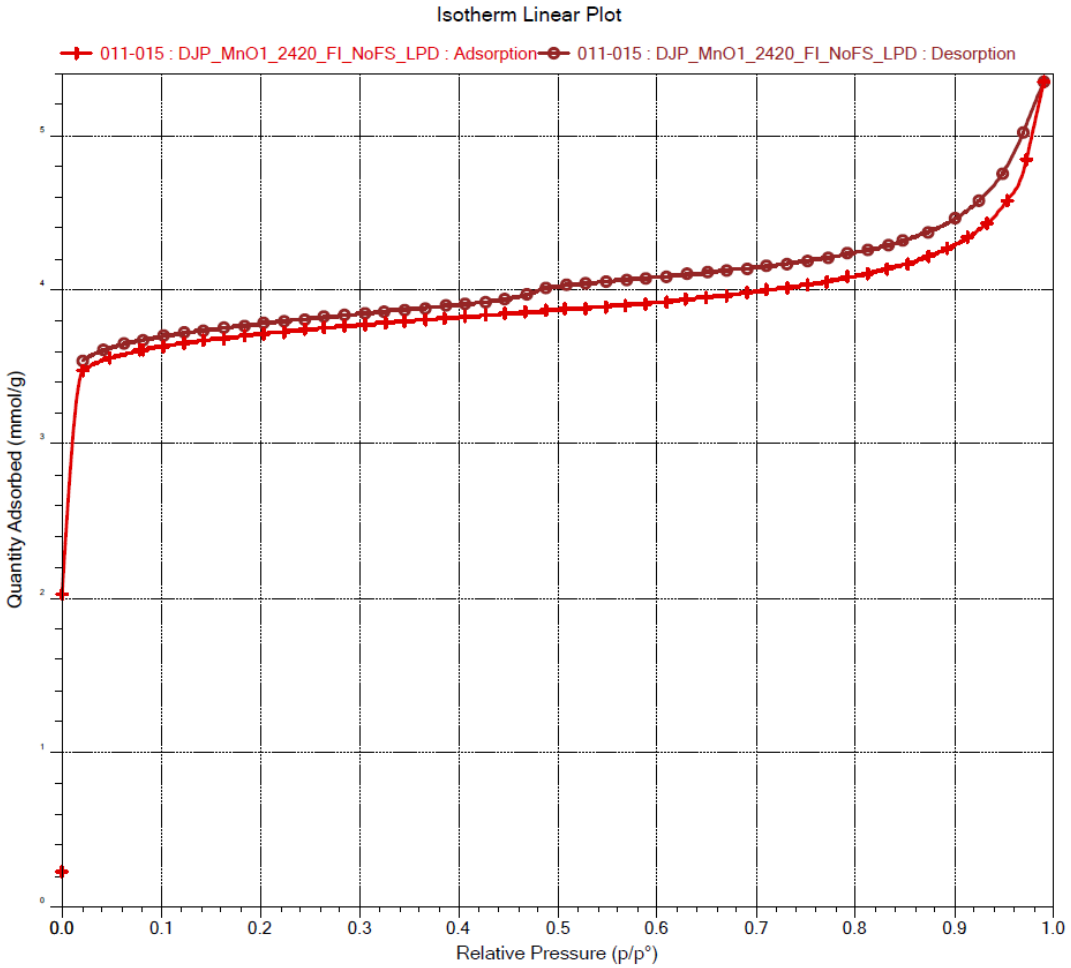

Surface Area		**Pore Volume**	
Single point at p/p^0 p/p^0 = 0.203895148	288.5833 m^2/g	**Maximum at p/p^0** p/p^0 = 0.143092162	0.127290 cm^3/g
BET	264.3157 m^2/g		
Langmuir	369.2411 m^2/g		

VI. Mordenite coated with S-HOP nitrogen adsorption isotherm

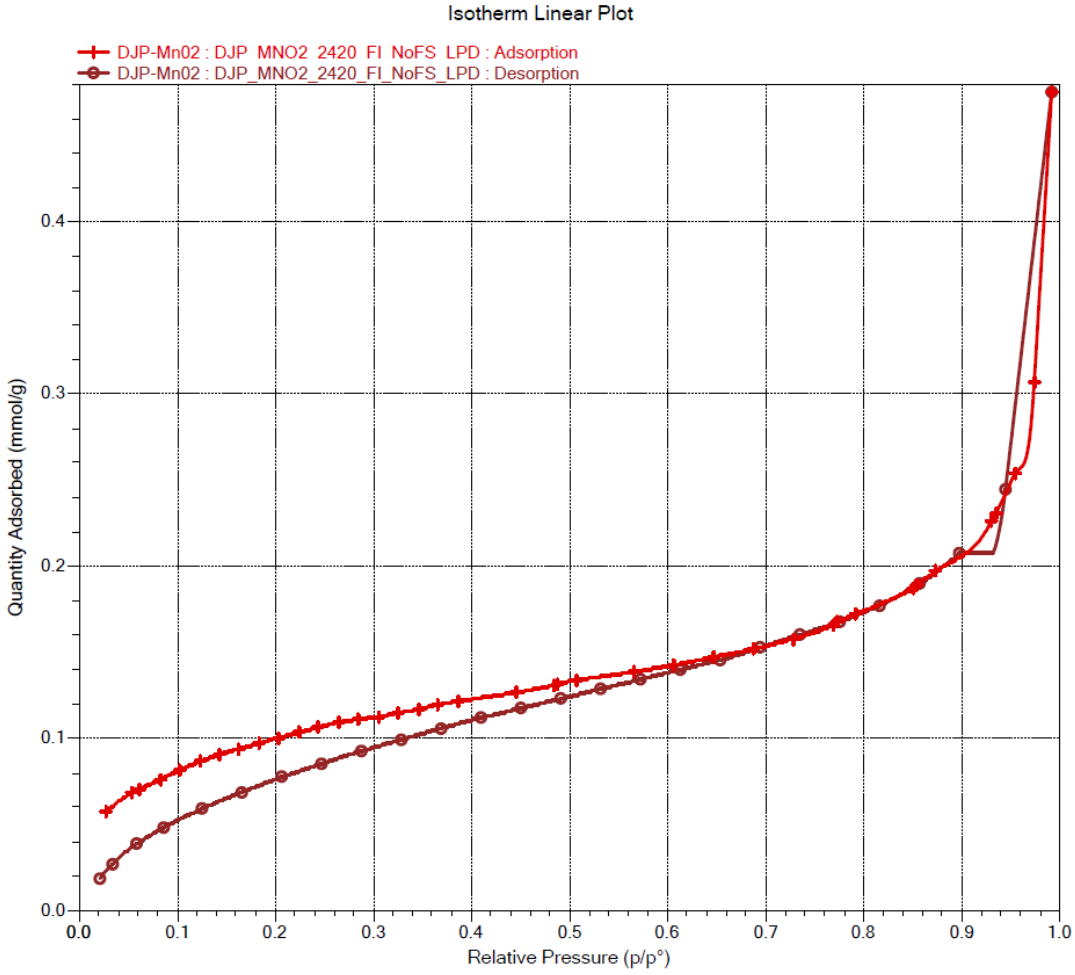

Surface Area		**Pore Volume**	
Single point at p/p^0 p/p^0 = 0.224123147	7.8329 m^2/g	**Maximum at p/p^0** p/p^0 = 0.143062566	0.003139 cm^3/g
BET	8.4099 m^2/g		
Langmuir	12.1096 m^2/g		

VII. Fumed silica nitrogen adsorption isotherm

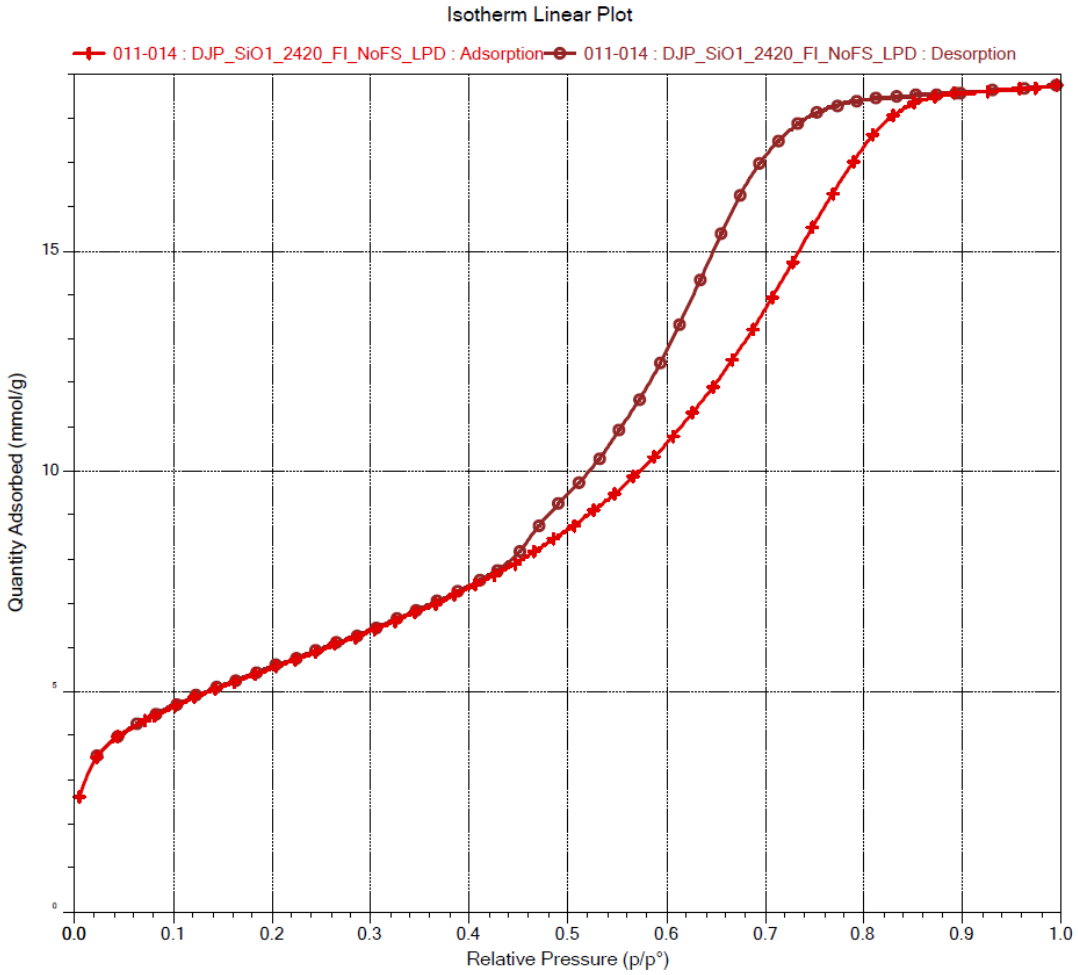

Surface Area		**Pore Volume**	
Single point at p/p^0 p/p^0 = 0.223378081	433.8354 m^2/g	**Maximum at p/p^0** p/p^0 = 0.142347155	0.175064 cm^3/g
BET	451.0932 m^2/g		
Langmuir	637.2742 m^2/g		

VIII. Fumed silica coated with S-HOP nitrogen adsorption isotherm

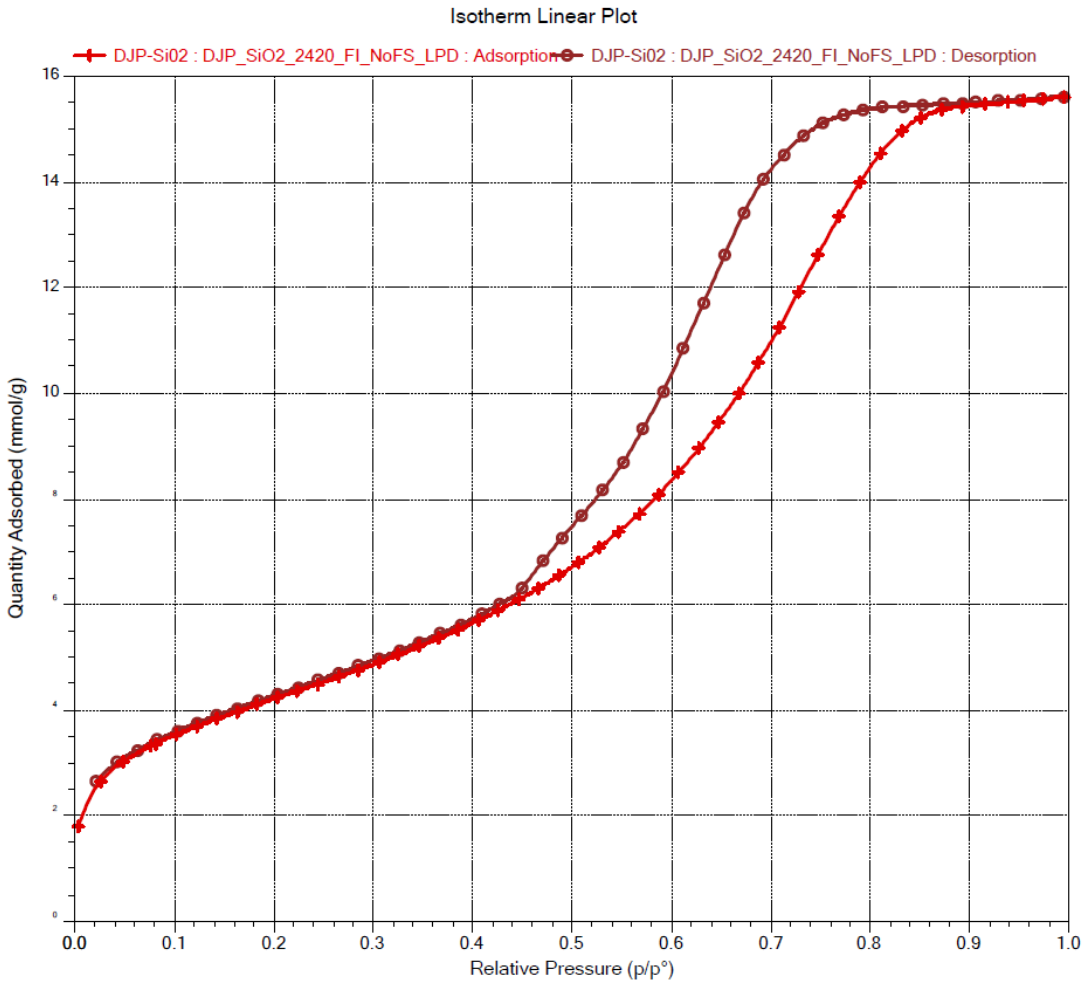

Surface Area		**Pore Volume**	
Single point at p/p^0 p/p^0 = 0.224171850	331.2852 m^2/g	**Maximum at p/p^0** p/p^0 = 0.142506367	0.132835 cm^3/g
BET	344.7394 m^2/g		
Langmuir	491.5443 m^2/g		